2D-Crystallization and 3D-Structures of Membrane Channels and Transporters

Inaugraldissertation

zur
Erlangung der Würde eines Doktors der Philosophie
vorgelegt der Philosophisch-Naturwissenschaftlichen
Fakultät der Universität Basel
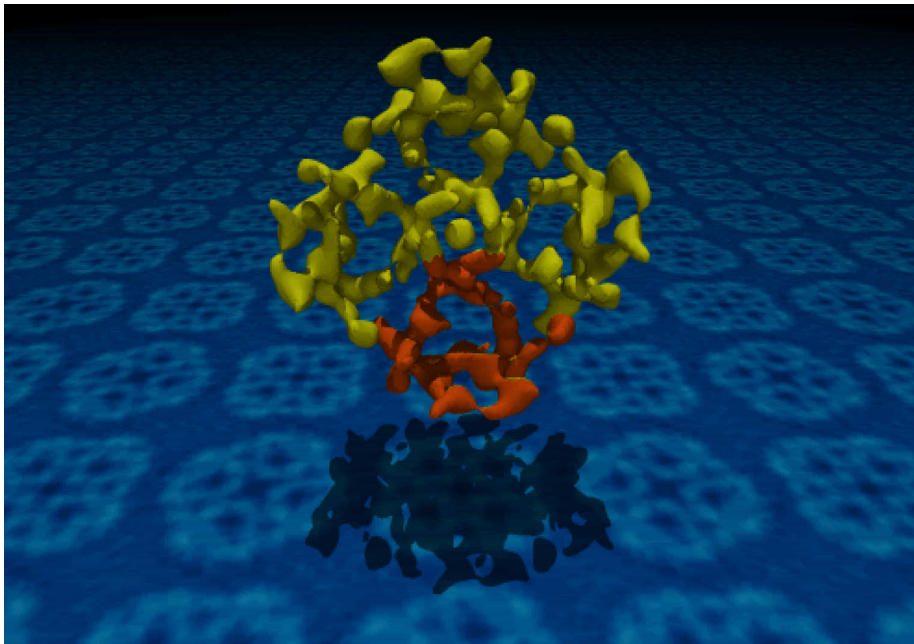
Von

Thomas Braun
aus Basel, Schweiz

Juli 2004

Genehmigt von der Naturwissenschaftlichen Fakultät
Auf Antrag von Professor Dr. Andreas Engel

Basel, den 1. Juli 2002
(Datum der Fakultätssitzung)

Professor Dr. Zuberbühler
Dekan

2D-Crystallization and 3D-Structures of Membrane Channels and Transporters

von
Thomas Braun
aus Basel, Schweiz

Biozentrum der Universität Basel
Klingelbergstrasse 70
CH-4056 Basel

ii

Short summary

The topic of this thesis was the structural exploration of membrane channels and transporters by two dimensional (2D) crystallization and transmission electron microscopy. Chapter 1 gives an introduction to the studied biological systems and summarizes the applied methods. Chapter 2 describes our attempts to 2D-crystallize LmrA, an ABC-transporter from *Lactococcus lactis*. Chapter 3 describes the successful 2D-crystallization of the glycerol channel GlpF from *Escherichia coli* and its structural analysis by electron microscopy and image processing.

Contents

List of Figures

List of Tables

Abbreviations

2D Two dimensional

3D Three dimensional

8-POE Polyoxyethylen ether (C_8E_y) mixture, also called Rosenbusch detergent

ABC-transporter ATP binding cassette transporter

ADP Adenosine-di-phosphate

AFM Atomic force microscope

AQP Aquaporin

AqpZ Aquaporin Z from *Escherichia coli*

ATP Adenosine tri-phosphate

$C_{12}E_9$ Polyoxyethylen(9)dodecyl ether

CH^RB30 MDR1 homologue in chinese hamster

CHAPS 3-[(3-cholamidopropyl)-demethylammonio]-1-propanesulfonate

CMC Critical micelle concentration

DDM n-Dodecyl-β-D-maltoside

DHPC 1,2-Diheptyl-sn-Glycero-3-Phosphocholine

DM n-Decyl-β-D-maltopyranoside

DMPC 1,2-Dimyristoyl-sn-Glycero-3-Phosphocholine

DMSO 3-[(3-cholamidopropyl)-demethylammonio]-1-propanesulfonate

DOPC 1,2-Dioleoyl-sn-Glycero-3-Phosphocholine

DOPG 1-Palmitoyl-2-Oleoyl-sn-Glycero-3-[Phospho-rac-(1-glycerol)]

EM Electron Microscopy

FPLC Fast Performance Liquid Chromatography

γ-S-ATP Slow hydrolyzable ATP analogon

GLP Glyceroporin

GlpF Glycerol facilitator from *Escherichia coli*

LmrA Multidrug ABC-transporter from *Lactococcus lactis*

LPR Lipid to protein ratio

MDR Multidrug resistance protein

MDR1 Mamilian multidrug resistance protein 1

MFP Membrane Fusion Protein

MIP Major intrinsic protein (channel of animal lense fiber cells)

MW Molecular weight

$\mathbf{n}_A$ Aggregation number

NB Nucleotide binding

NG n-Nonyl-β-D-glyopyronaoside

NiNTA Ni^{++}-Nitrilotriacetic acid

OG n-Octyl-β-D-glycopyranoside

OTG n-Octyl 1-β-D-glycopyranoside

o-vanadate Inorganic phosphate analogon

$\mathbf{P}_I$ Inorganic phosphate

PAA Polyacrylamid

PAGE Poyacrylamid gel electrophoresis

pfMdr1 ABC-exporter from *Plasmodium falciparum*

pH Negative logarith of proton concentration

PMSF Phenylmethylsulfonyl fluoride

Pril General biocentre washing agent (Henkel)

SDS Sodium-dodecylsulfat

SDS Sodiumdodecylsulfate

SNR Signal to noise ratio

STEM Scanning transmission electron microscope

TEM Transmission electron microscope

TEM Transmission electron microscope

TLC Thin layer chromatography

Triton X-100 Polyethylene glycol-p-isooctylphenyl ether

Chapter 1

Introduction

1.1 Membrane proteins: An overview

Membranes are one of the most fascinating structures in cells. They fulfill two main functions:

- Separation of the cell from the surrounding environment and division of the (eucaryotic) cell into compartments.

- Communication and interaction with the environment or different compartments.

At first view this is seemingly contradictory, but the two functions are closely related to the structural and chemical composition of biological membranes: The first is a property of the membrane lipids, which build up a barrier for water and water soluble solvents such as salts and sugars. The second function is primarily made possible by the presence of proteins. They mediate the "communication" with the outer world of the cell, which involves an extremely broad spectrum of biological functions:

- They control nutrition uptake and secretion of chemical compounds (transport)

- They act as sensors for chemical and physical effects and are transducing outer signals into the cell (signal transduction)

- They are essential for energy conversion

- They mediate cell mobility, cell adhesion and other structural functions

- They are important for some enzymatic activities

Therefore, it is not surprising that about 30% of all proteins are membrane spanning proteins [88, 80]. Interestingly their diversity of biological functions is not reflected by a large diversity of folding motifs in the transmembrane spanning regions: Because of the low dielectric constant of the membrane-phase, the entire hydrogen bonding capacity of the carbon back-bone has to be saturated. Therefore, only two types of transmembrane folds are found: α-helical motifs and β-barrel motifs. So far, the β-barrel type proteins have been exclusively

found in the outer membranes of gram negative bacteria, mitochondria and chloroplasts, whereas α-proteins are found in the cytoplasmic membrane and eucaryotic cells.

The structural analysis of membrane-proteins is a long (and sometimes painful) process. To date, only a few of the several thousand protein structures solved at atomic resolution are from membrane-proteins [46][1]: From the group of poly-topic membrane-proteins (plasma-membrane from bacteria, mitochondria and eucaryotic membrane-proteins), the structure of 31 proteins are known. Among them only 15 independent (unrelated) folds are observed. From the outer membrane of gram-negative bacteria 20 different protein-structures have been solved and from the group of the non-membrane-spanning (monotopic) proteins, the structures of only 4 proteins are known (2 unrelated). An pragmatic overview over the major structural-classes of the trans-membrane proteins is given in figure 1.1. Note, this table does not represent evolutionary relation-ships but is based on the *Structural Classification of Proteins (SCOP)* database [52][2]. Obviously, very important membrane protein-families such as the *Major Facilitator Superfamily* are not present in this overview.

1.2   Transporters and Channels

Biological membranes allow a tight control to be kept of the substances entering and leaving the cell. Only small amphiphilic compounds are able to diffuse across the lipid bilayer. Membrane crossing of other molecules is regulated by two groups of membrane proteins: The channels, which are molecular sieves, allow the diffusion of specific compounds along their electrochemical-potential gradient, and the transporters, which are pumps consuming energy to transport a substance in a specific direction even if this is energetically unfavorable.

A classification of transport proteins and channels is given in figure 1.2. The protein families were classified in two steps by Saier *et al.*, 2001 [47]: In the first step, the proteins were classified according to the transport mechanism: Channels, electro-chemical potential driven transporters, primary active transporters and group translocators. The transport-classes were further divided into subclasses according to class-specific criteria.

1.2.1   Multi drug resistance proteins

In the 1980s and 1990s, a dramatic increase in infectious diseases was observed. A major cause of the resurgent of these diseases are drug-resistant pathogenic bacteria, which were kept under control for more than half a century by antibiotics [47]. In recent years, the growing resistance of bacteria to drugs has become an enormous medical problem. The following examples illustrate this fact:

- Multidrug resistant *Mycobacterium tuberculosis* strains are ubiquitous [56]

- *Staphylococcus epdidermis* and *Enterecoccus faecium* have become resistant to most avaible antibiotics [47]

---

[1]URL: http://www.biophys.mpg.de/michel/public/memprotstruct.html
[2]URL: http://scop.mrc-lmb.cam.ac.uk/scop/
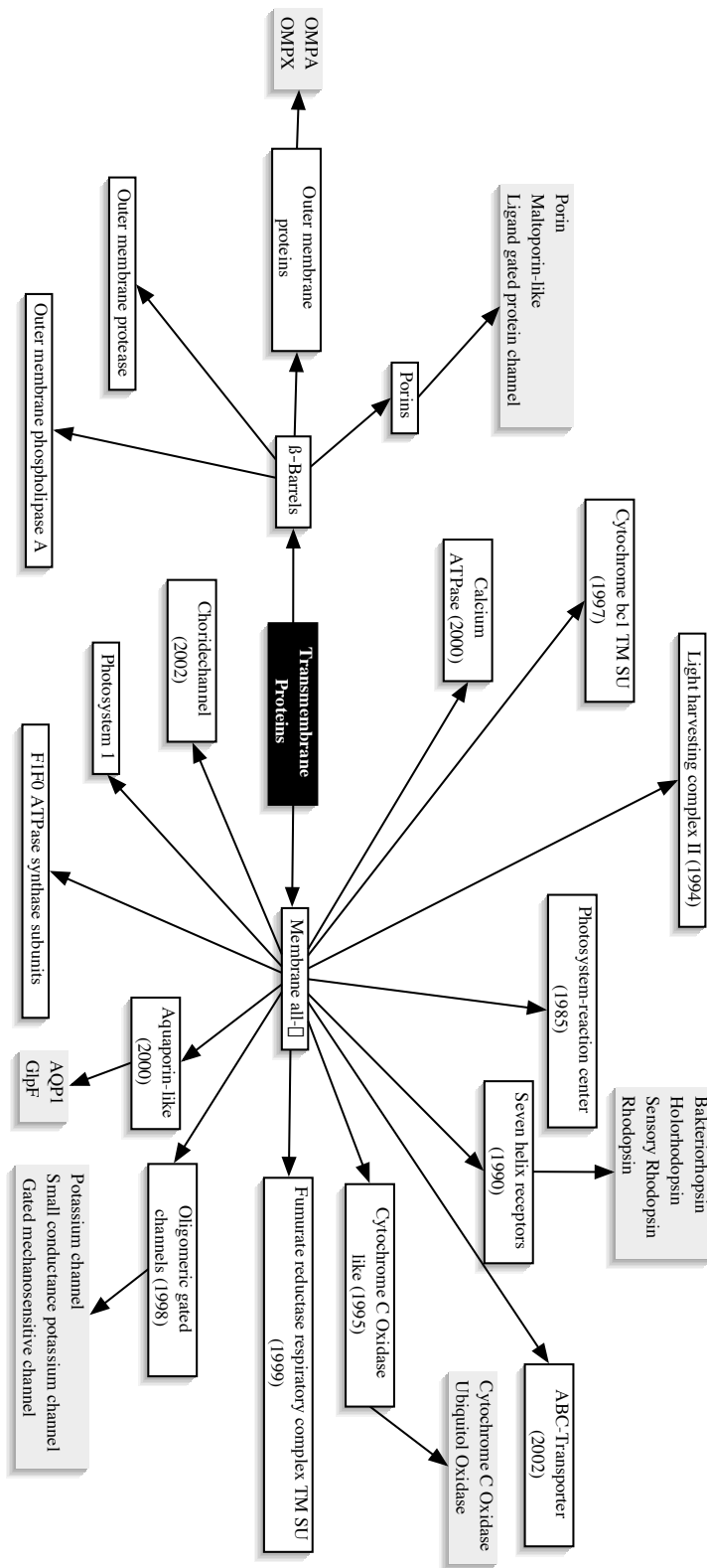
Figure 1.1: Overview over transmembrane proteins for which atomic structure is known. Toxins, non-transmembrane proteins and components of the immune-system are not included. The classification was done with the help of the SCOP [52], a database based on structural similarities of known atomic structures (as of Mai, 22nd 2002). TM: trans-Membrane, SU: SubUnit.
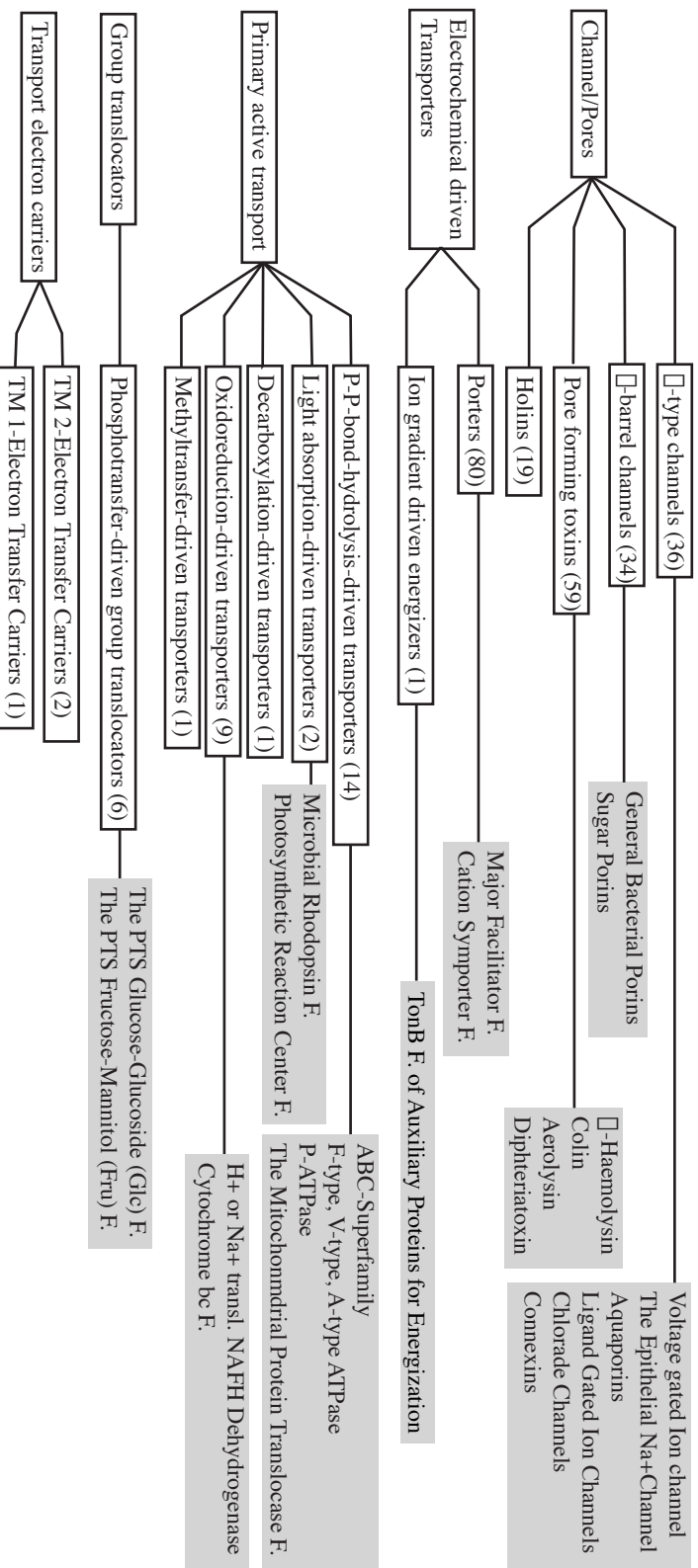
Figure 1.2: Classification of transporters and channels according to the *database for channels and transporters* [47]. The classification was made according to the transport-mechanism (most left white boxes). The different classes are divided into subclasses according to the energy source used to drive transport for primary active transporters, their general architecture (channels) or their function. For the subclasses, the number of known protein families is given in brackets. Examples of the protein families are written in gray boxes.

Table 1.1: Protein families containing MDR-pumps[a].

Energy	Distribution	Example
Major facilitator SF.		
Secondary	Ubiquitous	QacA of *Staphylococus aureus*
ABC-Transporter		
Primary	Ubiquitous	MDR1 of *Homo sapiens*
Resistance/nodulation/division SF.		
Secondary	Ubiquitous	HAE1 of Gram$^-$ bacteria
Drug/metabolite transport SF.		
Secondary	Ubiquitous	PUP1 of *Aridodopsis thaliana*
Multi antimicrobial extrusion F.		
Secondary	Ubiquitous	EmrE of *Escherichia coli*
Multidrug endosomal transporter		
Secondary	Eucaryotic	Mouse transporter protein

[a]after Paulsen *et al.*, 2001 [47]

- *Escherichia coli* is once again the major pathogen leading to infant mortality [47]

Drug resistance of a pathogen can be achieved in several ways [86, 47]:

- Using enzymes making the drug inactive.

- Eliminating entry ports for hydrophilic drugs, such as outer membrane porins in Gram-negative bacteria

- Alternating of the drug target

- Expelling the drug out of the cell by activated pump mechanisms. Since these pumps often have amazingly broad substrate specifity, they are commonly referred to as *Multidrug Resistance* pumps or simple MDR's.

The development of drug-resistance by cancer cells is also a major problem: During the first treatment by chemotherapeutic agents the expression of multidrug-resistance genes is induced, making the medicament ineffective in subsequent pulses.

Saier and Paulsen [47] have examined the phylogenetic origins of the MDR phenomena based on their database for channels and transporters (see also figure 1.2). They found that only 11 protein families out of 250 contain exporters, and only 6 families contain MDR proteins. Table 1.1 summarizes the phylogeny of known MDR-pumps. As more and more genomes are sequenced, more and more putative MDR pumps are being found.

About 90% of all research on MDR's has been done on members of the *Major Facilitator Family* and the *ATP-Binding Cassette Family* (ABC-Transporters) [33]. Besides these two classes, only the *The Small Multidrug Resistance Family* is somewhat better explored, including the structural information of a 7Å projection-map of EmrE 2D-crystals, a multidrug transporter from *Escherichia coli* [78].

Multidrug resistance proteins in the ABC-transporter family

The ABC-Transporters have some very prominent multidrug resistance pumps expelling drugs at the cost of ATP hydrolysis. Examples are:

MDR1 The *mammalian drug resistance protein* is a well known drug-resistance protein responsible for resistance to the chemotherapeutic agents used to treat many cancers.

MRP1...MRP5 The *multidrug resistance-associated protein.* Until now, 6 isoforms are known. These have been detected in many different drug resistant human cell lines, associated with a multidrug resistance phenotype.

LmrA a MDR1 homologue in *Lactococcus lactis.* Can complement MDR1 in fibroblast cell cultures and shows similar pharmacologic properties as MDR1.

pfMdr1 from *Plasmodium falciparum* responsible for the disease Malaria tropica. It's expression makes the Malaria parasites resistant to chloroquine.

The ABC-Transporters share a common domain organisation: Two hydrophobic transmembrane spanning domains (each containing six transmembrane α-helices in exporters, generally 5 helices for importers) and two hydrophilic and conserved nucleotide binding domains (NBD). The domains can be organized in one single peptide chain (as in the mammalian multidrug resistance transporter (MDR)), or the protein can be split up into several polypeptide-chains as in many prokaryotic systems. Furthermore, uptake systems often contain an additional protoplasmic domain or an associated soluble protein for substrate recognition. Further, some exporters found in *gram negative* bacteria need additional accessory proteins to ensure transport through the outer membrane (protein exporters). These includes members of the membrane fusion proteins (MFP) and a second helper protein in the outer membrane [4]. Generally, ABC-transporters show a highly flexible domain organization. This is one of the reasons for the high diversity in the ABC-protein superfamily, which is also reflected in the high substrate range of these transporters, including ions, phospholipids, steroids, polysaccharides, amino acids, peptides, and for many MDR1 homologue's, drugs [68].

Transport across the membrane is driven by the hydrolysis of ATP. ATP-binding and hydrolysis is performed by the NB-domain, the most conserved feature of ABC-transporters. This domain contains the Walker A and B motifs (the nucleotide binding-site) along with the ABC signature or C motif, for which several functions have been proposed, including the communication between the NB-domain und the transmembrane part of the protein [59]. In contrast to P-ATPases, the protein is not phosphorylated during the transport cycle.

LmrA: A multidrug resistance protein from *Lactococcus lactis*

The best characterized multidrug resistance pump so far is the MDR1 homologue LmrA from *Lactococcus lactis* [87, 83, 85, 86, 84]. However, the domain organization is significantly different: MDR1 is encoded in one single polypeptide chain, whereas LmrA is split into two halves, thus working presumably
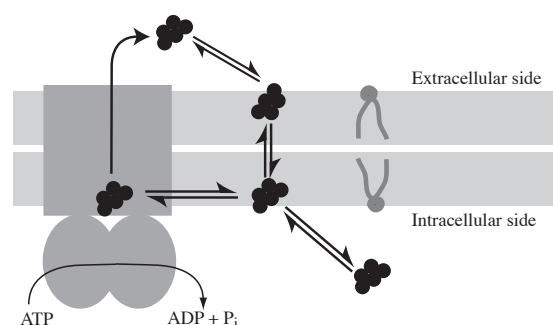
Figure 1.3: Proposed model of substrate export by ABC-MDR's. The drug is taken from the inner membrane leaflet und subsequently exported out of the cell [60]. The energy is provided by ATP-hydrolysis. Since the rate limiting step is the un-catalyzed flip-flop of the drug from the outer leaflet to the inner leaflet and the release of the drug from the membrane to the cytosol is not energetically favorable, this is a very efficient strategy.

as a homodimer. On the protein level, the similarity between the amino-acid sequences of LmrA und MDR1 is remarkable [87]: The membrane domains of LmrA and the N- and C-terminal halves of MDR1 are 23% and 27% identical, respectively, whereas the ABC domains of the proteins are 48% and 43% identical.

Functionally, LmrA can complement MDR1: Transfected human fibroblast cells have been shown to translate and target the LmrA protein to the cell membrane. These transfected cells showed the typical multidrug resistant phenotype with similar pharmacological properties. The experiments demonstrate that the bacterial LmrA and human P-glycoproteins are functionally interchangeable and that this type of multidrug efflux pump is evolutionary conserved from bacteria to human [83].

The general model for the function of ABC-MDR's is depicted in figure 1.3. In this model, the ABC-Transporter takes up the drug specifically from the inner membrane leaflet and pumps it out of the cell [60].

Based on equilibrium binding experiments, photoaffinity labeling and drug transport assays, it was speculated that LmrA works as a homodimer in an alternating, two cylinder mechanism [84]: LmrA possesses two binding sites, a transport competent binding site on the inner side of the membrane (high affinity site) and a drug release site (low affinity site) outside of the cell. The inter-conversion of these two sites is driven by ATP hydrolysis going through a transition intermediate. The two monomers are dependent on one other and work with a phase shift of half a transport cycle (see figure 1.4).

There are no direct structural data for LmrA itself, but the structure of a close homologue, the lipid flipase MsbA from *Escherichia coli* has been solved to 4.5Å resolution by x-ray crystallography [10]. This protein-dimer has a split two-leg structure, with NBD's separated by 50Å and non-parallel membrane domains that together form an open groove in the postulated membrane region (see figure 1.4). In contrast, fluorescent energy transfer measurements of vanadate-ADP-Mg^{++} trapped MDR CH^{R}B30 from Chinese hamster have indicated that the two NBD-domains are close together [59]. If these MDR1 homologue function
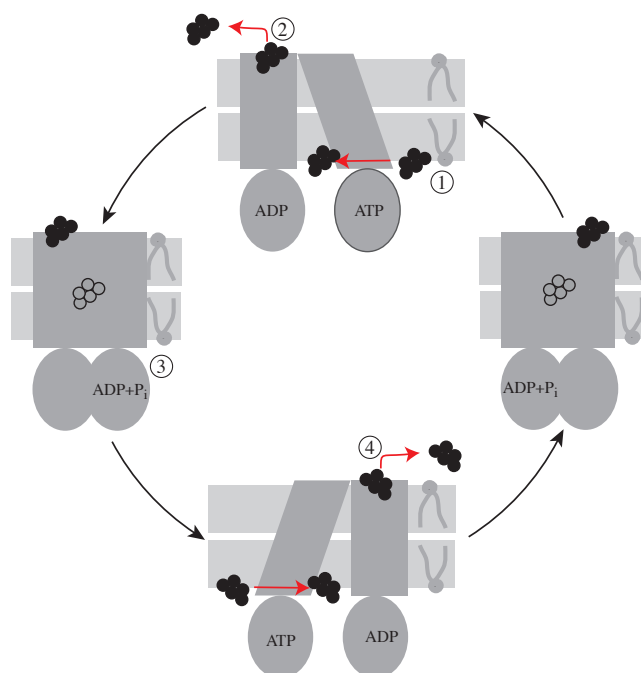
Figure 1.4: Speculative model for the transport mechanism of LmrA. The following working models were combined: The alternating two-site (two cylinder) transport model of LmrA after van Veen *et al.*, 2000 [84], the closing chamber model derived from the 4.5Å density map of MsbA, a flipase from *Escherichia coli.* (Chang *et al.*, 2001 [10]) and the closing of the structure found by Qu *et al.*, 2001 [59] (hamster MDR). The cytosolic ATP binding domain represented by an ellipse and the transmembrane domain by a rectangle. The drug substrate is represented by 5 circles. These are filled (black), if the corresponding binding site is accessible and empty, if the binding site is inaccessible for drugs. The ATP loaded LmrA monomer is associated with a high-affinity binding site on the inner surface of the cell-membrane (1). The ADP loaded protein is associated with the low-affinity (release) binding site (2). The ADP+P_i loaded LmrA monomer is not accessible for drug binding (3), so this state is thought to represent an occluded binding site during the pump cycle (a transient structure). In this state it was also found, that the two NBD's are close together. Corresponding to the model for MsbA, the drug would be in a unfavorable environment forced to do a kind of flip-flop across the membrane and be expelled from the protein (4). Note that the two monomers work in a dependent manner with an phase shift of half a transport cycle (180°).

by a general mechanism, this is an indication of large structural changes and domain movements during the pump cycle. This would explain the extremely long transmembrane α-helices of LmrA, since at least some of the helices would have to change their relative tilt to the membrane to high angles. A raw model for the transport mechanism is described in figure 1.4.

1.2.2 The Aquaporin protein-family

Water is the dominant chemical compound in living systems. It is not only the solvent for all the biochemical reactions, but also the driving force that holds the living cells together by the hydrophobic effect.

Therefore, osmoregulation in bacteria, plant, and animal cells requires the presence of membrane channels, specific for water and small non-ionic solutes to carefully control the water content. Despite the extreme importance of such control systems, water channels were discovered very late: Quite early it was noticed that biological membranes from different tissues had different water permeabilities. However, in general it was believed, that water could cross membranes through lipid fluctuations and unspecifically permeate through membrane proteins. The breakthrough was the discovery of the first water specific pore in the early 90's: Expression of aquaporin-1 (AQP1, the water channel of human erythrocytes) in *Xenopus* oocytes demonstrated the water permeation capacity [58] of this protein. This discovery initiated many functional and structural studies of the rapidly growing aquaporin superfamily.

The sequences of the known members od the aquaporin super-family share an internal repeat. Each half is predicted to comprise three transmembrane regions according to hydropathy profiling [25, 57]. Two NPA-motifs represent the prominent finger-print of the highly conserved loops B and E. These two loops are predicted to fold back into the core of the protein from the extra- and intra-cellular side to form a channel resembling an hourglass [36].

Phylogenetic analysis has revealed the existence of two clusters of subfamilies, the aquaporins (AQPs) and glycerol facilitators (GLPs) [31, 54], see figure 1.5. Five key amino acids distinguish between AQPs and GLPs [22]. Two further amino acids (F24 and L149) were hypothesized to play a functional role [30], which was confirmed by the 3.8Å structure of AQP1 [51]. In the majority of GLPs (79%), these residues are both Leu, whereas they are mostly Phe and Leu in the AQPs. Another difference between AQPs and GLPs concerns long inserts in the extracellular loops C and E.

Whereas all AQPs so far characterized are tetramers [19], it was speculated that the GLPs act as monomers [9, 38, 39]. However, all the higher resolution structures so far show a tetrameric architecture for GlpF, a member of the GLP subcluster. It was postulated that the inner α-helix nearest to the four-fold axis of the GlpF-tetramer are not long enough to span the membrane. Taken together, it seems that the tetramer is the stable physiological quaternary structure of GlpF [23].

The internal sequence repeat of the aquaporins is reflected in a pseudo two-fold symmetry within the monomer-structure, as well as in the non-directional diffusion of solutes through the pore. This pseudo two-fold symmetry (the inner and outer part of the monomer are very similar) complicated the sidedness assignment of the first high resolution density maps from the electron-microscopic analysis of 2D-crystals. Later, atomic force microscopy before and after pro-
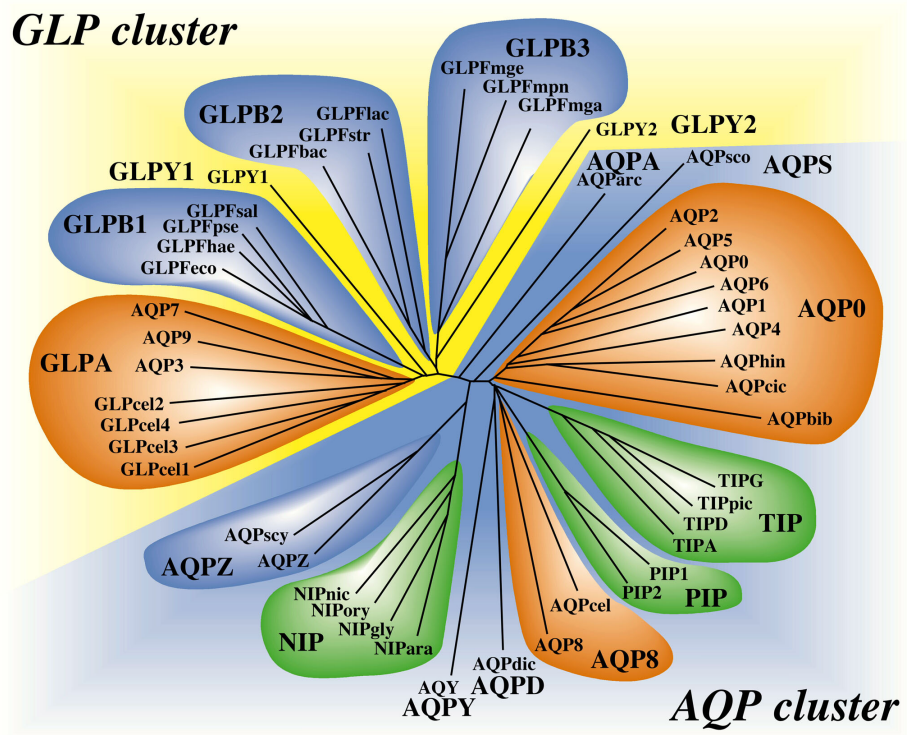
Figure 1.5: The aquaporin family (formerly known as MIP family) can be divided into two subgroups the aquaporins and the glyceroporins.

teolytic cleavage of N- and/or C-termini allowed the sidedness of AqpZ (the bacterial water channel) and MIP (the channel of animal lens fiber cells) to be determined [20, 70]. The sidedness of AQP1 was subsequently derived by comparing surface topography and projection maps of AqpZ with those of AQP1 [71], and by computationally fitting of helical segments to the 4.5Å map [16], an assignment corroborated by the 3.8Å electron-microscopy structure of AQP1 [51].

The electron-microscopic structures of AQP1 also confirmed the early predictions of the hourglass-model [11, 42, 91, 51]. The maps show the tetrameric organization of monomers each comprising a right-handed bundle of six highly tilted transmembrane helices that surround loops B and E, which fold back to meet in the center of the membrane. At 4.5Å resolution, parts of loop B and E were found to form two additional short helices within this central structure [48]. The first atomic model of AQP1 reveals one site of water selectivity to be close to the center of the monomer [51], as predicted by the hourglass-model. This eyelet is determined by four conserved hydrophobic residues in helix 1 (F24), helix 2 (I60), helix 5 (V176) and helix 4 (L149), two hydrophobic residues in loop B (L75) and loop E (I191) and the two conserved Asp (N76 and N192) of the NPA motifs (compare with figure 3.10e).

In the mean time atomic structures have become available for both, AQP1 and GlpF. This allows an interesting exploration of the physical mechanism of the water traveling through the channel. Further refinement of the atomic structure of AQP1 [14] and molecular-dynamics [15] answered many questions concerning the AQPs, such as: How does the aquaporin-protein achieve such high diffusion rates of H_2O? How are protons prevented from traversing the channel and why is the the rate of water permeation through the GlpF channel much lower even if this channel is wider than the one of AQP1? The findings of de Groot and Grubmüller are schematically presented in figure 1.6.

These simulations confirm the early biochemical finding, that the water does not travel through the central gap along the four-fold axis of the tetramer but through the central pore present in each monomer. In general, the GlpF-pore is wider than the AQP1-pore. But both channels are narrow enough only to let pass a single file of molecules. Each monomer seems to work independent of each other. This model with two restriction sites was also found by Jap *et al.* with the latest atomic model of AQP1 at 2.2Å (Jap *et al.*, 2002 [77]). Note that the dipoles of the water molecules have to rotate by 180° as they traverse the channel. With this mechanism there is no hydrogen-bond file through the channel possible and protons are hindered from traversing the channel.

The atomic structure of GlpF [23] revealed a greasy slide similar to the maltoporin [72], which orients the glycerol molecule and works as a selectivity filter. In AQP1 the hydrophobic slide is broken by hydrophilic amino-acids. Molecular dynamic simulations [35] indicate that there is a competition of water and glycerol for the hydrogen bonds. The NPA region was found to be most populated with glycerol molecule, the non-helical part of the two half-membrane-spanning segments are exposing their carbonyl-groups towards the channel interior to provide a "curve-linear conduction pathway" along this the glycerol molecules seem to move "step by step" breaking and forming hydrogen-bonds.
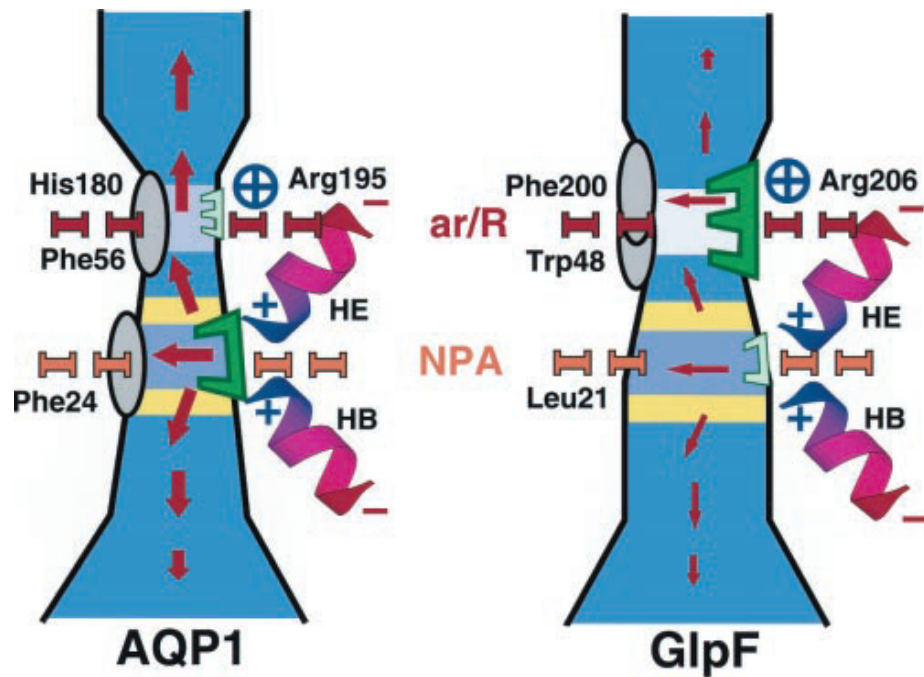
Figure 1.6: Schematic model of the permeation mechanism for AQP1 and GlpF. Directly taken from de Groot and Grubmüller, 2001 [15]. In this model, two restriction sites are responsible for selectivity: (1.) The ar/R region, this is the narrowest part of the channel. In the AQP1 structure this site is even more restricted than in GlpF. In this region, the hydrogen-bonds of the water are weakened (light-blue) than the bulk water (dark blue) and together with the two Arginines (Arg195, Arg206) a proton barrier is build up. (2.) The second filter is around the NPA-motif. This is mainly a size-exclusion selectivity filter. In both proteins, two rings of hydrophobic residues build up the highest energy-barrier, which is thus rate-limiting. Note that in both proteins the dipole-moment of the water has to rotate during the passage making the formation of a line of hydrogen-bonds through the channel impossible.
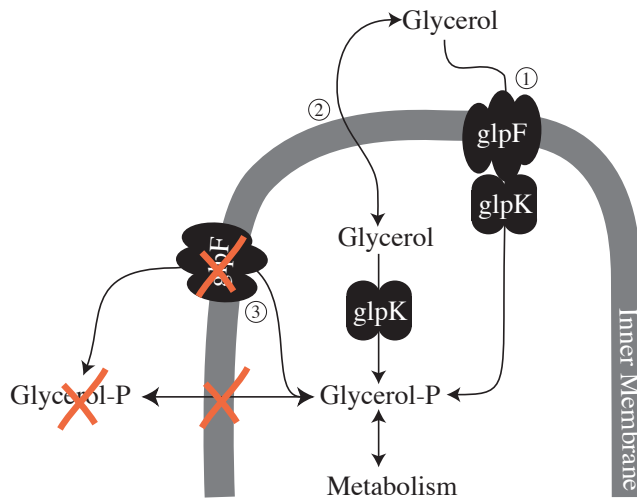
Figure 1.7: The biological function of GlpF as proposed in [89]. The GlpF tetramer acts as a glycerol channel facilitating its diffusion across the membrane (1). However, glycerol can also diffuse across biological membranes without channels with kinetics similar to channel containing cells (2), but the metabolization of the glycerol is much slower in these GlpF mutants. Therefore a direct interaction between GlpF and the tetrameric glycerol kinase GlpK is proposed (1). Note that phosphorylated glycerol can neither traverse the membrane nor the glycerol channel (3).

The glycerol channel of *Escherichia coli* (GlpF)

The glycerol uptake facilitator of *Escherichia coli* (GlpF; [5]) is one of the few known diffusion facilitators in the inner membrane of this bacterium and belongs to the GLP subcluster of the aquaporin super-family. Glycerol diffuses into the cell through GlpF and is phosphorylated by the glycerol kinase (GlpK), which prevents back-diffusion (see figure 1.7). In this way, glycerol is withdrawn from the distribution equilibrium, so that the GlpF-GlpK complex works a as primary active transport-system. Besides glycerol transport, the diffusion of polyols and urea derivatives through GlpF has been reported [44], but none of these substrates are transported in a phosphorylated state. Water permeation through the channel is 10-fold lower than that of glycerol [6]. On the other hand, the glycerol channel is strictly selective for non-ionic compounds, thus preventing the dissipation of the membrane potential. Kinetic studies of the *in vivo* uptake of glycerol into the facilitator-minus strain are significantly different from the kinetics of glycerol uptake in the wild type. Since the kinetics of the diffusion through the plasma-membrane of *Escherichia coli* cells is not the rate limiting step in the glycerol metabolization and unphosphorylated glycerol is not observed in the wild type cell. Voegele and colleagues [89] conclude that kinetics of glycerol phosphorylation are different, depending on the presence or absence of the facilitator protein. They suggest that there is an interaction between the glycerol facilitator protein and glycerol kinase that stimulates kinase activity, analogous to the hexokinase- and glycerol kinase-porin interactions in mitochondria.

1.3 2D-crystallography and electron microscopy of membrane proteins

The exploration of the structure of membrane proteins has been and still is a major challenge for biologist and biophysicist. Major breakthroughs have been reported in the last years, such as the atomic structures of F_1F_0 ATPase [76], the P-ATPase [79] or the aquaporins [23, 51]. However, leading structures for some very important protein-families are still missing, e. g. for the *Major Facilitator Proteinsuperfamily*. Medical and pharmacologically important membrane-proteins should be analyzed more routinely.

A powerful method to collect structural information of such proteins is the two dimensional (2D) crystallization with subsequent electron-microscopical structure-analysis. This crystallographic approach delivers high-resolution 3D-information of membrane-proteins under physiological conditions [29, 28, 27, 81]. Furthermore, 2D-crystals are ideal substrates for the atomic force microscope (AFM), which gives real-time information of the surface-topography in buffer solution. When used together, electron microscopy and AFM complement each other in a powerful way: Whereas the AFM is not able to record 3D-volume-information it delivers information about the flexible part of membrane-proteins, which are not detected by the crystallographic approach of electron microscopy.

1.3.1 Crystallization of membrane proteins

The structural analysis of membrane proteins is a long (and sometimes painful) story. In a time where several thousands of soluble proteins are solved, only few membrane proteins are known at atomic level (stand 27.5.2002, see [46][3]): From the group of poly-topic membrane-proteins (plasma-membrane from bacteria, mitochondria and eucaryotic membrane-proteins), 31 proteins are solved among them 15 unrelated proteins. From the outer membrane of gram-negative bacteria 20 different proteins are solved and for the group of the non-membrane-spanning (mono-topic) proteins 4 proteins are solved (2 unrelated).

Due to the amphiphilic nature of membrane-proteins, these have to be stabilized by detergents during purification and 3D-crystallization. Most membrane-proteins are much less stable in the solubilized form than when embedded in membranes. For this reason, 2D-crystallization is a convenient method: With this technique, the protein is solubilized and purified in the conventional way, but is subsequently reconstituted into lipid-membranes (see figure 1.8) allowing the exposure of the protein to detergent to be reduced to a matter of hours.

The critical moment in the life of a membrane-protein during the crystallization-process is the time-point at which the lipid-molecules have to take over the protein-stabilizing function in a lipid-detergent-protein mix. The problem is depicted in figure 1.9. The absorption-desorption kinetic of the detergent-molecule is not necessarily the same for the protein and the mixed-micelles or the lipid-molecules, respectively. Thus the critical transition-moment for the protein is not necessarily the critical micelle concentration (CMC). The chance for the protein to catch the right lipids early enough increases if the crystallization cocktail can be incubated before the detergent is removed (personal communication Thomas Walz and Lorenz Hasler). For many proteins it has been reported that

---

[3]URL: http://www.biophys.mpg.de/michel/public/memprotstruct.html
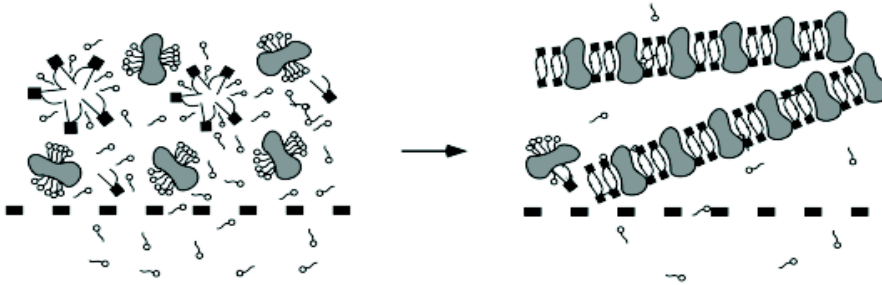
Figure 1.8: Principle of the 2D-crystallization of membrane-proteins. After purification, the solubilized protein is mixed with solubilized lipids (mixed micelles) and the detergent is subsequently removed, in this example by dialysis against a buffer without detergent. If the conditions are right, the protein is reconstituted into the membrane in a crystalline arrangement.
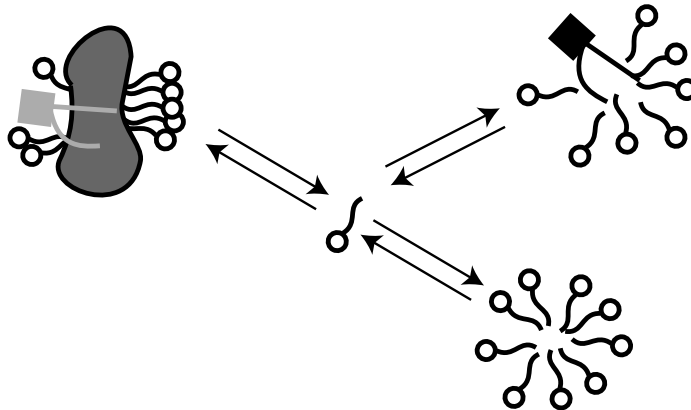
Figure 1.9: Simplified interaction-pattern of the detergent-molecules with the protein and the lipid. The adsorption and desorption kinetics of the detergent molecules from lipid-containing micelles, detergent micelles and the protein are not necessary the same. Note, the protein brings its own lipids into the crystallization system (grey).

associated lipids are crucial for their stability. Harsh purification-methods (such as Ion-exchange columns) can harm the protein by stripping stabilizing lipids off. The lipids associated with the protein are a crucial factor for crystallization and should be controlled during protein-purification.

Intuitively, two different crystallization-mechanisms can be proposed [62]:

1. Direct crystallization: The protein falls together into 2D-dimensional crystals below a critical detergent-concentration. Proteins are self-arranging in a plane and the detergent-molecules are subsequently replaced by lipid-molecules.

2. Crystallization in a two-step process: The protein is first incorporated in a lipid-bilayer and subsequently orders itself into 2D-crystals. For this model, a direct and indirect insertion-pathways have been described [62]:

   (a) The detergent is slowly removed and the protein-lipid-detergent-micelle becomes unstable. The proteins are sticking together to avoid water-contact. As a result, vesicles with incorporated protein and detergent-molecule are build.

   (b) First, detergent-soaked vesicles are formed and the protein is still stabilized by lipid-detergent micelles. Subsequently, at lower detergent concentration, the protein inserts into the previously formed membranes.

Thus, for some proteins it can be favorable to add lipid-vesicles instead of mixed micelles to the 2D-crystallization cocktail. All the described models stress the importance of trying a variety of crystallization methods, such as detergent-removal by dialysis [34] or by bio-beads [64, 63] or crystallization on functionalized surfaces (monolayer-technique, see Levy *et al.*, 1999 [41]).

2D-crystallization is generally a two step process: First, initial crystallization conditions have to be found. A potential systematic approach is described in chapter 2 in which first a screen for conditions stabilizing the protein in the solubilized form is performed, followed by a screen for lipids in which the protein can be reconstituted. In a second step, the initial crystallization conditions have to be refined. Of course, some of the parameters will already have been tested during the initial screen. The following factors can be modified:

The membrane: This can be modified using different lipid-compositions and additions, such as cholesterol or organic solvents such as DMSO or iso-propanol. Of course, the lipid to protein ratio (LPR) is a major factor.

The protein: By varying the purification conditions, lipids can be stripped off by ion-exchange columns such as reported for EmrE leading to better crystal quality [78] or the protein can be brought into a specific biochemical state by the use of inhibitors and/or phosphorylation. A major parameter is the pH of the used buffer, which is mainly believed to affect the protein.

The buffer: The bulk-phase can be changed in various ways. This also affects the properties of the membrane and the protein. The hydrophobic effect can be weakened by the addition of chaotropic substances such as urea, or can be pronounced by high salt concentration which also shields electrostatic interactions between the protein. Addition of double-charged

cations (such as Mg^{++}) are reported to have a major influence on protein-reconstitution and crystallization [34].

1.3.2 Electron-microscopy of 2D-crystals and image processing

Two major problems in the electron-crystallography have to be overcome to reach high-resolution 3D-structures: First, the strong interaction of electrons with matter leads to rapid sample destruction and, second, the crystals have to be prepared in a way, that the high-resolution structures are preserved and the sample is suitable for electron microscopy (high vacuum, thin layer). Interestingly, the same answer was found for both problems by one technique: Cryo electron microscopy (see Dubochet *et al.*, 1988 [18]). With this technique, the crystal is absorbed onto a thin carbon-layer, surplus material is blotted away and the sample is frozen very fast in liquid ethane. By this preparation-method, the crystals are embedded in a thin layer of amorphous ice, which can easily be penetrated by the electron beam and the fine-structures are conserved to high-resolution. Due to the low temperature of the sample (at least liquid nitrogen temperature of $-180°C$), the sample withstands the electron-beam much better, allowing images to be recorded at higher electron doses (approx. $500e^-/nm^2$). If the sample is cooled down to liquid helium temperature ($4.2K$), electron doses of $2000e^-/nm^2$ are possible without intolerable sample damage [24].

However, images recorded by this technique have an extremely low signal to noise ratio (SNR) and no structures are recognizable without image-processing. The periodic arrangement of the protein in 2D-crystals leads to a periodic signal in the recorded image. The Fourier-transformation of such images shows discrete spots, in which the structural information is concentrated. This allows noise-reduction by a Fourier-peak-filtering. After this simple image-processing step, some structural feature can already be recognized. In contrast to the x-ray crystallography, not only the amplitude of the diffraction pattern can be measured but also the corresponding phases. This allows a correction of lattice distortion of the 2D-crystal. For this, a crosscorrelation of a small reference area of the image (or a synthetic reference if a structure is already known) is calculated with the original image and the real position of the unit-cells is detected. This information can be compared to the theoretical lattice vectors and a field of shift-vectors describing the crystal-distortions can be calculated. This information is used to interpolate the original image for unbending the crystal-structure. By this procedure in real-space, the diffraction-spots are focused. This combination of crystallographic methods in Fourier-space and image-processing methods in real-space allows to improve the resolution by a factor of two [27, 81, 28, 29].

The amplitude information of the images can also be directly recorded by electron diffraction. Since the back-transformation of the back-focal information of electron-microscopic lenses introduces severe image artefactss, this information is of great value for the correction of these. Further-more, since there is no interference between the high-diffraction and low-diffraction information, incoherence in the electron-beam does not effect the observed resolution, thus a direct evaluation of crystal-information to high resolution analogue to the x-ray technique is possible (e. g. crystal quality, see figure 3.3 panel B p. 52).

To get a three-dimensional structure, the 2D-crystal has to be tilted in the electron-microscope so that "side-views" of the protein are recorded (see figure

3.6 p. 59) . These images are noise-filtered and unbent in the same way as the untilted ones. In a final step, all images (tilted and untilted) are merged together by a so called back-projection. The final result is a 3D mass density-map of the unit cell (an example is shown in figure 3.8 p. 61)

Chapter 2

Attempts to Crystallize an ABC-Transporter

Christine Widmer and Thomas Braun

2.1 Introduction

This chapter is a progress report on our attempts to crystallize the multidrug transporter LmrA from *Lactococcus lactis*. The primary goal is not only to give hard fact results but also to outline and demonstrate some possible strategies as a general approach to 2D-crystallization of highly flexible membrane protein such as ABC-transporters.

The general strategy for LmrA-crystallization is outlined in figure 2.1. In the first step, the purification was optimized for our needs. This was accompanied by a first series of crystallization experiments, since the outcome of the LmrA purification seemed to be of good quality (direct crystallization assays in figure 2.1). In these initial experiments, major problems were observed: LmrA was regularly degraded by proteases. This could be overcome by adjusting of purification protocols (section 2.4.1) and the use of strong Ser-protease inhibitors. Furthermore, it became obvious that the reconstitution of LmrA would be difficult. Therefore new experiments were planned:

1. A pre-screen with the goal to search for suitable detergents and, subsequently, a lipid screen to search for detergent-lipid combinations promoting the reconstitution of LmrA was performed.
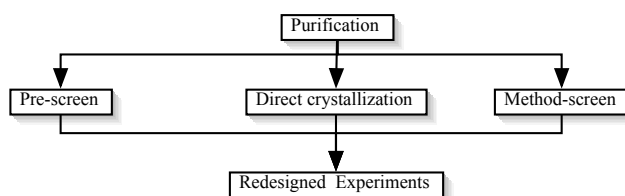
Figure 2.1: Strategy used for the crystallization attempts for LmrA (see text).

2. Different reconstitution methods were tested under conditions known to stabilize LmrA.

Since the direct crystallization approach failed, only a very short summary of some observations is listed in section 2.2.3 (p. 33).

2.2   Results

2.2.1   Purification of LmrA

To facilitate protein purification, LmrA was tagged with 6 histidines at the N-terminus. Over-expression was done in *Lactococcus lactis* using a Nis A induced promoter on a pNHIlmrA plasmid. The protein-expression was highly efficient; around 30% of the total membrane-protein was LmrA (Margalles *et al.*, 1999 [43]).

The main purification step was an affinity-binding on a NiNTA-column based on the His-tag of LmrA. But due to the already mentioned proteolytic digestion of the LmrA protein during the subsequent crystallization experiments, other purification-steps were introduced to minimize this effect:

Membrane pre-wash :   The LmrA-containing membrane-vesicles were washed before the purification to strip off peripheral proteins (e. g. proteases)

Anion-exchange chromatography: An Anion-exchange was performed directly after solubilization as a fast pre-purification. This was done with the intention to obtain a more homogeneous quality of the starting material, since differences in the quality of the obtained membrane batches were observed.

Note that the purification protocols varied for different experiments, only the NiNTA-affinity purification was part of all procedures.

Membrane pre-washes   Pre-washes of LmrA containing *Lactococcus lactis*-membranes were either done in wash-buffer without any special additives (50 mM KP$_i$, 10% glycerol, 100 mM NaCl) or in buffer containing additionally 1% cholate. For this, the membranes were homogenized in a glass-potter, centrifuged to harvest the membrane vesicles and resuspended in a phosphate-buffer (without cholate). The cholate-wash was shown to not affect the transport activity of LmrA containing *Lactococcus lactis*-membranes (personal communication Gerrit Poelarends). However, in some membrane batches a significant loss of LmrA was observed during the cholate washing step (data not shown), so that the cholate was omitted for the experiments presented in this thesis.

Purification over NiNTA-column   In the presented experiment, LmrA containing membrane-vesicles (without pre-wash) were solubilized with 4% DM by incubating for $30min$ at 4°C. The solubilized protein was centrifuged at $100'000 \times g$ and the supernatant was incubated with a minimal volume NiNTA-beads (1 ml beads for 8 mg LmrA) for 3 h. Finally, the NiNTA-beads were poured into a Promega-column, which was subsequently washed with two different wash-buffers, at pH 8.0 (1 mM histidine) and pH 7.0 (2 mM histidine),
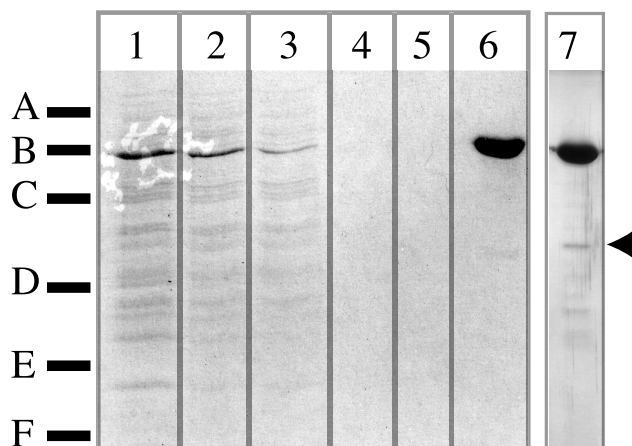
Figure 2.2: Purification of LmrA with a NiNTA-column (in the detergent DM). To analyze the quality of the purification, SDS-polyacryamide gels were run and stained with Coomassieblue (lanes 1-6) and silver-staining (lane 7) Lane 1: Total membranes; 2: Solubilized membranes; 3: LmrA not bound to NiNTA-matrix (flow through); 4: wash 1; 5: wash 2; 6: eluted protein (ca. $2, 2\ \mu g$), 7: eluted protein (ca. $0.3\ \mu g$). Triangle: 35 kDa contamination found in most purifications. A to F: Molecular weight standards in kDa (A: 97,4; B: 66,2; C: 42.7; D: 31; E: 21.5; F: 16.7).

respectively. The LmrA protein was finally eluted with an elution buffer containing 200 mM Histidine (pH 7.0). As quality control, coomassie-blue stained SDS-PAGE and silver-stain SDS-PAGE was performed. The result of a typical purification is shown in figure 2.2. Note that a minimal amount of NiNTA-beads was used, which led to incomplete binding of LmrA (lane 3 figure 2.2). The measured molecular weight for LmrA of ca. 60 kDa is in good accordance with the theoretical mass of 65 kDa. The protein concentration of LmrA was estimated by measuring the absorption at 280 nm and using the theoretical extinction coefficient of $\epsilon = 45090$. The measured protein concentrations were in good agreement with the values obtained by biochemical methods such as bradford (Bio-rad).

Furthermore, the solubilized and purified protein was prepared by the negative-stain technique and analyzed as single particles in the electron microscope. The electron-micrographs showed a rather homogenous size-distribution of the particles with a diameter of ca. 10 nm (figure 2.3).

Anion-exchange To have a more consistent purification of LmrA, a fast pre-purification with an anion-exchange column was performed on a FPLC equipement: The membranes were solubilized at pH 8.0 with 2% DDM, centrifuged to remove unsolubilized material and directly loaded on a Q-Sepharose column equilibrated with a low-salt buffer (phosphate buffer at pH 8.0 without NaCl). Subsequently, the protein was eluted with an NaCl-gradient (see figure 2.4): The LmrA protein started to elute at a NaCl-concentration of ca.
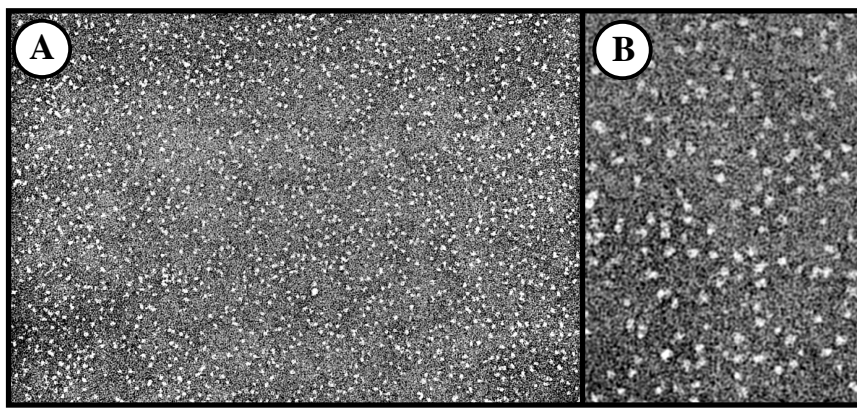
Figure 2.3: Negative stain electron microscopy of LmrA solubilized in DM. *Panel A*: Large overview showing the homogeneous size-distribution of LmrA. The scale bar corresponds to 100 *nm*. *Panel B*: View at higher magnification. Scale bar: 50 *nm*

250 *mM*. Note that the elution peak of LmrA from the anion-exchange column is relatively broad due to the large volume (8 *ml*) of the solubilized membrane loaded on the column.

The apparent removal of proteases by this method allowed to bind the LmrA-protein over night on the NiNTA-column without degradation of LmrA (see figure 2.4) which was not possible without this pre-purification-step.

Since ion-exchange columns are known to destabilize proteins by stripping off structurally important lipids, a single-particle analysis in the electron microscope of solubilized LmrA prepared with an anion-exchange and NiNTA-column) was done: Even after one week storage at $4°C$ in 0.5% DDM, the negative stain preparations revealed the same particle-shapes (data not shown) as LmrA freshly prepared in DM (figure 2.3).

Test for lipids associated with the protein   To ensure protein-stability and for 2D-crystallization experiments it is not only important to have pure protein, but also to have a control over the lipids associated with it. For this, an additional quality-control measurement was introduced: The variability in phospholipids and neutral-lipids associated with LmrA during purification was monitored by thin-layer chromatography (TLC) and detected by a charring method with phosphoric acid and cupric sulfate [69]. The result for the anion-exchange experiment (figure 2.4) is presented in figure 2.5 as an example. Note that not all bands can be compared directly, since the volume applied to the TLC-plate was kept constant, even with different dilutions of the starting material. Directly comparable to each other are lanes 1 to 5 and 6 to 11.

2.2.2   Pre-screen for crystallization conditions

To minimize the number of experiments during the crystallization screen, a crystallization pre-screen for two parameters was performed:

1. A detergent screen to find suitable detergents stabilizing the protein.
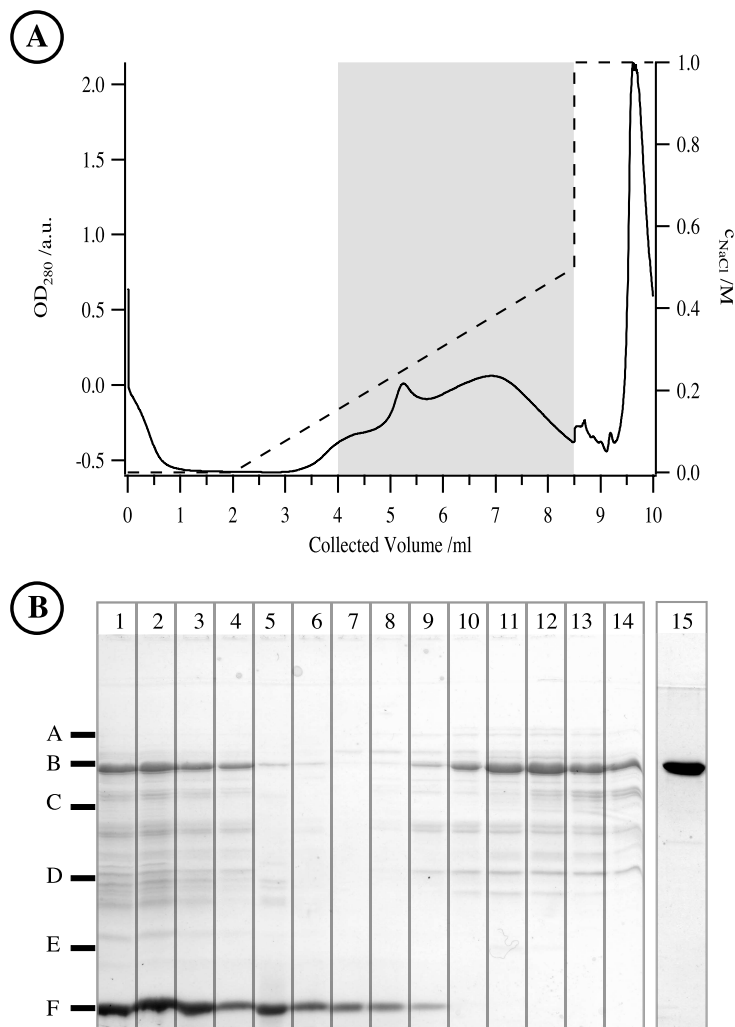
Figure 2.4: Pre-purification of LmrA with an anion-exchange column in the detergent DDM. *Panel A:* Elution profile of LmrA from the anion-exchange column (solid curve). The LmrA protein was bound at low salt concentration (ca. 50mM NaCl), washed with phosphate-buffer without NaCl and eluted with a sodium-chloride-gradient (dashed line). The fractions loaded on the SDS-PAGE (panel B, lane 9 to 16) are indicated by a gray box in panel A. *Panel B:* Coomassie-blue SDS-polyacrylamid gel of anion-exchange and NiNTA-column purification steps. Lane 1: Solubilization-mix of LmrA before incubation at 4°C ; 2: Solubilization-mix of LmrA after incubation; 3: Diluted protein before centrifugation; 4: Diluted protein after centrifugation (supernatant); 5: Resuspended pellet 6: Flow-through anion-exchange column; lanes 7 to 14: Fractions 9 to 16 of anion-exchange. A to F: Molecular weight standards in kDa (A: 97,4; B: 66,2; C: 42.7; D: 31; E: 21.5; F: 16.7)
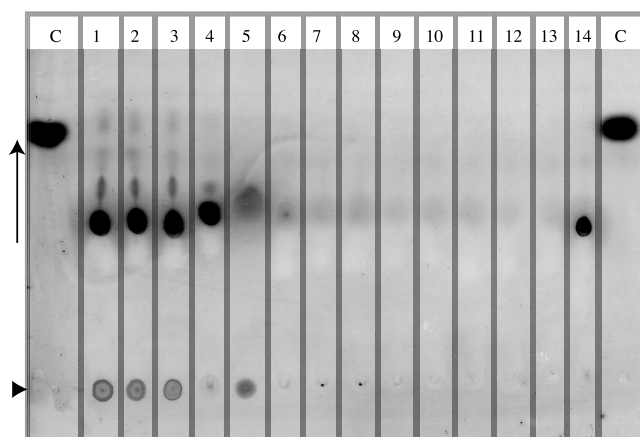
Figure 2.5: Thin layer chromatography (TLC) and detection of neutral- and phospholipids during the purification of LmrA by anion-exchange and NiNTA-column. The triangle marks the line where the sample was blotted on the TLC-plate, the arrow indicates separation-direction. C: Positive control with cholesterol (2.5 μg). Negative controls of all buffers were made without any signal (data not shown). Lane 1: Solubilization-mix before incubation, 2: Solubilization-mix after incubation; 3: Diluted before centrifugation; 4: Supernatant (solubilized LmrA); 5: Pellet, insoluble material; 6: Protein after FPLC in NiNTA binding-buffer, before incubation; 7: NiNTA-binding-buffer after incubation; 8: flow through NiNTA; 9: wash 1; 10: wash 2; 11: Eluted Protein; 12: flow-through up-concentration 1 (centricon); 13: flow through up-concentration 2; 14: final (up-concentrated) protein
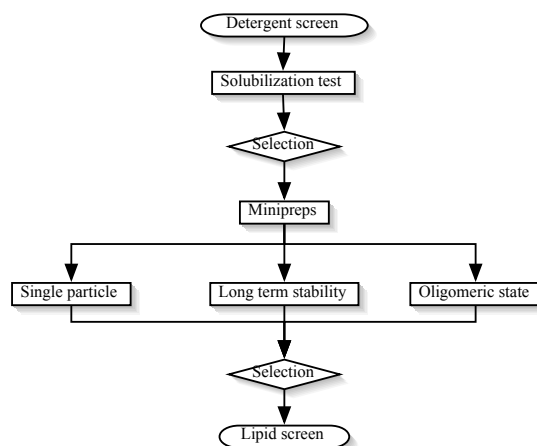
Figure 2.6: Proposed systematic approach for 2D-crystallization. In a first step, detergents are selected for their ability to solubilize and stabilize the protein (and its oligomeric) structure. Finally, the detergent chosen is used in a screening for suitable lipids by the mono-layer technique.

2. A lipid-screen with the selected detergents to find detergent-lipid-combinations promoting LmrA reconstitution into membranes.

An outline of this systematic approach is given in figure 2.6. Due to the fact that there is no activity test known for solubilized LmrA, only indirect methods could be used for detergent-selection. To monitor the ability of a test-detergent to keep LmrA in a state suitable for subsequent reconstitution experiments, following parameters were tested:

- The solubilization capacity of the test-detergent for *Lactococcus lactis*-membranes.

- The quality of LmrA purification in a specific detergent.

- The stability of solubilized LmrA in the test-detergent

- The oligomeric state of LmrA tested by sucrose-gradients.

- The visual appearance of solubilized LmrA by negative stain electron microscopy.

agraphSolubilization and NiNTA-binding tests The detergents tested are listed in table 2.1, together with their physico-chemical characteristics. As a first step, solubilization tests were performed: In these tests, small aliquots of LmrA containing membranes were incubated for 30 min at $4°C$ with an appropriate amount of detergent, considering the CMC and the capacity (aggregation-number n_A) of the detergent. To separate the solubilized material from the insoluble membrane-parts and aggregated LmrA, the solubilization-mix was centrifuged at $100'000 \times g$ for 30 min. Since LmrA is visible as characteristic protein band in coomassie blue stained SDS-PAGE, no special detection method (such as western-blotting) was needed. The results are presented in figure 2.7 panel A.

Table 2.1: Tested detergents in crystallization pre-screen.

Detergent	MW^a /g/mol	CMC^b /%	$n_A{}^c$	Solub. /%	Elution /%
DM	482.6	0.08	70	4	0.5
DDM	510.6	0.008	85	2	0.05
OG	292.4	0.7	78-90	8	3
OTG	306.4	0.3	-	5	1.5
NG	306.4	0.2	-	3	1
8-POE	-	0.25	-	3	1
C_8E_6	406.3	0.2	32	10	1
$C_{12}E_8$	538.8	0.005	120	2	0.05
$C_{12}E_9$	582.8	0.002	128	1	0.02
Triton X-100	-	0.02	100-155	1	0.5
CHAPS	614	0.49	10	10	2
Pril	-	-	-	1	0.3

^{a}MW: Molecular weight
^{b}CMC: critical micelle concentration
^{c}n_A: Aggregation-number of micelles
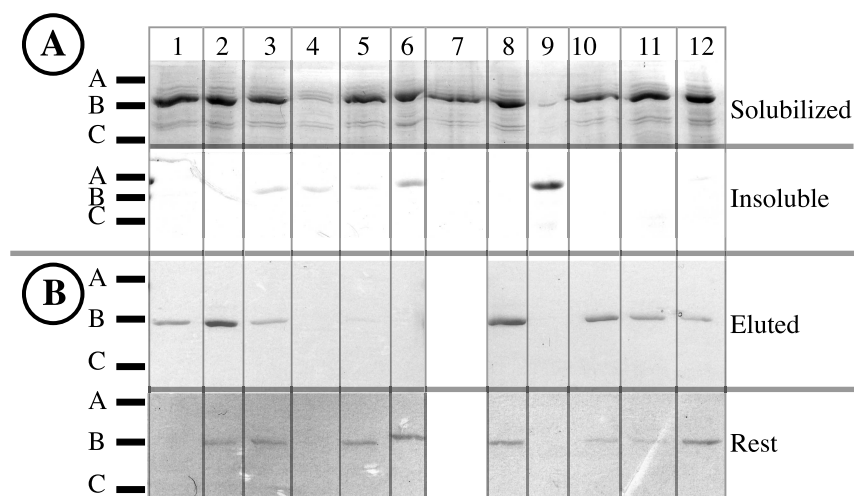
Figure 2.7: Initial solubilization and NiNTA-binding tests of LmrA with different detergents. This experiment was repeated with 3 different detergent-concentrations confirming these results. *Panel A*: Solubilization tests. The upper SDS-polyacrylamid gel represents the supernatant after centrifugation, the lower one the in 1% SDS re-solubilized pellets. *Panel B*: NiNTA-binding tests. Upper gel: eluted protein, lower gel: Not eluted protein released by SDS-sample buffer from the NiNTA-matrix. Lane 1: DM; 2: DDM; 3: OG; 4: OTG; 5: NG; 6: 8-POE; 7: C_8E_6 (sample for binding experiment lost); 8: $C_{12}E_8$; 9: $C_{12}E_9$; 10: Triton X-100; 11: CHAPS; 12: Pril. A to C: Molecular weight markers in kDa (A: 97,4; B: 66,2; C: 42.7)

To test the NiNTA-binding in these detergents, the supernatants of the solubilization tests were incubated with ca. 20 μl of NiNTA-beads for 2 h at 4°C, washed with washing buffer (50 mM KP$_i$ pH 8.0, 100 mM NaCl, 1 mM histidine and detergent) and eluted with elution-buffer containing 200 mM histidine at pH 7.0. To check for not eluted protein, the NiNTA-beads were incubated with SDS-sample buffer (see figure 2.7, panel B).

From the 12 tested detergents, only OTG and C$_{12}$E$_9$ did not properly solubilize LmrA. In contrast to that, only a few detergents were able to keep LmrA in a state so that it could be eluted from the NiNTA-beads: With the detergents DM, DDM, C$_8$E$_6$ and Triton X-100 most of the protein was properly eluted. Prepared in CHAPS and Pril, LmrA did only partially elute from the NiNTA-Matrix. The detergents NG, 8-POE and OG successfully solubilized the protein but the following elution from the NiNTA-beads was problematic.

Mini-preparations of LmrA To further explore the detergent dependency of LmrA, small amounts were purified with NiNTA-beads (as described in section 2.4.1) and analyzed on SDS-PAGE and with negative stain in the electron microscope. From the initial experiment, the following detergents were selected: C$_8$E$_6$, C$_{12}$E$_8$, Triton X100, CHAPS and Pril (DM and DDM were not tested because these detergents had already been used routinely, as example see figure 2.2 and figure 2.4).

The result of the purification is shown in figure 2.8, panel A. Obviously, there are significant differences in the protein-concentration between the different detergents tested: Whereas C$_{12}$E$_9$ and Triton X-100 have strong LmrA bands, the C$_8$E$_6$ band is significantly narrower indicating a lower concentration. CHAPS and Pril only indicate very low protein concentrations. All concentrations were measured via the Bradford-method (Bio-rad, see legend of figure 2.8).

To test the long-term stability of LmrA in the various detergents, the eluted protein was stored for one week at 4 °C and analyzed again by SDS-PAGE as shown in panel B of figure 2.8. In all detergents degradation of LmrA could be observed. The relative amount of degradation seemed to be approximately the same for C$_8$E$_6$, C$_{12}$E$_8$ and Triton-X100 but the amount of intact protein was considerable less in CHAPS and Pril: LmrA prepared in these detergents was almost completely digested.

To obtain a more complete picture, negative stain grids were prepared using aliquotes of the solubilized protein and examined for single particles and aggregates. An overview of the grids is given in figure 2.9. LmrA prepared in the detergent C$_8$E$_6$ formed significantly more aggregates than that prepared in the low CMC detergents Triton X-100 (and others, data not shown). At higher magnification, the Triton X100-solubilized preparation revealed many distinct particles whereas the C$_8$E$_6$-preparation showed a comparatively low number of well defined particles. It was impossible to detect any single particles for CHAPS and Pril (data not shown).

Sucrose-gradients To compare the oligomeric state of LmrA in various detergents, sucrose-gradients (7.5%-20%) in buffer containing the test-detergent were run. With this technique it is difficult to estimate the exact molecular weight of a protein, but it gives a good estimate of the condition of the protein. A comparison between LmrA solubilized in DDM, C$_{12}$E$_8$ and C$_8$E$_6$ is shown in
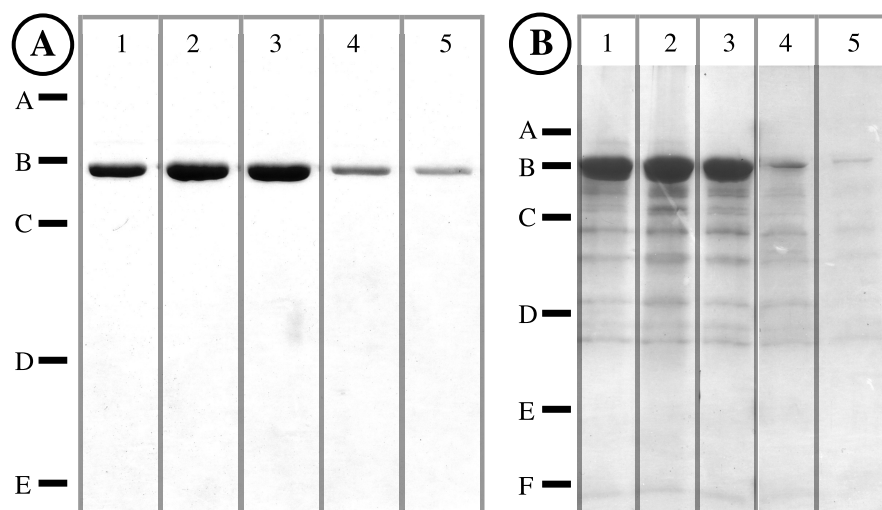
Figure 2.8: LmrA low-scale purifications in selected detergents: Coomassie-blue stained SDS-PAGE of the eluted LmrA-protein from NiNTA-columns. Lane 1: C_8E_6 (1 *mg/ml*); 2: $C_{12}E_8$ (0.98 *mg/ml*); 3: Triton X100 (0.76 *mg/ml*); 4: CHAPS (0.56 *mg/ml*); 5: Pril (0.5 *mg/ml*) *Panel A*: Immidiately after elution, *Panel B*: After one-week storage at 4°C. A to E: Molecular weight markers in kDa (A: 97,4; B: 66,2; C: 42.7; D: 31; E: 21.5)

figure 2.10.

Note that the molecular-weight markers migrated similarly in all three detergents. Three different behaviors can be observed: The detergents DDM, $C_{12}E_8$, DM and Triton X-100 seem to keep solubilized LmrA in a state where not all protein goes to the pellet, whereas LmrA solubilized in CHAPS and C_8E_6 was exclusively found in the pellet. These results have to be studied carefully since different detergents were added to every test-run, which changed the density of the media. Furthermore, the used molecular-weight markers were soluble-proteins and it is not clear how they interact with the detergent. Even so, a significant difference can be observed between LmrA solubilized in $C_{12}E_8$ and DDM: LmrA in $C_{12}E_8$ revealed a band approximately at the position expected for a dimer but also higher aggregates were detectable, whereas LmrA solubilized in DDM migrated almost exclusively to positions of higher molecular-weight despite very narrow bands at the dimer position. However, it is not clear how much the detergent belt stabilizing the protein accounts to the observed protein-mass (see discussion). The observed migration profile of LmrA in Triton X-100 is comparable to the one in $C_{12}E_8$. LmrA solubilized in DM and LmrA in DDM were detected in the equivalent fractions of the sucrose gradients (data not shown).

Lipid-screen   During the detergent-removal of the crystallization process, a complex and not well understood interaction between detergent, protein and lipid-molecules takes place. As outlined in the introduction, not every detergent lipid mixture will probably be a good combination. Therefor, the detergents known to favor a stable solubilized LmrA were tested against various lipids and
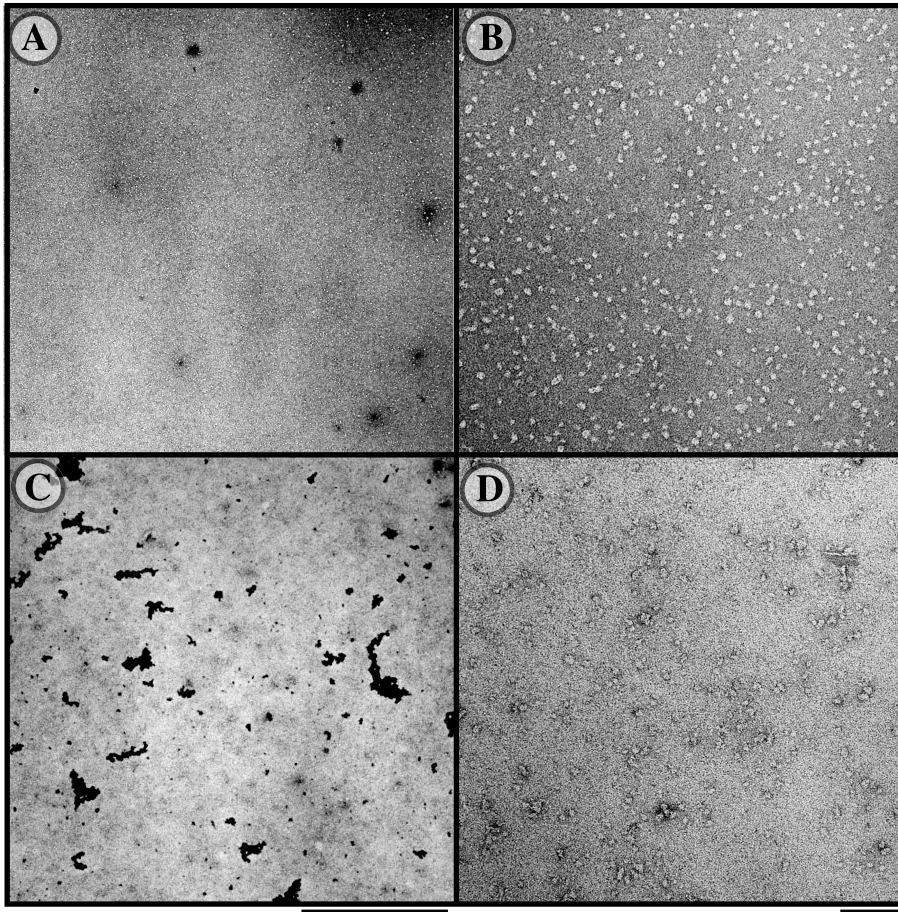
Figure 2.9: Comparison of the mini-preparations of LmrA-particles solubilized with the detergents Triton X-100 and C_8E_6 by negative stain electron microscopy. The samples were prepared directly after the NiNTA-column. A and B: LmrA solubilized in Triton X-100, C and D: LmrA solubilized in C_8E_6. A and C give an overview of the two detergents. Scale-bar corresponds to 1 μM. B and D: Detail-views showing the single LmrA-particles. Scale bar: 100 nm
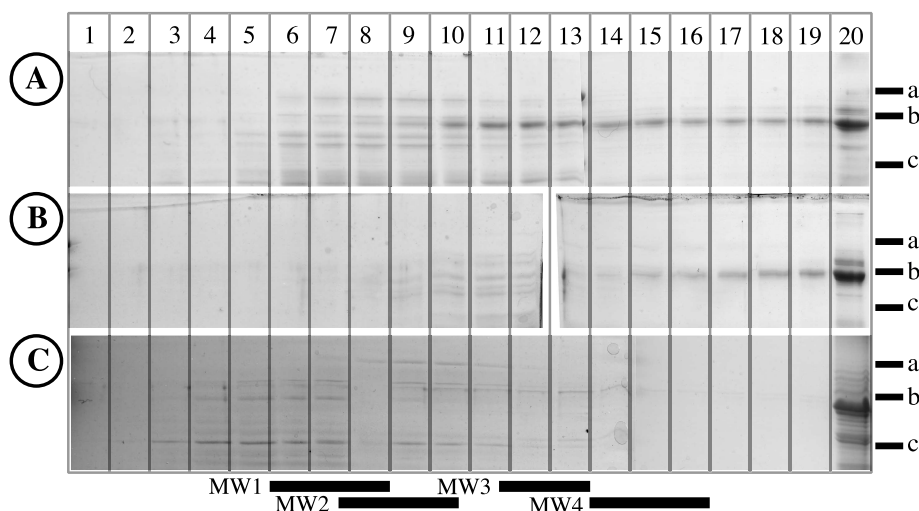
Figure 2.10: Analysis of selected sucrose-gradients by coomassieblue SDS-PAGE. Lanes 1-20: Fractions of sucrose gradient. Fraction 20 corresponds to the gradient pellet. *Panel A:* $C_{12}E_8$; *B:* DDM, *C:* C_8E_6. Molecular-weight markers for sucrose-gradient: MW1: 29 kDa, MW2: 64 kDa; MW3: 150 kDa; MW4 200 kDa . a to c: Molecular weight standards for SDS-PAGE in kDa (A: 97,4; B: 66,2; C: 42.7)

lipid-mixtures for protein-incorporation into membranes.

To do this lipid-screen, the mono-layer method [41, 64] was chosen. The advantages of this technique are:

- Only a very small amount of protein is needed.

- The interpretation of the observed structure is simplified, since the protein attaches to the mono-layer surface before the detergent is removed by bio-beads. In this way, the recorded TEM pictures are not overpopulated by the general lipid-structures such as vesicles, which are formed after detergent-removal.

A disadvantage of this approach is that it is limited to low-CMC detergents (stability of the monolayer). But since DM is the only high-CMC detergent, which proofed successful for LmrA-purification, this limitation was not a problem in this case. Since DM and DDM had already been used for crystallization trials, only $C_{12}E_8$ and Triton X-100 were tested in this first experiment.

The monolayers were prepared in advance by deposing 0.6 μl of a 0.1 mg/ml DOGS:NiNTA-DOGS=1:1 lipid solution (chloroform) on the surface of the crystallization buffer placed in a teflon cavity. After 4 h of evaporation of the organic solvent, the monolayer was ready for the lipid-screen experiments: LmrA was purified as described with the same detergent-concentration for Triton X-100 and $C_{12}E_8$ (Solubilization: 2%, wash-buffers and elution-buffer: 0.5%). Histidine was removed from the elution-buffer with two consecutive mini-Sephadex-G25 columns (the removal was tested with thin-layer-chromatography and Ninhydrin-detection). The protein (500 $\mu g/ml$) was first incubated with vesicles of the test-lipid at 4°C for 2h at a nominal detergent concentration of 0.5% (Triton X-100, $C_{12}E_8$) with stirring. After that, the protein was injected into

the sub-phase of the NiNTA-monolayer for overnight binding. The detergent was removed at room temperature with 5 μl densely packed Bio-bead solution over a period of 5 h.

The following lipids and lipid-mixtures have been tested: DMPC, DOPC, DOPG, *Escherichia coli*-lipid-extract, Cardiolipin:DOPG=2:1 mix, DOPE:POPG=8:2 mix, Heart lipid extracts, Cholesterol:DOPC=2:8 mix and DLPS. To ensure that not the amount of lipid was the limiting factor for protein reconstitution, a relatively high LPR of 2 was used, with the idea that common vesicles after the detergent-removal remain in the sub-phase. The crystallization-tests were analyzed with the electron microscope by picking up the mono-layer using a hydrophobic carbon coated electron-microscope grid.

Only preliminary results for this reconstitution-test are available at the moment. The results of this experiment should also be confirmed with other reconstitution techniques (see discussion). Some representative photographs are displayed in figure 2.11.

The results are looking quite different for different detergent-lipid combinations, many of the tested conditions are not interpretable. A common phenomenon is the observation of different "phases" (rough structured areas *vs.* smoke-like lighter structures) as it is seen in the *Escherichia coli*-lipid and also the POPG experiments (see images A, B, E, F and G of 2.11). It is not clear if this should be interpreted as differently packed proteins or if it is a staining artifact due to the uncharged grid. The reconstitution experiments with the different lipids gave the following results:

Escherichia coli-lipid: See figure 2.11A and B. Besides the smoke-like structures also observed with other lipids (most probably stain artifacts on the carbon film), supposable membrane areas were visible using the detergent $C_{12}E_8$ for the reconstitution: Most of these structures were very rough and could be based on bulky membrane peripheries. However, it can not be excluded that they were denatured protein. Beside these structures, larger flat membrane areas were observed (arrow). With the detergent Triton X-100, only very thin structures were detected, possibly the solubilized LmrA did not bind to the monolayer for some reason.

DMPC: Figure 2.11C and D. With the lipid DMPC, very different results were obtained: Using the detergent Triton X-100, small membrane areas were observed with bulky borders. Besides these structures, more flat and larger membrane-patches have been observed (arrow, panel D). In the reconstitution-experiment with $C_{12}E_8$ only thin structures were visible.

POPG: Figure 2.11E and F. In combination with the detergent $C_{12}E_8$ similar results as with *Escherichia coli*-lipid with the same detergent were obtained: This can be interpreted as denatured protein or as small membrane areas with bulky peripheries. Interestingly POPG showed in the detergent Triton X-100 also stacked structures besides the flat membrane areas (panel F, arrows).

Cardiolipin:POPG-mixture: Figure 2.11G and H. With this lipid-mixture, huge membrane areas with bulky borders were observed in combination with $C_{12}E_8$. Inside the supposed membrane structures particles similar to the observed structures in single particle analysis were observed (see
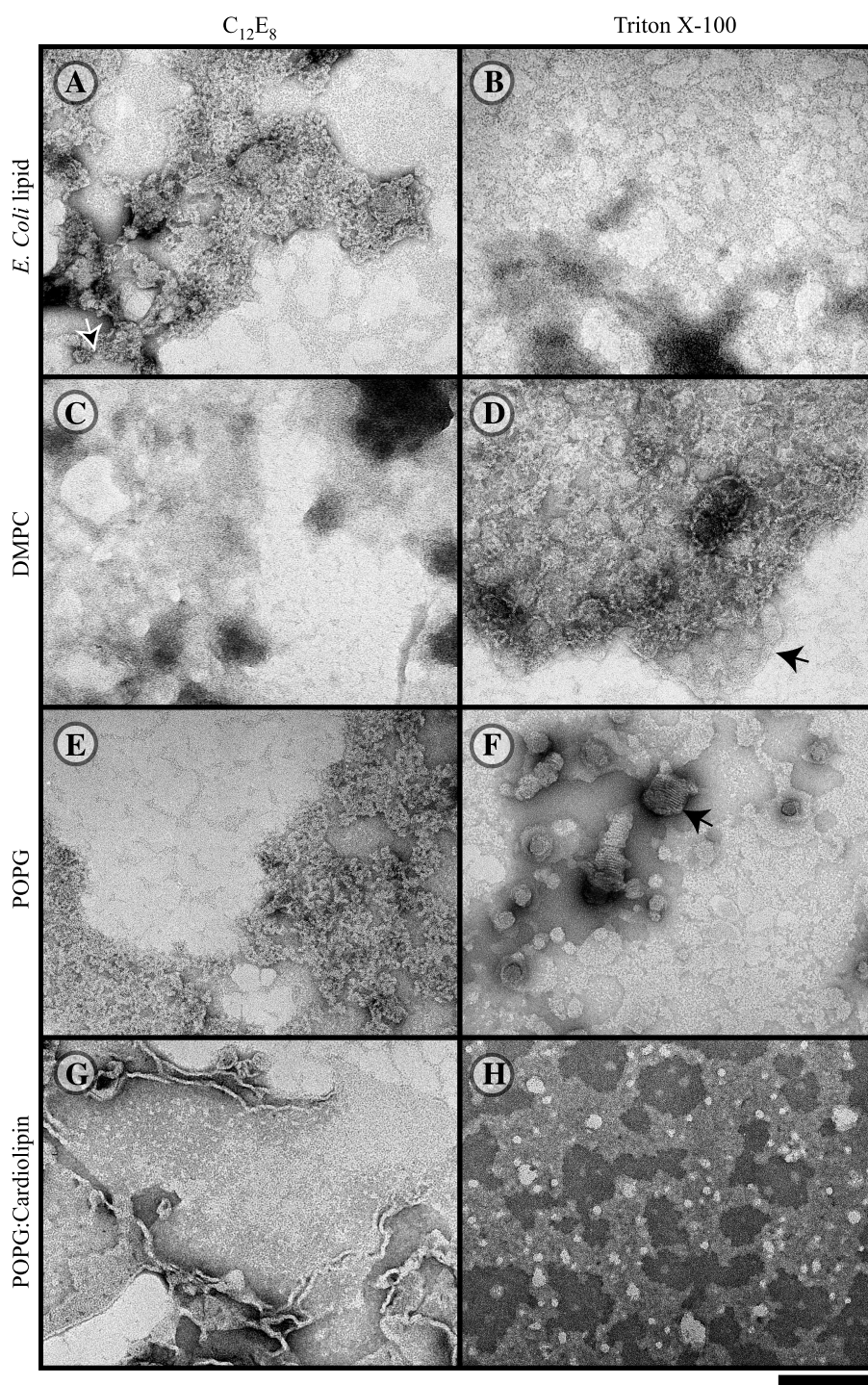
Figure 2.11: Lipid-screen with the detergents $C_{12}E_8$ and Triton X100. A: *Escherichia coli*-lipid ($C_{12}E_8$); B: *Escherichia coli*-lipid (Triton X100); C: DMPC ($C_{12}E_8$); D: DMPC (Triton X100); E: POPG ($C_{12}E_8$); F: POPG (Triton X100); G: POPG:Cardiolipin ($C_{12}E_8$); H: POPG:Cardiolipin (Triton X-100). For further explanation (arrows) see text. Scale bar corresponds to 200 nm

figure 2.3). However, only thin structure were detected with the detergent Triton X-100.

2.2.3 Crystallization assays

Initial crystallization screens

In the initial crystallization-experiments with DM as detergent, a screen for lipids and LmrA-inhibitors was performed. First, a good set-up for dialysis against small buffer-volumes had to be found, since the inhibitors of LmrA are often poisons and expensive. A comfortable solution was the use of 24-well cell culture plates (Falcon), in which the crystallization probe could be moved from slot to slot, leading to a similar dilution factor as the normal batch procedure with dialysis buttons [67]. In the culture-plate setup the sample was placed in a Eppendorf-cap covered by a piece of dialysis-membrane. The sample was dialyzed 3 times against 2.5 ml buffer. For a 50 μl sample this meant a dilution-factor for the detergent of 125'000. The buffer was prepared freshly before every buffer-change, since some of the inhibitors are unstable (γ-S-ATP) or condensate to polymers (o-vanadate) in aqueous solutions. After four days, the detergent dialysis was complete and the negatively stained specimens were analyzed in the electron microscope.

As already outlined at the beginning of this chapter, the most important results of these experiments were the solutions to the problems we encountered: At the beginning, almost all of the protein was degraded. This could be solved by performing membrane-prewashes and using Ser-protease inhibitors. A remaining problem was the proper reconstitution of LmrA into membranes. Some interesting results, which will be helpful in the future, were obtained (data are not shown since these results are conclusions from many experiments):

- LmrA seems to be more stable at higher pH (pH 8).

- LmrA seems to be stabilized by the addition of DHPC (Diheptylphosphatidylcholine) to the reconstitution experiment.

- *Escherichia coli* lipids seemed to incorporate LmrA (However, additional uncommon lipid-phases were observed and the reproducibility was bad with the dialyzing method for detergent removal).

Test of different methods of detergent-removal

To resolve the problems observed in the initial crystallization-screen, more fundamental experiments were performed to answer questions such as:

- How does LmrA reconstitute with different reconstitution methods?

- Does it matter in which way lipids are added to the protein?

These tests were performed using DDM as detergent, since DDM was believed to preserve LmrA very well in phosphate-buffers (personal communication Gerrit Poelarends). Given the experience from the initial screens, these tests were performed with DMPC and *Escherichia coli*-lipids, but *Lactococcus lactis*-like lipid-mixtures were also taken into account. Three different approaches were tested:

- Batch-methods using the bio-bead-technique for detergent removal, followed by reconstitution experiments through dialysis.

- Different ways of lipid-additions, such as lipids solubilized in different detergents or addition of lipids as vesicles.

- The monolayer technique.

agraphReconstitution with Bio-beads First, simple reconstitution experiments were done in phosphate-buffers known to stabilize LmrA with the bio-beads-method (see Rigaud *et al.* 1998 [63]): LmrA was purified in DDM and incubated over night with *Escherichia coli* lipid-vesicles at $4°C$ in a buffer containing a nominal detergent concentration of 0.5% DDM. The detergent was subsequently removed by stepwise bio-bead addition and the reconstitution experiments were analyzed by negative-stain electron microscopy. A typical result with *Escherichia coli*-lipid of such a reconstitution-experiment is depicted in figure 2.12. Panel B shows worm-like structures. These were interpreted as membranes and have an estimated thickness of 14 nm, which is about twice the thickness of a biological membrane with embedded proteins. This suggests that the observed structures were collapsed vesicles and not capped membrane sheets which could possibly be observed in samples with remaining detergent. Note the spikes that point out of the membrane (arrows): These most likely represent the soluble domain of LmrA (see discussion).

Similar vesicles were also observed with POPG as lipid, but the membrane-areas were generally smaller. DMPC and cardiolipin also appeared to be able to incorporate LmrA, but the data are much less clear and the observed membrane areas were still very small (data not shown).

agraphTest of different lipid-additions Unfortunately, the observed membrane-areas of the reconstitution experiments of LmrA from DDM into *Escherichia coli*-lipid were relatively small (between 0.1 to 0.2 μm). To have a better starting point for subsequent crystallization experiments, the influence of the way of lipid-addition on the size of the obtained membrane patches was tested. For this, lipid-vesicles and mixed-micelles (lipid solubilized in DDM, DM, OG and OTG) were incubated with the LmrA protein and reconstituted by the bio-beads method described in the previous experiment. To get rid of the high background noise in the electron-micrographs taken from negatively-stained reconstitution samples, and to remove potential remaining detergent, the reconstituted material was washed 4 times in the crystallization-buffer(by low-spin centrifugation and resuspension). A comparison between the different addition-methods is shown in figure 2.13. The differences are minimal. Generally, it is very hard to see LmrA particles sticking out of the membrane in these experiments (possibly in 2.13, panel C). However, in the sample with DDM-lipid mixed-micelles, large and flat areas were seen in the background (arrow of panel C). It is unclear if LmrA was incorporated in these membrane areas or not. It is also to mention that at least the reconstitution-experiments with OTG mixed-micelles (presumably also with OG) revealed a similar appearance of the observed structures than the reconstitution-experiments with vesicles and mixed micelles. Thus LmrA seems to be temporarily stable in the presence of these high-CMC detergents and *Escherichia coli*-lipid.

agraphDetergent removal by dialysis and Bio-beads-dialysis combination To increase the membrane-patch sizes, other detergent-removal experiments were
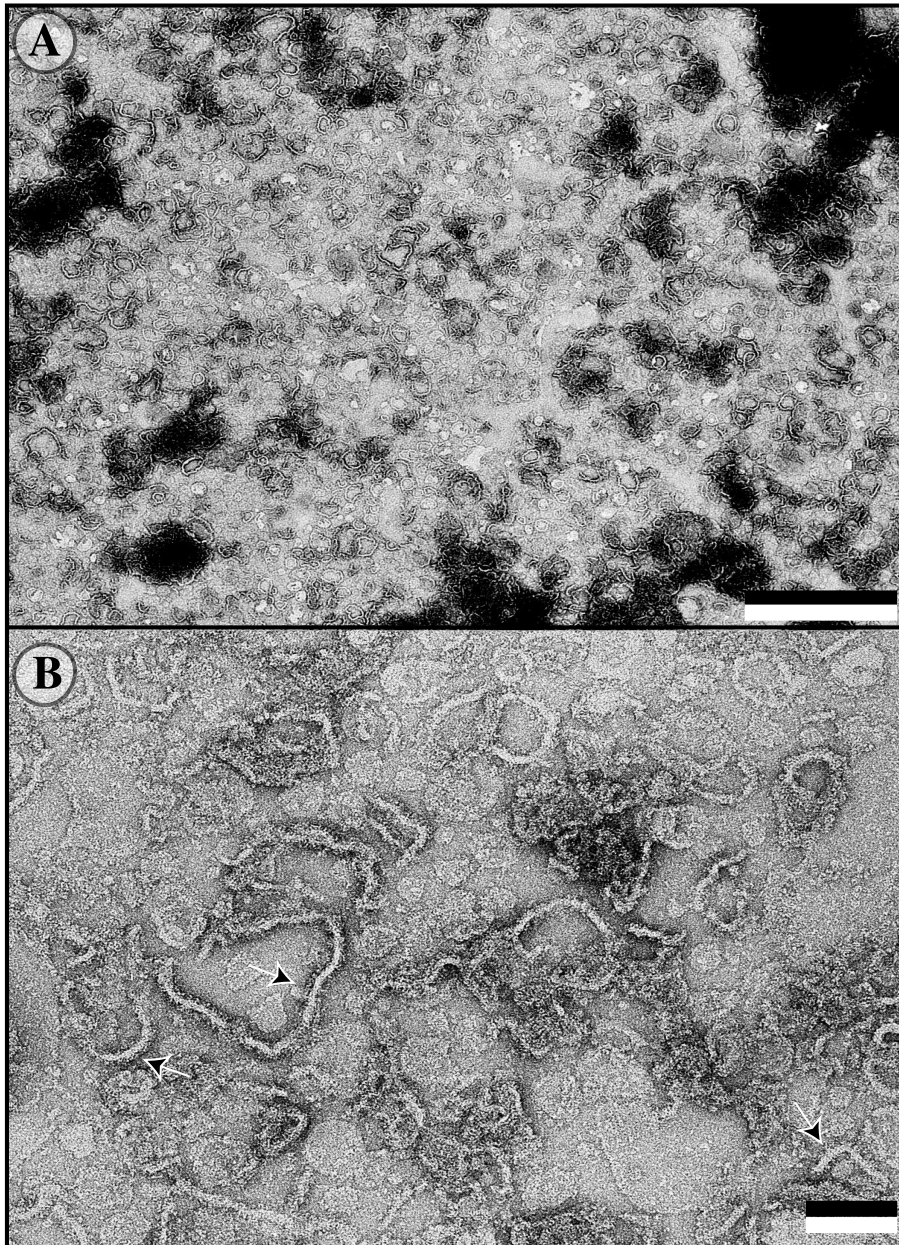
Figure 2.12: Reconstitution-experiments of LmrA with *Escherichia coli*-lipids. *Panel A*: Overview image. The scale-bar corresponds to 1μ *m*. *B*: Detail view at higher magnification. Note the fungi-like structures that are sticking out of the membrane with a hight of about 6 *nm* (arrows). The membrane-structures are more than twice as thick than expected for biological membranes, indicating that these structures are the border of collapsed vesicles. The scale-bar correspond to 100 *nm*
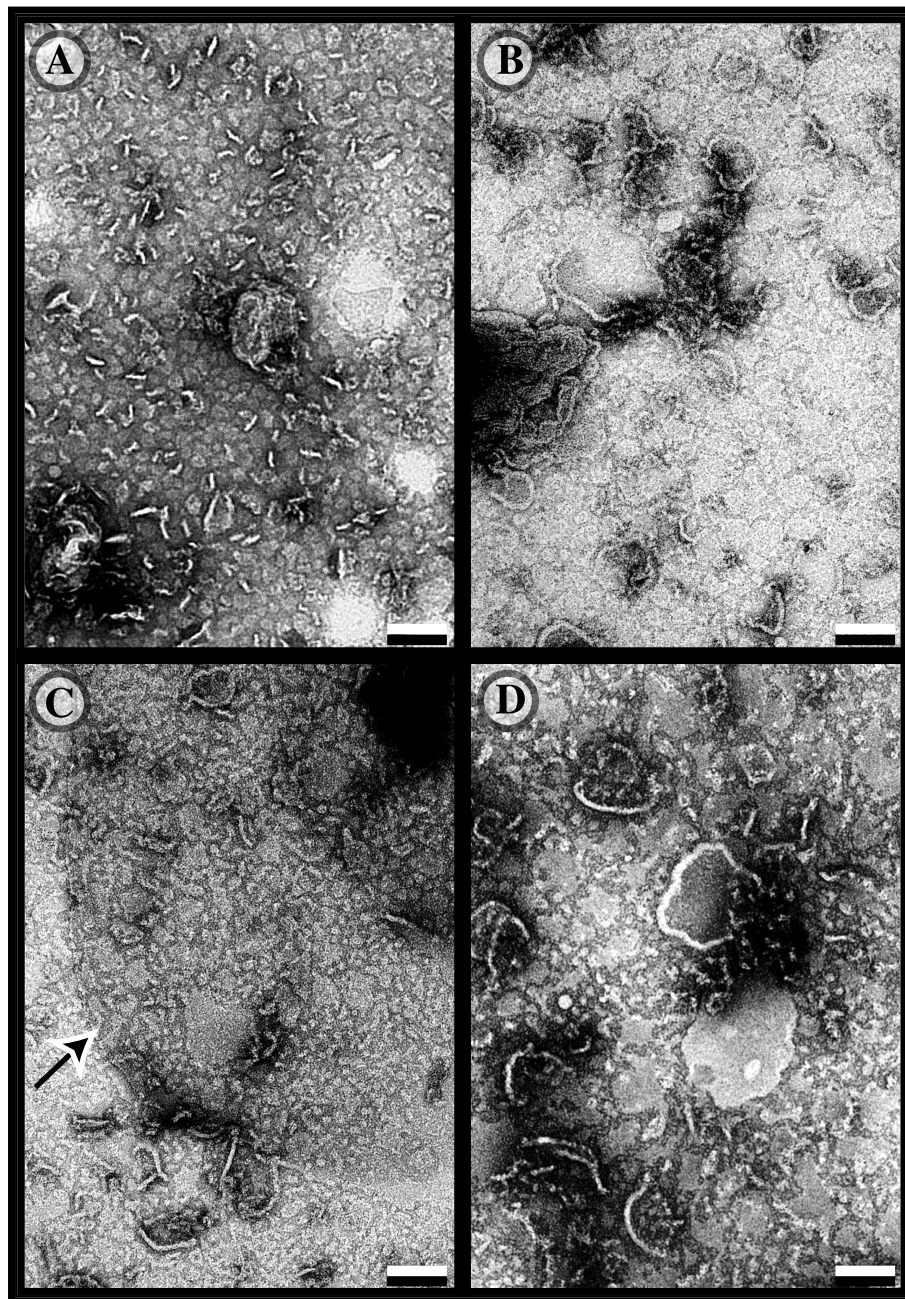
Figure 2.13: Tests of different ways of lipid-additions (*Escherichia coli*-lipid) to LmrA to increase membrane-patch size. A: Solubilized in 5% DM (5 *mg/ml* lipid); B: Solubilized in 6% OTG; C: Solubilized in 3% DDM. The arrow indicates the periphery of a large vesicle ; D: Solubilized in 6% OG. Scale bars correspond to 100 *nm*

performed: In a first experiment, the lipid-vesicles (without detergent) were incubated with the solubilized LmrA at a nominal detergent-concentration of 0.5% DDM, incubated at $4°C$ for $2~h$ and injected into slide-a-lyzer (Pierce). The advantage of this dialyzing device is the large dialysis-membrane surface compared to the sample volume. This allows a shorter dialysis time which is especially of advantage with low CMC detergents. The samples were dialyzed for 17 days at $4°C$. In the electron microscope these experiments revealed densely packed vesicles on a background with much less noise than the bio-bead reconstitution experiments. However, the observed membrane-patch sizes were much smaller than in the bio-bead reconstitution (data not shown).

The tests to fuse the small vesicles by partially re-solubilizing and/or desta-bilizing the membranes by dialysis against the CMC concentrations of OG and OTG respectively, or by freeze-thaw cycles with liquid nitrogen, failed. In an-other experiment, some of the detergent was first removed with bio-beads and the sample solution was then placed into dialysis-buttons for further detergent removal. The latter experiments gave no interpretable results (data not shown).

agraphMonolayer experiments As an alternative, the monolayer method was tested for crystallization of LmrA. In this experiment, LmrA was mixed with lipids presolubilized in 3% DDM (*Escherichia coli*-lipid and DMPC) at an LPR of 1 and a protein-concentration of 0.5 mg/ml, incubated for $2~h$ at $4°C$ with stirring. Then it was injected into the sub-phase of the previously pre-pared monolayer (50% NiNTA-contents). The final protein-concentration was 0.05 mg/ml and the nominal detergent-concentration 0.05% DDM.

Some results of the monolayer-experiments are shown in figure 2.14. The monolayer surfaces with the lipid DMPC were much smoother than the recon-stitution experiments with *Escherichia coli*-lipid (compare panel B and D of figure 2.14). Other monolayer-sheets with DMPC showed more rough struc-tures, but these seemed to be related with small membrane patches at the ob-served surface. The presented patch of DMPC-monolayer reveals a very smooth surface. However, this appearance was accompanied by a multi-layered struc-ture. This behavior was also observed with other lipids, such as POPG (see figure 2.11 p. 32). It is difficult to explain such an appearance by the mono-layer technique. Therefore, these stacked sheets could also be absorbed from the sub-phase on the grid. Note the areas of oriented structures (lines) in the DMPC experiment (white arrow-heads in figure 2.14, panel B). It is not known if these structures are related with the LmrA-protein. The periodicity of these lines were in the order of 9 nm, this could be a sign that indeed LmrA was in-corparated. The reconstitution-experiments with the *Escherichia coli*-lipid re-vealed a very rough structure and it looked as if the protein did not reconstitute (no real membrane borders were visible) and might thus have been denatured after detergent-removal.

2.3 Discussion and Outlook

2.3.1 Purification

In general, the purification of LmrA gave satisfactory results. Typical elution-concentrations of LmrA after the NiNTA-column were around 1 to 1.4 mg/ml. The purity of LmrA after successful purification were estimated of higher than
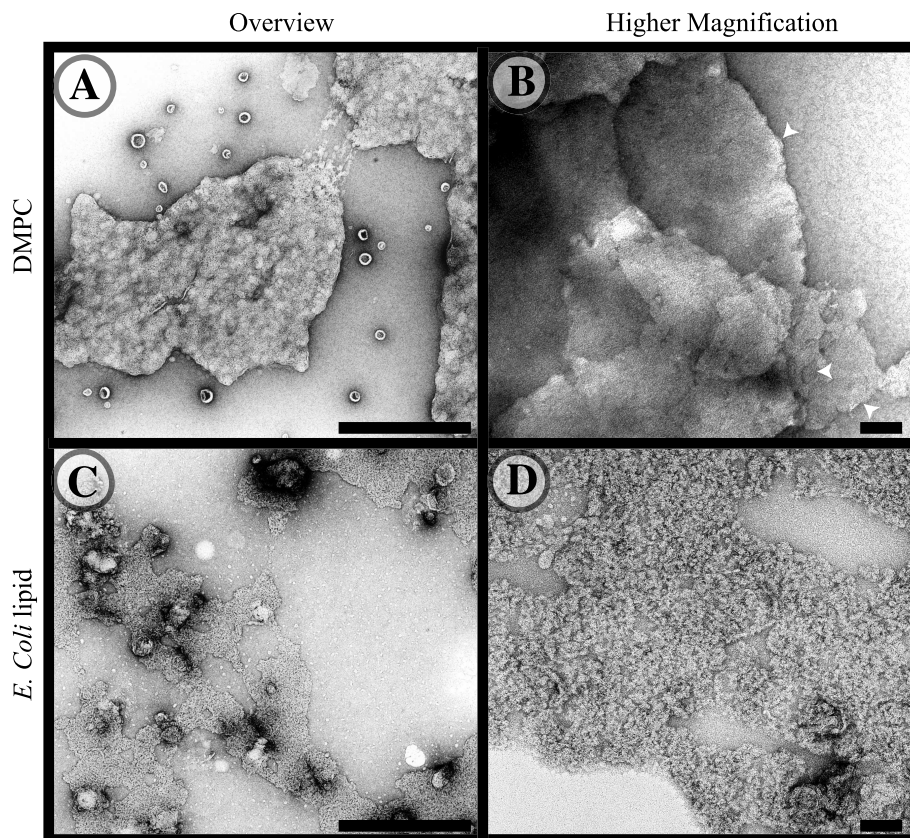
Figure 2.14: Crystallization-experiments with the monolayer-method. Used lipids were DMPC (A, B) and *Escherichia coli*-lipids (C, D). *Panel A and C* are presenting overviews of protein-decorated monolayers, the scale-bar corresponds to 1 μm. *Panel B and D* display the higher magnification views. Note the oriented structures in panel B. Scale bar: 100 nm.

99%. In most preparations a weak band of 35 kDa (see figure 2.2 triangle) was observed. This most probably represents a cleavage product of LmrA since a cleavage product of similar size was observed in crystallization trials. This weak band could partially be removed by further protein concentration through membrane-filtration (vivaspin, vivascience, Germany) with a cut-off of 100 kDa. With this concentration method, LmrA concentrations of 3 mg/ml could be reached, both with DM and DDM as detergent.

The good purification was therefore a promising basis for 2D-crystallization trials. However, major differences in the quality between different membrane batches were observed. Especially, proteolytic degradation of LmrA during the purification was a problem in some of the membrane-preparations. Using such protein in crystallization assays led to major protein-degradation during the reconstitution-process. The degradation of LmrA observed seemed to be mainly due to Ser-proteases since the use of strong Ser-protease inhibitors such as PMSF (Sigma) and BEFA-block (Roche) prevented degradation efficiently during purification and crystallization. Since protease-inhibitors like PMSF can modify proteins also in an unspecific way, we first tried to reduce the protein-degradation-problem by a cholate-wash. This wash was shown not to harm the LmrA activity of LmrA containing *Lactococcus lactis*-vesicles (personal communication Gerrit), but this procedure led to the loss of LmrA from some of the membrane batches. This could be a sign that LmrA was not properly folded or incorrectly inserted into the membrane or that the membrane composition changed from batch to batch.

To have a better control over the quality of the starting-material, an anion-exchange chromatography step was introduced directly after the solubilization step. The removal of most protease activity by this additional purification step also allowed the binding of LmrA to the NiNTA-column over night in the presence of BEFA-block as protease-inhibitors. This procedure did not seem to destabilize LmrA, but caution should be taken, since ion-exchange columns are known to remove lipids very efficient from proteins. In some cases reported (personal communication Andreas Engel, [45]), important stabilizing lipids (such as POPE) were stripped off and the protein has been destabilized.

To analyze the lipids associated with the LmrA-protein, thin-layer-chromatography was performed. The lipids were detected by a Cu-phosphoric acid bath. This method stains neutral and phospholipids in the sub-nanomolar range according to Ruiz *et al.*, 1997 [69]. The results presented are preliminary and allowed only a qualitative interpretation of the associated lipids. For a more precise and quantitative analysis, this technique could be further improved: 1.) Synthetic lipid-markers, 2) Densitometric quantification of the bands, 3.) Previous extraction of the lipids with a chloroform:methanol (3:1) mixture and concentration by the evaporation of the organic solvents. This would also allow to analyze relative amounts of every fraction so that these could be compared directly.

Our lipid-analysis, however, still allowed a qualitative interpretation: A major band was observed in raw membranes (figure 2.5 lane 1) with 3 minor bands migrating further. These minor bands were lost after solubilization (lane 3 and 4). Interestingly, comparison of the major band of lane 4 and 5 showed that most of the lipids were solubilized. After the anion-exchange column, the lipids were diluted. Their concentrations fell under the lower detection limit of the system. However, after concentration with a membrane-concentrator (vivaspin), a clear band migrating with the same rate as the major band in the total

membrane fraction (lanes 14 and 1) was present. This indicates that indeed a substantial amount of lipid is present with the purified protein. This could be a good sign regarding the stability of the protein purified with this procedure (anion-exchange followed by a NiNTA-column). For further experiments and crystallization trials, this technique will have to be further improved as indicated above. Different protein-purification methods should be tested for their influence on the protein-associated lipids. With synthetic markers it could be possible to identify specific lipids that remain associated with the LmrA-protein.

Interestingly, a very strong 28 kDa-band was observed during all LmrA purifications (see molecular-weight marker F in figure 2.4). This protein seemed to be even higher expressed than LmrA and was easily purified by a cation-exchange column at pH 6 (binding at low salt condition, elution with high-salt, data not shown) and was also separated in sucrose-gradients from the LmrA fractions. We first interpreted this protein as a degradation product. However, since the physico-chemical behavior of this protein was completely different than that of LmrA (bound strongly to cation-exchange material, but LmrA did not bind at all under this conditions or was denatured at low pH and low salt concentration) it seemed not to be derived from LmrA. Wether it was a regulatory factor as speculated (Margreet Moos, personal communication), remains to be clarified. A protein sequencing analysis should shine light onto this.

2.3.2   Crystallization pre-screen

In order to approach the 2D-crystallization as broadly as possible, a screen for suitable detergents was performed. Since there were no transport-assay known for solubilized LmrA, indirect methods had to be used to measure the integrity of the purified LmrA-protein. Unfortunately, there were no "black and white" methods for doing this and many different methods had to be combined to find "good" detergents.

Some of the detergents tested were very efficient in LmrA-solubilization. Other detergents failed to solubilize LmrA or led to quick aggregation of the protein. Many of the successfully solubilizing detergents failed in the NiNTA-binding test. Due to the very small volumes, this experiments have to be repeated several times with different detergent concentrations to confirm these preliminary results.

Of all detergents tested, only the low CMC detergents DDM, $C_{12}E_8$ and Triton X-100, and the high-CMC detergents DM and C_8E_6 were successful in LmrA purification. However, in C_8E_6 the protein aggregated significantly faster than in the presence of low CMC-detergents and DM. Furthermore, in sucrose-gradients C_8E_6 did not keep LmrA in a solubilized state and the protein was only detected in the pellet. During sucrose-gradients, the protein is exposed for a relatively long time (around 20 h) to the test-detergent. However, LmrA purified in $C_{12}E_8$ could be stored for one week at $4°C$ without a major decrease of the concentration of the observed LmrA band in Coomassieblue stained SDS-PAGE (see figure 2.8). This long-term stability test could be improved by a high-speed centrifugation at $100000 \times g$ to pellet aggregated protein before the SDS-PAGE were performed. Possibly, LmrA denatured slowly in C_8E_6 or this detergent solublized LmrA efficiently but in a denatured form. A similar effect was observed with CHAPS in sucrose-gradients, but CHAPS failed also in some

Table 2.2: Lipid-composition of the *Lactococcus lactis*-membrane[a].

Phospholipid	%	Glycolipids	%
Phosphatidyglycerol	14.1	Glycerophosphatidylglycolipid	21.8
Cardiolipin	31.7	Dihexosyldiclyceride	22.6
Lysophosphatidylglycerol	3.2	Monohexosyldiglyceride	3.0
Unidentified	3.3	Unidentified	3.3
total	52.3	total	47.7

[a] Taken from Driessen *et al.*, 1988 [17]

purification test. Interestingly, the C_8E_x-mix 8-POE seemed to be more harsh than C_8E_6 alone, since no purification of LmrA was possible with this mixed detergent.

Due to the broad peaks in sucrose-gradients it was not possible to accurately estimate the oligomeric state of LmrA in the corresponding detergent. However, LmrA solubilized in DM and DDM was detected in the same gradient fractions of the sucrose-gradient, indicating a comparable oligomeric state of the protein in both detergents (data not shown). But major differences in the gradient profiles between DDM, $C_{12}E_8$ and Triton X-100 were observed: in DDM, LmrA revealed a much higher oligomeric state than LmrA solubilized in $C_{12}E_8$ and Triton X-100. The latter two conditions showed a molecular weight compatible with the dimer of LmrA (ca. 128 kDa) plus a micelle (ca. 50 kDa). This could be a sign, that DDM was not the best suitable detergent for LmrA crystallization. However, single particle analysis did not reveal significant differences between LmrA solubilized in DDM and $C_{12}E_8$ or Triton X-100. As already outlined in the result-section, these experiments should be interpreted with care since it was not clear how the detergent belt (and lipid) around the hydrophobic areas of the protein increases the measured protein mass. These findings should be confirmed with other techniques such as size-exclusion experiments, ultracentrifugation and mass measurements by the scanning transmission microscope (STEM). In summary, the sucrose gradient was successful in discriminating detergents stabilizing the LmrA protein (DM, DDM, $C_{12}E_8$, Triton X-100) and detergents leading to aggregation (C_8E_6, CHAPS) but a more detailed discussion about the oligomeric state was difficult.

Intuitively, the oligomeric state of a protein to crystallize is not so important for 2D-crystallization than for the growing of x-ray crystals since the protein is reconstituted into a lipid bilayer where it has a chance to build up the right oligomeric state again. However, the postulated direct crystallization mechanism (see introduction, section 1.3.1) is hindered if the oligomeric state of the protein is not correct in the solubilized form of the protein.

The lipid-screen revealed major differences between the various lipid-detergent-combinations. Best results were obtained with a cardiolipin:POPG-mix, which gave large membrane-areas in combination with $C_{12}E_8$, but not with Triton X100. POPG and *Escherichia coli*-lipids also gave membrane areas, but by far not to the extent as with the above mix. Highly interesting was that the lipid-mix used mimics the lipid-composition of the *Lactococcus lactis* plasma membrane (compare with table 2.2). This result indicates the atractiveness of the use of natural *Lactococcus lactis*-lipids for reconstitution assays. However, around 50% of the *Lactococcus lactis* lipids are glycolipids. This makes them

very difficult to isolate by ethanol-precipitation: Isolated membranes showed very different characteristics such as the solubilization point from isolated batch to batch (personal communication Arnold Driessen and Gerrit Poelarends). Interestingly, there is a complete lack of PE and PS lipids in *Lactococcus lactis*. In contrast a large fraction of the lipids is cardiolipin (31.7%). It is the major component of the unglycosylated lipids. The differences between POPG and the cardiolipin:POPG-mix also stresses the possible important role of cardiolipin for LmrA reconstitution.

The monolayer results were corroborated by the findings of the crystallization experiments: POPG and cardiolipin were building vesicles with bulky borders, a sign for the presence of reconstituted LmrA. Besides these lipids, DMPC could also be a likely candidate for further crystallization trials.

The proposed lipid-screen was only half successful so far, mainly for four reasons:

1. Technically, the monolayer method was very sensitive to mechanical distortions, much more as it was the case for bulk-experiments. This was also due to the fact that very small amounts of materials were used.

2. It was not possible to control the state of the protein by SDS-PAGE after the crystallization process had completed.

3. Since the carbon-film of the grids was not glow-discharged, an irregular staining of the specimens was observed. This complicated the interpretation.

4. The rate of detergent-removal was difficult to control, it is not to exclude that some detergent-lipid combination will be suitable under different detergent-removal-rates than it was usually obtained with the monolayer approach.

However, this technique can be improved in various ways: The crystallization-process can possibly be followed by light-microscopic techniques. The reconstituted lipids can be visualized with fluorescent dyes or brewster-angle microscopy. Detergent-removal could be better controlled by washing away the detergent with buffer (if necessary containing lipid) at slow rates since the protein is bound to the monolayer (personal communication Mohamed Chami). Such technical improvement could make this technique suitable for a high-throughput screening of possible crystallization conditions, which then could be further refined in other crystallization trials.

2.3.3   Crystallization assays

The crystallization assays so far did not lead to LmrA crystals. However, by putting together all the information obtained, the most promising direction for further experiments became apparent: LmrA could be reconstituted in *Escherichia coli*-lipids. This was clearly observed in the reconstitution-experiments with the bio-beads method (figure 2.12). The hight of the spikes sticking out of the membranes were estimated to be around 6 nm. This fits well to the 4.5 Å resolution 3D-structure, in which the not membrane-embedded part had a length of 68 Å (see Chang *et al.*, 2001 [10]). Similar results were observed with POPG and possibly with cardiolipin, but the latter was very difficult to interpret

since the membrane structures were folded together. These results fit very nicely to the findings of the lipid-screen performed with the monolayer-technique, in which POPG and especially POPG:cardiolipin mixtures gave larger and flat membrane-sheets. *Escherichia coli*-lipid extracts also contain around 10% cardiolipin. Interesting are the contrasting results, which were obtained with *Escherichia coli*-lipid: in the batch-method, vesicles were obtained, whereas with all the monolayer-experiments only very rough surfaces have been observed. Since the protein bound with the large (soluble) domain to the monolayer, the small extracellular side of the protein was oriented to the negative stain during the grid preparation. If the protein is properly reconstituted, a flat surface would have been expected. This would then be difficult to distinguish from empty lipid bilayers, although these are not expected to accumulate at the monolayer surface. Given these difficulties it seemed that the monolayer-technique was not a good approach for the *Escherichia coli*-lipid. This raises the question how far the result from one technique can be translated to the other. Furthermore, LmrA could be a bad example for the monolayer technique due to the large and somewhat bulky non-membrane (soluble) part of the protein.

The results of the monolayer technique with DMPC looked interesting but were very difficult to reproduce. DMPC seemed also to be an interesting lipid for the crystallization of LmrA. However, batch-assays with bio-bead detergent-removal have so far only resulted in small vesicles with stiff and bulky borders. If LmrA was properly reconstituted is to the present unclear.

Highly interesting were the results from the detergent-screen: $C_{12}E_8$ and Triton X-100 seemed to stabilize LmrA in a different oligomeric state than DDM. In future, all described experiments should also be done with these detergents. It is recommended that future work on LmrA will focus on the lipids from *Escherichia coli*, POPG, cardiolipin and DMPC. The influence of cardiolipin on the reconstitution of LmrA should be tested systematically. $C_{12}E_8$ and Triton X-100 are the most promising detergents, but also DDM should be used in a standard way. Very important seems to be the method chosen for reconstitution. Especially the rate of detergent-removal seems to be crucial. This should be explored in more precise way in the future. A very useful way to do this could be the dilution machine [61].

2.4 Materials and Methods

2.4.1 Protein-purification

agraphMembrane pre-wash The membranes (1 ml membrane, ca. 25 mg total protein) were first thawed and resuspended in $13ml$ washing-buffer (50 mM KP$_i$ pH 8.0, 10% Glycerol and 100 mM NaCl). In some experiments (see Results) this buffer was supplemented with 1% cholate. The membranes were homogenized with a glass-potter (tight pestle A, three strokes) and centrifuged at 47000 rpm in TFT75.13 rotor (Centrikon) for 30 min at 4°C. The membrane pellet was resuspended with a glass-potter to a homogenous resuspension in the washing buffer without cholate. For the cholate wash, this procedure was repeated without cholate containing buffers to get rid of remaining detergent molecules.

agraphSolubilization For protein-purification, membrane aliquots were first

thawed and complemented with solubilization-buffer (final composition: 50 mM KP_i pH 8.0, 10% Glycerol and 100 mM NaCl). Then the detergent was added (final concentration for DM: 4% or DDM: 2%). The membranes were incubated for $30min$ at 4°C with shaking. To remove insoluble material, the solubilization-cocktail was centrifuged at 47000 rpm in a Centrikon rotor TFT75.13 for 40 min. To prevent proteindegradation, either "comlete preotease-inhibitor" tabs (Roche) or $4mM$ BEFA-bloc (Roche) were used.

agraphPurification over NiNTA-column For binding of LmrA on NiNTA-columns (QIAGEN, Super flow quality), the beads were washed (2 times in H_2O, 2 times in wash buffer 2, see below) and incubated with the solubilized LmrA in a total volume of 40 ml for 3 h at 4°C with gentle shaking in 50 ml Falcon tubes (1 ml for 8 mg LmrA protein). The composition of the binding-buffer was: $50mM$ KP_i pH 8.0, 10% Glycerol, 100 mM NaCl, 1 mM Histidine and detergent (0.5% DM or 0.05% DDM). To prevent protein degradation, the binding-buffer was supplemented with a "complete protease inhibitor tab" (Roche). After binding, the beads were allowed to settle in a Promega column via gravity flow. Subsequently, the NiNTA-bound protein was washed with wash-buffer 1 (50 mM KP_i pH 8.0, 10% Glycerol 100 mM NaCl, 1 mM Histidine and detergent (0.5% DM or 0.05% DDM)) and wash-buffer 2 (50 mM KP_i pH 7.0, 10% Glycerol 100 mM NaCl, $2mM$ Histidine and detergent (0.5% DM or 0.05% DDM)). To remove remaining wash-buffer (and contaminants) the column was centrifuged with 2000 rpm in a Heraus table-top-centrifuge for $1min$. Finally, elution buffer was added to the NiNTA-beads in the smallest possible volume (bed volume) and incubated for 1 h at 4°C (elution-buffer: 50 mM KP_i pH 7.0, 10% Glycerol, 100 mM NaCl, 200 mM Histidine and detergent (0.5% DM or 0.1% DDM)).

agraphAnion-exchange column A 1 ml column was packed with Q-Sepharose (fast flow, Pharmacia) and equilibrated with a low-salt buffer (20 mM KP_i pH 8.0, 0.5% DDM). For all chromatographic work the SMART-system (Pharmacia) was used at 4°C. The solubilized protein was diluted by a factor of two with the low-salt buffer, to give a final volume of 8 ml and loaded on the column with a 10 ml-loop. Finally, the protein was eluted with a NaCl-gradient (high-salt buffer: 20 mM KP_i pH 8.0, 0.5% DDM, 1 M NaCl) and a flow rate of 500 $\mu l/min$. The following program was used: A 4 min wash with the low-salt buffer, then a gradient up to a concentration of 50% high-salt buffer from 4 min to 17 min. Then the column was flooded for 2 min with 100% high-salt buffer and one minute with the low-salt buffer. Fractions of 500 μl were collected, directly supplemented with 5 μl of a strong protease-inhibitor cocktail (1 mM PMSF, 5 mg/ml leupeptin and pepstatin)

agraphThin layer chromatography for lipid analyzation After the protocol developed by Ruiz *et al.*, 1997 [69]. The plates for the thin layer chromatography were prepared as followed: The plates (TLC Silicalgel G-25 20x20cm, 0.25 mm thick, glass-backed Marcherey-Nagel 809013) were impregnated with 1 mM EDTA, pH5.5, by an ascending development, dried in the air overnight and then at 110°C for 1 h. Before separation, the plate were washed overnight in Chloroform:methanol:water=60:40:10 (v/v/v) in the same direction as the impregnation, dried under a stream of hot air (hair dryer) and activated at 110°C for 30 min.

Samples of 1 to 5 μl were spotted 1 cm from the edge of the plate and dried with the hair dryer from the back of the plate. Applications were first

concentrated as fine bands with chloroform:methanol:water=60:40:10 (v/v/v), allowing the solvent to move 1 cm, and then dried by directing a hot air stream towards the back of the TLC plate, ensuring complete removal of water. The lipids were separated stepwise as follows:

- Chloroform:methanol:water=65:40:5 (v/v/v) (to 2 cm)

- Ethylacetate:2-propanol:ethanol:chloroform:methanol:0,25%Kcl= 35:5:20:22:15:9 (to 5 cm)

- toluene:diethylether:ethanol=60:40:3 (v/v/v) (to 7.5 cm)

- n-heptane- diethylether 94: 8 (v/v) (to 10.5 cm)

- n-heptane pure (to 12.5 cm)

Between each step the plates were dried as described above. For the visualization of the neutral and phospholipids, the TLC was first dipped in a solution of 10% cupric sulfate (w/v) and then in phosphoric acid 8% (v/v) for 10 sec. The plate was thoroughly dried under a Stream of hot air until the lipid spots became evident and immediately heated at 200°C for 10 min.

2.4.2 Detergent-screen

agraphSolubilization and NiNTA-binding tests To test solubilization, 40 μl LmrA containing membranes (ca. 0.8 mg total protein) were mixed with 40 μl Buffer A (200 mM KP$_i$ pH 8.0, 400 mM NaCl, 40% Glycerol) and 80 μl detergent (2 times final concentration, see table 2.1). The samples were mixed and incubated for 30 min at 4°C. To separate the solubilized LmrA from the insoluble material, the samples were centrifuged in a Beckmann TLA 100.2 rotor at 55$krpm$ (100000 × g) for 30 min (4°C). 10 μl of the supernatant (corresponding to ca. 5 μg protein) were taken as sample for SDS-PAGE. The pellet was resuspended in 40μl sample buffer (1% SDS, 50% Glycerol, 250 mM Tris pH 6.8, 0.1% Bromphonol blue, 5% Mercaptoethanol) and 10 μl (ca. 20 μg LmrA, if nothing was solubilized) were loaded on the SDS-PAGE.

To test NiNTA-binding, ca. 20 μl Ni-NTA superflow were added to the Supernatant and incubated for 2 h at 4°C. The beads were washed by pelleting the NiNTA-beads by a short centrifugation (Eppendorf centrifuge for 2 min at 2000 rpm) and the resins were resuspended in the wash 1 Buffer (see protocol for LmrA purification). To elute the protein, the resins were pelleted as described and 80μl elution-buffer was added and incubated for 1 h at 4°C. To separate the elution-buffer from the NiNTA-beads, a hole was made in the Eppendorf-tube with a fine needle. The elution-buffer was centrifuged into a second Eppendorf-tube. 10 μl of eluted protein was analyzed on the Coomassie-blue stained SDS-PAGE. The resins were further incubated with 80μl sample-buffer and 20 μl was analyzed on SDS-PAGE as a control for not-eluted protein.

agraphLow scale purification of LmrA For solubilization, 1 ml (ca. 25 mg/ml total protein) of LmrA-containing membranes was mixed with 1 ml of Buffer A (200 mM KP$_i$ pH 8.0,400 mM NaCl, 40% Glycerol) and 2 ml detergent stock (2 times final concentration, see table 2.1, p. 26) and incubated for 30 min at 4°C. To separate solubilized and insoluble material, the samples were centrifuged in a Beckmann centrifuge with a TLA 100.2 rotor for 30 min at 55 $krpm$.

The supernatant was incubated for 2 h at 4°C with 200 μl densely packed NiNTA-beads. Promega-columns were loaded and washed with 10 ml wash-buffer 1 (see protocol for LmrA purification 2.4.1). The protein was eluted with 200 μl elution-buffer (50 mM KP$_i$ pH 7.0, 10% Glycerol 100 mM NaCl, 200mM Histidine and detergent (see table 2.1)). The concentration was determined with Bradford protein assay (Bio-rad).

agraphSucrose-gradients To solubilize the membranes, 50 μl of washed membranes were added to 150 μl of 2xSolubilization buffer (40 mM KP$_i$, 200 mM NaCl, 8mM PEFA-block from Roche) and 150 μl 2xDetergent-stock. The solubilization-cocktail was incubated for 30min at 4°C. Then, the insoluble material was pelleted by centrifugation at 55 $krpm$ (100000 × g) in a Beckmann TLA 100.2 rotor for 45 min.

A modified version of the sucrose gradient described in [94] was used. The sucrose gradients were layered using 533 μl of 7.5%, 10%, 12.5%, 15%, 17.5% and 20% Sucorose-solutions in 5mM KP$_i$, 5mM EDTA, 4 mM BEFA-block and were supplemented with the corresponding detergent (concentration as for the elution-concentration in the low-scale purification-experiments (table 2.1). The solubilized and centrifuged material was layered onto the gradient and centrifuged with a Beckmann TST60.4 rotor (39000 rpm, 150000 × g) for 16 h at 8°C (brakes switched off). Finally, the gradients was dissected in 200 μl fractions and analyzed on SDS-PAGES (Coomassie-blue staining).

2.4.3 Lipid-screen

LmrA was purified as described with the detergent-concentrations indicated in table 2.1. The Histidine was removed with two Sephadex G25 (Pharmacia) spin columns, which were equilibrated overnight in detergent containing buffer. The protein (final concentration of 500 $\mu g/ml$) was mixed with lipid-vesicles (LPR of 2) at a final detergentconcentration of 0.5% for C$_{12}$E$_8$ and Triton X-100, and incubated for 2h at 4°C. Finally, 6 μl of the crystallization-cocktail was injected into the sub-phase of the monolayer (50 mM KP$_i$, 10% Glycerol, 100 mM NaCl and incubated over night for protein binding. To remove the detergent, 5 μl of a densely packed Bio-beads suspension was added, incubated first for 3 h without stirring at room temperature and two additional hours with stirring to complete the detergent-removal. Negative stain (0.75% uranyl formate) electron microscopy grids were prepared without glow-discharging.

Monolayers were prepared as follows: NiNTA lipids (Ni^{2+}-NTA-DOGS and DOGS (Avanti Polar Lipids) were solved in a chloroform:methanol = 9 : 1 mixture at a final concentration of 0.1 mg/ml. 60 μl of the reconstitution buffer was placed in a teflon-well (see Levy *et al.*, 1999 [41]) and 0.6 μl of the monolayer-mix was carefully deposited onto the buffer-droplet. To evaporate the organic solvent, the monolayer were prepared at least 4 h before protein injection.

agraphElectron microscopy of single particles For single particle analysis 3.5 μl of the protein containing solution (100 $\mu g/ml$), was absorbed for 5 s onto glow discharged carbon film-coated copper grids, washed 4 times in distilled water for 5 s and stained with 0.75% uranyl formate. Images were recorded with a Hitachi H-8000 transmission electron microscope (TEM) at 200kV and nominal magnification of 50'000 or 70'000 times on Kodak SO-163 films.

agraphCrystallization with bio-beads LmrA was purified in DDM as described above (p. 44). For crystallization assays, the protein (1 mg/ml) was incubated with *Escherichia coli*-vesicles in 0.5% DDM over night on ice in a total volume of 50 μl. LPRs of 0.5 and 1 were tested, a control mimicking a LPR of 1 was performed without protein. To remove the detergent, bio-beads were added in 4 steps: After overnight incubation, 5μl densely packed Bio-bead suspension was added. This was repeated 3 h and 7.5 h later. The mixture was again incubated overnight and the rest of detergent was removed by the addition of 10 μl Bio-beads. To analyze the crystallization experiments, 3.5 μl sample was absorbed for 30 s onto glow-discharged grids and stained in 0.75% uranyl formate. The lipid (5 mg/ml *Escherichia coli*-lipid) for the lipid-addition experiments was solubilized in 3% DDM, 5% DM, 6% OTG or 6% OG respectively. The final DDM concentration of the crystallization experiments was adjusted to 0.5%.

agraphCrystallization with slide-a-lyzer The crystallization sample was prepared as described for the bio-beads experiments. The lipids 5 mg/ml were solubilized in 3% DDM. 100 μl sample were injected into a slide-a-lyzer device (Pirece, Illinois) and dialyzed against a phosphate buffer 50 mM KP$_i$ pH 8.0, 100 mM NaCl, 10% Glycerol) for 17 days.

agraphCrystallization with monolayer See also protocol for the lipid-screen. The lipids (DMPC, *Escherichia coli*-lipid exctracts, 5 mg/ml) were solubilized in 3% DDM.

Acknowledgments

Chapter 3

The Glycerol Channel of *Escherichia coli*

3.1 The 3.7Å projection map of the glycerol facilitator GlpF: a variant of the aquaporin tetramer [8]

Thomas Braun[1], Ansgar Philippsen[2], Sabine Wirtz[1], Mario J. Borgnia[3], Peter Agre[3], Werner Kühlbrandt[4], Andreas Engel[1] and Henning Stahlberg[1]

[a]M. E. Müller Institute for Microscopy, Universität Basel, Switzerland
[b]Departement of Strcutural Biology, Biozentrum, Universität Basel, Switzerland
[c]Department of Biological Chemistry, Johns Hopkins University School, Baltimore, USA
[d]Max-Planck institute for Biophysics, Frankfurt, Germany

3.1.1 Summary

GlpF, the glycerol facilitator protein of *Escherichia coli*, is an archetypal member of the aquaporin superfamily. To assess its structure, recombinant histidine tagged protein was overexpressed, solubilized in octylglucoside (OG) and purified to homogeneity. Negative stain electron microscopy of solubilized GlpF protein revealed a tetrameric structure of approximately 80 Å sidelength. Scanning transmission electron microscopy yielded a mass of 170 kDa corroborating the tetrameric nature of GlpF. Reconstitution of GlpF in the presence of lipids produced highly ordered two dimensional crystals, which diffracted electrons to 3.6 Å resolution. Cryo electron microscopy provided a 3.7 Å projection map exhibiting a unit cell comprised of two tetramers. In projection, GlpF is similar to AQP1, the erythrocyte water channel. However, the major density minimum within each monomer is distinctly larger in GlpF than in AQP1.

3.1.2 Results

Protein expression and single particle analysis

GlpF carrying ten C-terminal histidine residues was overexpressed in *Escherichia coli*, solubilized and purified in octyl-β-D-glucopyranoside (OG) as de-
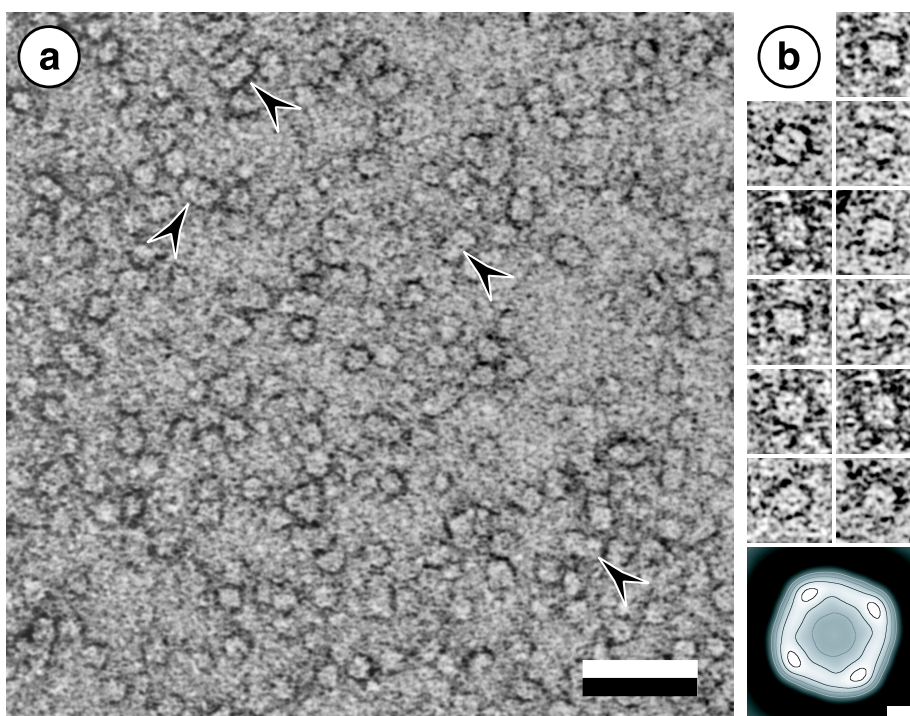
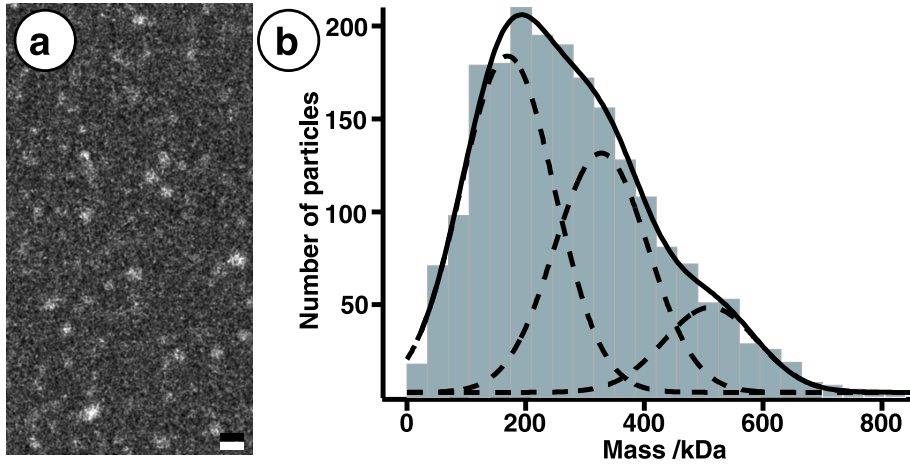**Figure 3.1:** Transmission electron microscopy of solubilized GlpF. *Panel A:* Overview of negatively stained solubilized GlpF in TEM. Randomly oriented particles, often presenting a square shape, are predominant, but complexes of approx. twice the size are also seen (arrows). Scale bar corresponds to 450 Å. *Panel B:* Selected square-shaped particles. Image side length corresponds to 230 Å. Large inset: 4 fold symmetrized average after reference free single particle analysis. Scale bar corresponds to 20 Å.

scribed in [7]. Analysis of purified and solubilized GlpF by SDS-PAGE revealed a prominent band at an apparent molecular weight of 30 kDa. GlpF purified in this way is functionally active (Borgnia *et al.*, personal communication). Transmission electron microscopy (TEM) of negatively stained solubilized GlpF revealed two different particle populations (figure 3.1, panel A): Smaller, often square shaped particles and larger complexes of about twice the size of the small ones (arrows). Tilting of the tetramers possibly related to the histidine tag [66] may explain the heterogeneous appearance of the small particles. Nevertheless, 1294 single particles were selected automatically (figure 3.1B), windowed and subjected to reference-free alignment [55]. The resulting square-shaped average projection that had a side-length of about 80Å and four weak peripheral densities (figure 3.1B; large inset) .

Purified GlpF particles were also freeze-dried and imaged with a scanning transmission electron microscope (STEM) for mass-measurements [49]. The low dose dark-field image in figure 3.2A shows particles of different brightness and size, whose masses were calculated and sorted in a histogram after mass-loss correction (figure 3.2B); [50]. The mass histogram resulting from the analysis of 100 images (2073 particles in total) exhibits a broad asymmetric distribution with a single maximum at about 190 kDa. Two independent Marquardt al-

Figure 3.2: Scanning transmission electron microscopy (STEM) of solubilized GlpF. *Panel A:* Dark-field STEM image of freeze-dried solubilized GlpF recorded at 3.3 e/Å^2. Scale bar corresponds to 100 Å. *Panel B:* Result of STEM mass–measurements. The mass histogram comprising 2073 measurements was fitted with two significant Gauss peaks at 170 kDa (total error of $\pm 12 kDa$) and $327 \pm 20 kDa$ respectively, and a minor peak at $511 \pm 31 kDa$.

gorithms (see Methods) produced a three-peak fit with Gauss-profiles having a standard deviation of 111 kDa were located at 170 kDa, 327 kDa, and 511 kDa. The experimental errors for these three peaks were estimated to 12 kDa, 20 kDa and 31 kDa, respectively, taking the standard deviation, the number of particles within a peak and the calibration accuracy into account. 170 kDa is compatible with a GlpF tetramer including the four His-tags and their spacers (12 kDa), plus 60 kDa of octylglucoside accounting for two micelles [92]. Thus, 327 kDa corresponds to an octamer and 511 kDa to a dodecamer. The abundance of tetrameric particles documented by the mass histogram is consistent with the results from negatively stained preparations (figure 3.1A) .

Two-dimensional crystallization

Solubilized GlpF was reproducibly crystallised using a continuous flow dialysing device [34] as described in the Methods section. Analysis in the TEM showed polycrystalline vesicles with diameters up to $40\mu m$ and mostly mono-crystalline double layered sheets with rectangular shapes and diameters up to 8 μm (figure 3.3A) . Some tubular structures were seen in many reconstitution experiments. However their crystallinity was far inferior to that of the double layered sheets. The crystal quality of the latter was assessed by electron diffraction of frozen-hydrated samples. The diffraction pattern recorded with a $1k \times 1k$ CCD camera shows spots beyond 3.6 Å (figure 3.3B) but weak structure factors between 7 and 5 Å. The 4 (28,7) orders marked by arrows corresponds to a resolution of 3.6 Å. Since the two layers were rotated with respect to each other, two lattices are indicated.
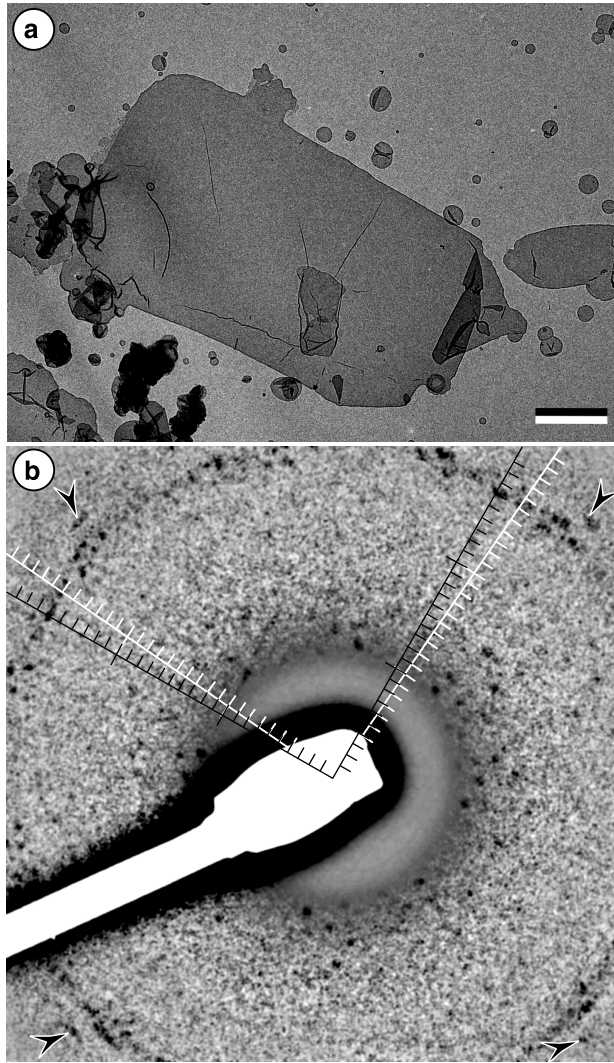
Figure 3.3: Two-dimensional (2D) crystal of GlpF reconstituted in the presence of lipid. *Panel A:* The rectangular double layered crystals were usually mono-crystalline and well ordered and had sizes of several micrometers in diameter. Scale bar corresponds to $2\mu m$. *Panel B:* The electron diffraction pattern of a frozen hydrated 2D-crystal demonstrates the excellent crystallinity of such rectangular crystals. Two different lattices of the double layered crystal are overlaid. Two hair crosses indicate the superimposed lattices. Diffraction orders marked by arrows correspond to a resolution of 3.6 Å. The scale bar represents $1/10$ Å^{-1}.

Electron Microscopy and Image treatment

Images of negatively stained crystals were recorded in a TEM and analysed by correlation averaging [2]. The unit cell containing two tetrameric structures exhibited a p4 symmetry. Adjacent tetramers were differently stained similar to AQP1 crystals [92], indicating their up-down orientation (data not shown).

Images of frozen hydrated crystals recorded at low dose revealed sharp spots when examined by optical diffraction out to a resolution of 7 Å. The 8 best images were digitised and processed by the MRC program package [27, 28]. The unit cell size was determined to 104 Å. The phase residuals of the merged data obtained after lattice unbending and transfer function correction indicated significant information up to a resolution of 3.7 Å (table 3.1), yielding the projection map shown in figure 3.4. In contrast to AQP1 crystals with $p42_12$ symmetry, the GlpF crystals exhibit a p4 symmetry (table 3.2), since oppositely oriented tetramers are rotated about their four-fold axes by different amounts. Thus, the striking similarity of the two oppositely handed tetramers shown in figure 3.4 demonstrates the quality of the map.

**Table 3.1:** Phase residuals in resolution ranges (random=90°)

Resolution	IQ value[a] $\left(\frac{Signal}{Noise} \approx \frac{8}{IQ}\right)$							Weight.[b]
from − to /Å	1	2	3	4	5	6	7	residual:
200 − 9.9	5.7	14.8	23.0	37.7	41.0	48.5	47.6	14.4
	299	324	212	123	109	74	44	1185
9.8 − 7.0	7.6	10.1	17.2	24.0	40.5	47.7	44.6	24.3
	17	64	143	161	131	120	70	706
7.0 − 5.7		31.9	18.2	30.9	37.0	47.4	44.6	24.3
		1	25	70	128	97	84	405
5.7 − 4.9		40.4	32.3	32.0	47.3	47.6	66.9	39.1
		1	17	40	92	86	93	329
4.9 − 4.4			47.5	55.9	57.3	69.0	64.6	60.9
			13	49	92	86	80	320
4.4 − 4.0			47.5	55.9	57.3	69.0	64.6	60.9
			15	45	71	97	81	309
4.0 − 3.7			62.8	41.8	57.0	62.3	55.7	55.9
			3	38	86	105	84	316
3.7 − 3.5			26.3	62.1	77.2	79.4	82.6	74.0
			8	27	63	80	79	257
3.5 − 3.3			59.8	87.8	75.2	91.4	79.9	82.0
			6	27	65	73	70	241

[a]Spots are classified according to [28]. Phase residuals (in degree, top line) during merging and the number of spots (bottom line) in each class are given for different resolution ranges.
[b]IQ-weighted phase residuals: The phase was multiplied with a corresponding weightening factor to the IQ value (ex. the phases of IQ1 spots were multiplied with 9).

3.1.3 Discussion

Here we present the first structural analysis of GlpF, the archetypal member of the GlpF subcluster of the aquaporin superfamily [31]. Negative stain electron
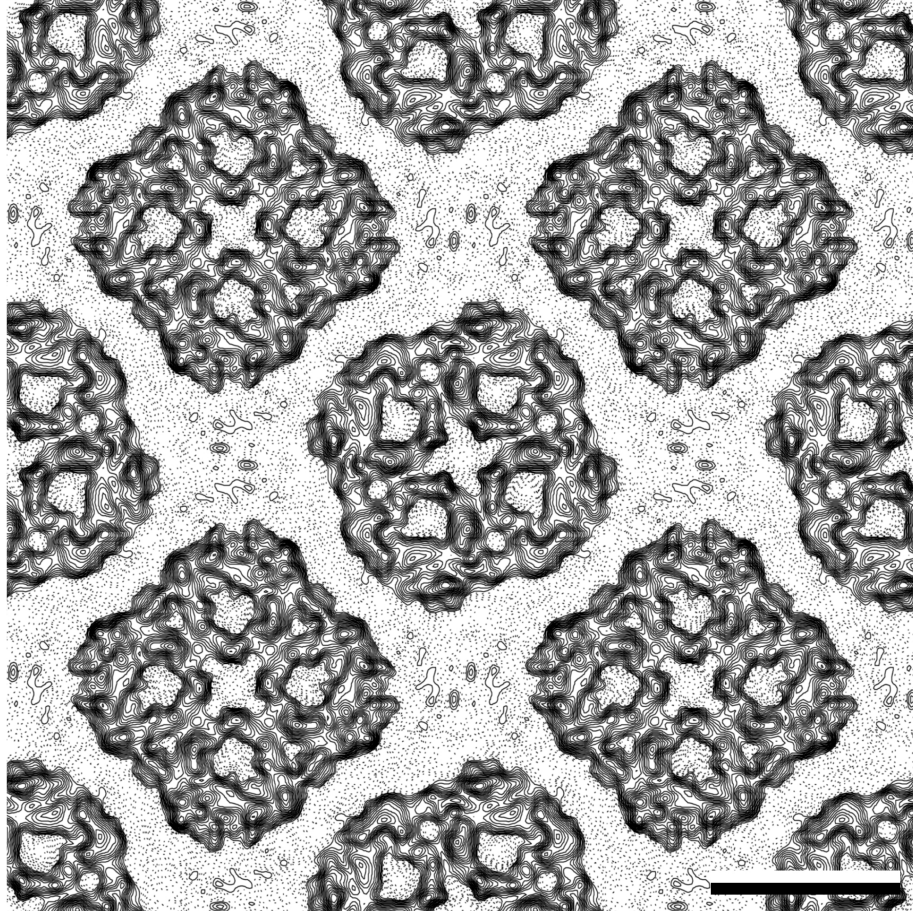
Figure 3.4: The p4-symmetrized 3.7 Å projection structure of GlpF. The map was calculated by merging 8 electron micrographs after unbending crystal distortions and correcting the transfer function. The phase residuals indicated significant information up to 3.5 Å resolution (see Table 3.1). A negative temperature factor of –20 Å^2 was applied. Scale bar corresponds to 50 Å.

Table 3.2: Lattice data of GlpF crystals

|	
Plane Group Symmetry:	p4
Lattice constants	$a = b = 104$Å
Number of Images:	8
Resolution limit for merging:	3.7Å

microscopy and mass-measurements of freeze-dried unstained preparations in the STEM demonstrate that octylglucoside solubilized GlpF exhibits the same tetrameric structure as other aquaporins previously studied: AQP1 [74, 92], AqpZ [66], MIP [26], and TIP [13]. This result is in contrast with reports of monomeric GlpF and the hypothesis that glycerol facilitators are monomeric whereas water channels require tetramerization [9, 40]. However, the apparent tetrameric nature of GlpF reported here is consistent with the model proposed by [89] that GlpF interacts with the tetrameric glycerol kinase GlpF to stimulate glycerol phosphorylation.

In our hands, GlpF crystallised under similar conditions as AQP1 [93], but at pH 8.5 instead of pH 6 and at much lower $MgCl_2$ concentration. The p4 unit cell houses eight GlpF monomers, has a side length of 104 Å and is thus 8% larger than the $p42_12$ unit cell of AQP1 (96 Å; [92]). Electron diffraction experiments, yielding diffraction maxima to 3.6 Å, document the crystalline quality of these double-layered sheets and suggest their suitability for structure determination at atomic resolution. This is further supported by the 3.7 Å projection map obtained by processing images of frozen-hydrated crystals recorded at liquid helium temperature. It is interesting to compare the first high-resolution projection structure of the archetypal member of the GLP sub-cluster with that of AQP1, the first aquaporin structurally analyzed to high resolution (figure 3.5; [11, 42, 48, 91, 92]). The density maxima marked in the AQP1 (figure 3.5B) map appear to be slightly shifted and of different amplitude than the maxima in the GlpF map (figure 3.5A). They are related to six tilted helices that surround a central structure produced by loops B and E [48]. According to the hourglass model [36], these loops are close to the channel (marked by an X in figure 3.5). Thus differences between GlpF and AQP1 in this region are of particular interest. While the projection map of AQP1 shows a weak density at this position, GlpF seems to have a much larger hole with no inner structure discernible in the projection map.

The striking similarity of the GlpF tetramers of opposing handedness in figure 3.3 suggests that that their four-fold axes were parallel to the optical axis of the microscope, similar to the situation of the AQP1 crystals. Hence, tilting of tetramers can be excluded as a major reason for the differences observed. Another possibility could be that the pore of GlpF is parallel to the four-fold axis of the tetramer, whereas the AQP1 channel is tilted. Nevertheless it is more compelling to speculate that the apparently larger pore is required for the diffusion of glycerol and other small anionic solutes [44]. How such a pore prevents passage of protons and other ions is a mystery still to be enlightened. The highly ordered 2D crystals presented here are a first essential step towards this goal.

3.1.4 Methods

Protein expression A construct of GlpF with a 10-Histidine tag at the N-terminus was overexpressed in *Escherichia coli*, solubilized in octyl-β-D-glucopyranoside (OG) and isolated by Ni-chelation chromatography [7, 66]. The solubilized protein was stable in 3% OG at 4°C for weeks and could be concentrated by centrifugation to 12 mg/ml without precipitation.
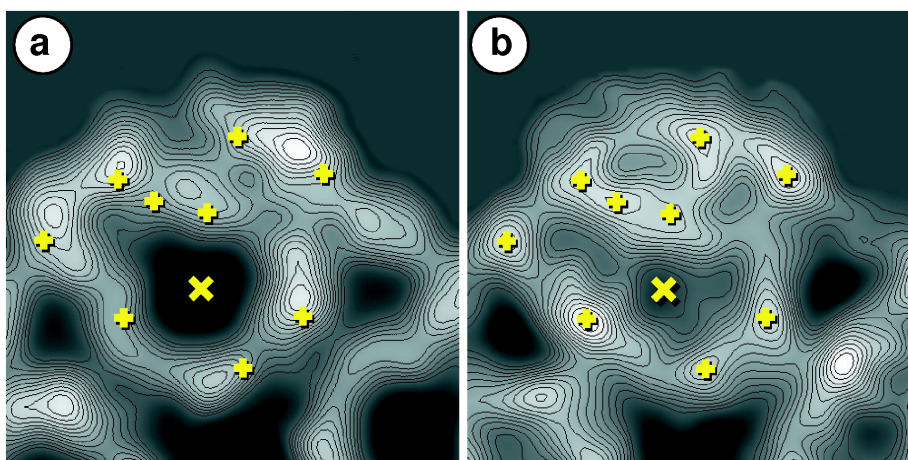
Figure 3.5: Comparison of GlpF and AQP1 at 4 Å resolution. *Panel A:* GlpF monomer. *Panel B:* AQP1 monomer. Overlaid crosses mark the position of density maxima found in AQP1. The depression in the AQP1 monomer, thought to represent the pore, is marked by an "X". The most prominent difference revealed by the GlpF monomer is the central depression of approx. 10 Å diameter, which is significantly larger than the one in AQP1 that exhibits a complex shape. Further differences are seen in the surrounding density maxima. They correspond to the projection of over-lapping highly tilted helices. The minima around the four–fold axes and between the monomers are rather similar. The image side length corresponds to 41 Å.

Crystallization   The GlpF was dialyzed in a continuous flow dialysis machine [34] against a buffer containing 10 mM Tricine pH 8.5, 5 mM $MgCl_2$, $100mM$ $NaCl$, 10 mM DTT and *Escherichia coli*-lipid (Avanti Polar lipids, Inc. USA) with a lipid-to-protein ratio (LPR) ranging from 0.6 to 1.4 (w/w) using the following temperature profile: 25°C for 12 h, a linear increase to $40°C$ over the next 12 h, 40°C for 24 h and a linear decrease to 25°C over 6 h. Protein concentrations between 1 and 3 mg/ml were used.

STEM mass determination   Purified GlpF (50 $\mu g/ml$) was absorbed to thin carbon films, extensively washed with quartz distilled water, freeze-dried, and imaged with a Vacuum Generators HB5 STEM at doses of approx. 3.3 $e/Å^2$ [49]. The IMPSYS software package was used to extract mass values of all particles discernible on the dark field images. These values were corrected for the experimentally measured dose-associated mass-loss [50], distributed in a histogram and approximated by Gaussian curve fitting with a Marquardt algorithm [3]. The mass values were also analysed using a commercial program (Igor pro[1]) for Histogram calculations and Gauss-peak fitting by a Levenberg-Marquardt algorithm. The total experimental error was calculated as the standard error of the mean, plus 5% of the measured particle mass to account for the absolute calibration uncertainty.

Transmission Electron Microscopy   For single particle analysis the protein (50 $\mu g/ml$) sample was absorbed for 5 s onto glow discharged carbon film-

---

[1] www.wavemetrics.com

coated copper grids, washed 3 times in distilled water for 5 s and stained with 0.75% uranyl formate. Images were recorded under low-dose conditions with a Hitachi H-8000 transmission electron microscope (TEM) at 200kV and nominal magnification of 50'000 on Kodak SO-163 films. For cryo-electron microscopy grids were prepared by the back-injection technique [32] with 1 % trehalose, quickly frozen in liquid ethane and transferred with a Gatan 626 cryo holder into a Hitachi H-8000 TEM. Images were recorded at 90 K at 200 kV and 50'000x nominal magnification on Kodak SO-163 film, using a home made spot-scan and low dose set-up programmed on the Tietz CCD remote control system (Tietz Video & Imaging Processing System, Gauting, Germany). The dose per negative was 5 $e/\text{Å}^2$. Electron diffraction patterns of vitrified crystals were acquired by the $1k \times 1k$ Tietz-CCD camera. Alternatively, images were recorded with a JEOL 3000SFF (MPI for Biophysics, Frankfurt) in spot scan mode and operated at 300kV, 4.2 K and 70'000x nominal magnification. The dose for recording an image was 17 $e/\text{Å}^2$.

Image processing   Micrographs of negatively stained samples were digitised using a Leafscan-45 scanner (Leaf Systems, Inc., Westborough, MA, USA) at 4Å/$pixel$ at the specimen level. Single particles were picked automatically, windowed, aligned with a reference-free alignment procedure [55], and classified, using the SPIDER software [21].

Cryo-TEM negatives of 2D crystals were digitised using a ZEISS Phodis scanner (Carl Zeiss, Oberkochen, Germany) at 1 Å/$pixel$ on the specimen level. Image processing was performed with the MRC-software package [27, 28]. In a first run, images were unbent three times, using the Fourier-filtered images themselves as a reference. The merged amplitudes and phases from 8 images were then used with the program MAKETRAN to create two synthetic references, applying two different negative temperature factors. All images were now unbent using the reference with the smaller negative temperature factor. The unbent images were then refined by unbending them a second time, using the reference with the stronger negative temperature factor, this time allowing only very small (5 $pixel/unitcell$) displacements of the units cells.

To compare the GlpF and AQP1 monomers, the SEMPER software was used. First, the non-crystalline symmetry in the GlpF crystals was applied (mirroring and rotational alignment of the two adjacent tetramers) to approach the $p42_12$-symmetrization used for AQP1. The monomers of GlpF and AQP1 were then interpolated to the same scale, aligned translationally and rotationally, and displayed with identical gray-value level-ranges and contours to aid comparison.

Acknowledgments

3.2 The 6.9 Å structure of GlpF: a basis for homology modeling of the glycerol channel from *Escherichia coli* [75]

Henning Stahlberg[12], Thomas Braun[12], Bert de Groot[4], Ansgar Philippsen[3], Mario J. Borgnia[5], Peter Agre[5], Werner Kühlbrandt[6] and Andreas Engel[2]

[a]These authors contributed equally to this work

[b]M. E. Müller Institute for Microscopy, Universität Basel, Switzerland

[c]Departement of Strcutural Biology, Biozentrum, Universität Basel, Switzerland

[d]Max-Planck-Institut for Biophysical Chemistry, Göttingen, Germany

[e]Department of Biological Chemistry, Johns Hopkins University School, Baltimore, USA

[f]Max-Planck institute for Biophysics, Frankfurt, Germany

3.2.1   Summary

The three-dimensional structure of GlpF, the glycerol facilitator of *Escherichia coli*, was determined by cryo-electron microscopy. The 6.9 Å density map calculated from images of two-dimensional crystals shows the GlpF helices to be similar to those of AQP1, the erythrocyte water channel. While the helix arrangement of GlpF does not reflect the larger pore diameter as seen in the projection map, additional peripheral densities observed in GlpF are compatible with the 31 additional residues in loops C and E, which accordingly do not interfere with the inner channel construction. Therefore, the atomic structure of AQP1 was used as a basis for homology modeling of the GlpF channel, which is predicted to be free of bends, wider, and more vertically oriented than the AQP1 channel. Furthermore, the residues facing the GlpF channel exhibit an amphiphilic nature, being hydrophobic on one side and hydrophilic on the other side. This property may partially explain the contradiction of glycerol diffusion but limited water capacity.

3.2.2   Results and Discussion

Data collection and processing

Figure 3.6 shows IQ-plots [28] of an untilted and a 60° tilted lattice recorded in a spot scan mode by a JEOL 3000 SFF electron microscope. The corresponding projection maps were calculated after lattice unbending and contrast transfer function correction, using the MRC program package [12]. Since highly ordered GlpF lattices consisted always of two layers, both were processed, requiring determination of the sidedness. This was unambiguous for the 0°, 30° and 45° images, but difficult for the 60° images, of which only those 5 with clearly distinguishable sidedness were included in the merging process. After determining sidedness and phase origin, the images were merged, imposing p4 symmetry.

The azimuthal projection of the collected three-dimensional data set is shown in figure 3.7a . To calculate the 3D-map, lattice lines were fitted and interpolated (3.7b). The phase residuals of the merged data indicated significant structure information up to 6.9 Å (table 3.3). Because spots from the two overlapping lattices were not sufficiently separated in the electron diffraction patterns recorded with our 1k CCD, amplitude data obtained from the images were taken to calculate the 3D density map.
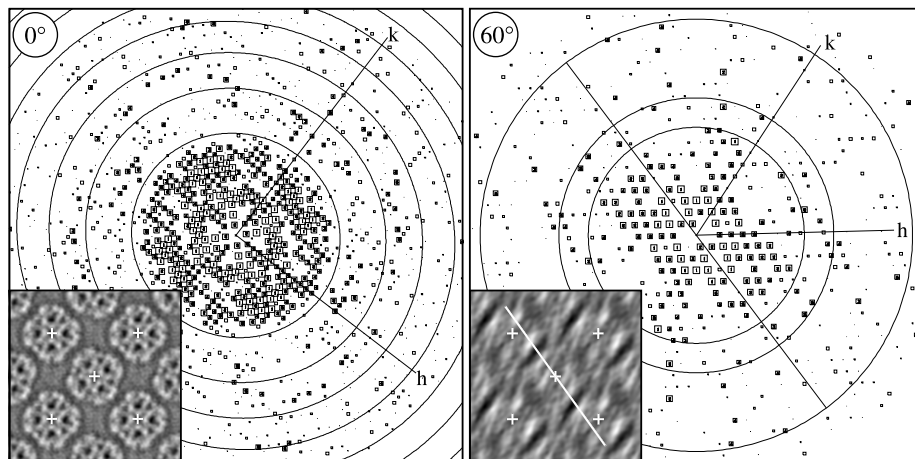
Figure 3.6: Power spectra (IQ-plots)[28] of the unbent images and calculated projection maps (insets) of an untilted sample (left) and a 60° tilted sample (right). The reciprocal lattice axis are indicated (h and k). In the 0° IQ-plot, the zero crossings of the contrast transfer function are marked by the concentric lines. In the 60° IQ-plot, the circles indicate resolution limits of 7.5, 5.0 and 3.5 Å, respectively. The tilt axis is represented by a straight line in the IQ-plot and in the projection map. The projection maps show four unit cells, which have dimensions $a = b = 104$ Å. The crosses mark the centers of the tetramers.

Table 3.3: Phase residuals in resolution ranges

Crystallographic data:[a]	
Plane group symmetry	p4
Unit cell	$a = b = 104$Å
Number of processed images:	48
Number of processed lattices:	73 (0˚: 9; 30˚: 28; 45˚: 31; 65˚: 5)
Number of merged phases:	16273
Maximum tilt angle:	61°
Phase residual (200–6.9Å):	Overall: 49˚ (IQ-weighted: 25˚)
R-factor (200–6.9Å):	Overall: 0.540 (IQ-weighted: 0.767)
Resolution limit for merging:	In plane (x,y): 6.9Å
Normal to plane (z): 10Å	
Completeness:[b]	68.0%

[a]Phase residuals, R-factors and Number of merged phases were calculated with the program LATLINED.

[b]Only reflections within the resolution volume having a figure of merit over 0.5 were included; the missing cone comprises 13% of this volume.
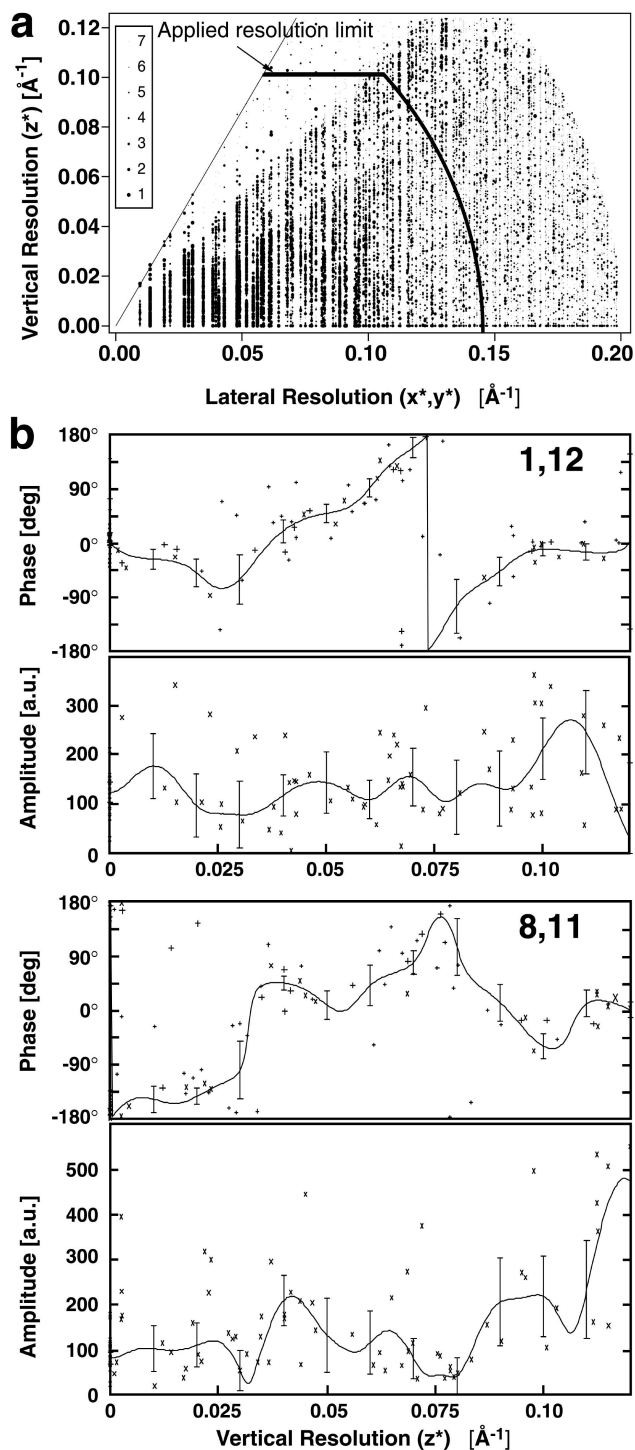
Figure 3.7: *Panel A:* Azimuthal projection of the three-dimensional data in the asymmetric quadrant, showing the data sampling. The limit of the missing cone is marked by a thin line. The size of the data points indicates their IQ-value[28], a reference scale is given in the inset. The largest spots correspond to IQ=1, the smallest to IQ=7. Changes in sampling densities reflect the data collection at 30°, 45° and 60°. Despite the presence of data at higher resolution, the resolution limit was set to $(6.9 \text{ Å})^{-1}$, in z-direction to $(10 \text{ Å})^{-1}$, as indicated by the solid line (Table 1). *Panel B:* Amplitudes and phases along the lattice line 1,12 and 8,11. The curves were calculated by a least-square algorithm from the experimental values of 73 images: 9 from untilted samples, 28 at 30° tilt, 31 at 45° tilt and 5 at 60° tilt. These curves were sampled at $(100\text{Å})^{-1}$ to obtain a 3D data set of structure factors. The error bars are a measure of the data quality.
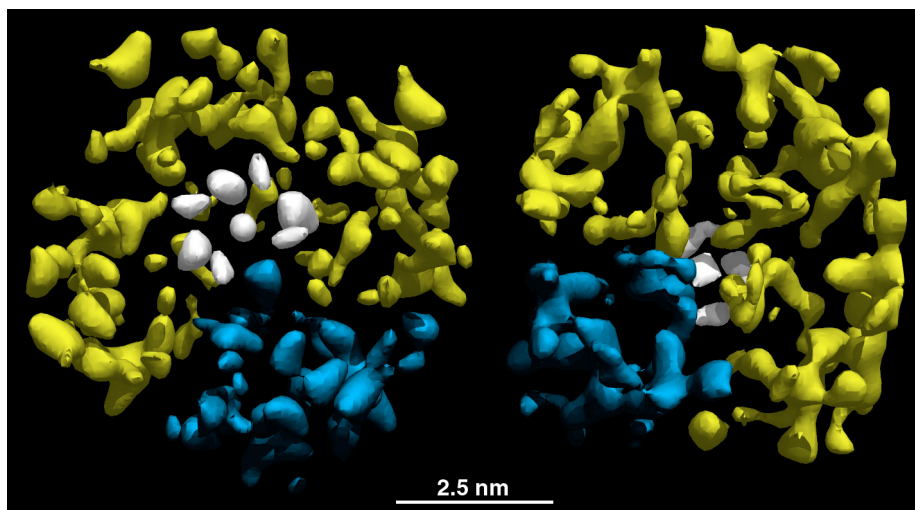
**Figure 3.8:** The two oppositely oriented tetramers of one unit cell, seen at $20°$ normal to the membrane plane. One monomer of each tetramer is highlighted in blue. The periplasmic density about the four-fold symmetry axis is shown in white. Due to the non-crystallographic symmetry between the two tetramers, data were merged imposing p4 symmetry. Rotating the left tetramer by $180°$ around the horizontal axis and then by $30°$ around its four-fold axis superposes it on the right tetramer. The in-plane distance between the tetramer centers is 73.5 Å.

The 6.9 Å 3D map of GlpF The emerging 3D density map (figure 3.8) reveals two tetramers in opposite orientations (correlation coefficient 0.69 after aligning one tetramer with the inverted second tetramer, but 0.50 without inversion). The tetramers exhibit an overall similarity to the AQP1 tetramer [91], but show on one side a density peak about the four-fold axis.

The GlpF monomer (figure 3.9) comprises six highly tilted rod-like structures that surround a central density. Since the two tetramers of one unit cell are not related by crystallographic symmetry [8], the reproducibility of pertinent features can be assessed by superposition of the two independent monomers (figure 3.9a, b; shaded and wire frame surfaces). The resolution estimated from their Fourier shell correlation coefficient is 8.1 Å [82], compatible with the resolution limits imposed for merging the data (table 3.3; figure 3.7). Compared to the AQP1 monomer rendered at 6.9 Å resolution (figure 3.9c), GlpF exhibits distinct additional domains (D1-D5) that are present in both independent 3D maps, although D3 is weaker in the shaded map (figure 3.9a, b). Therefore, these domains are genuine features of the GlpF structure that are probably related to sequence differences between GlpF and AQP1.

Comparison of GlpF with AQP1

To compare the 6.9 Å structure of GlpF with the atomic model of AQP1 [51], the independent GlpF monomers shown in figure 3.9 were merged and their sidedness determined by three criteria: (1) The side protruding further out of the membrane was identified as extracellular as observed for AQP0, AQP1 and AqpZ by atomic force microscopy [19]. (2) A systematic search for the best-
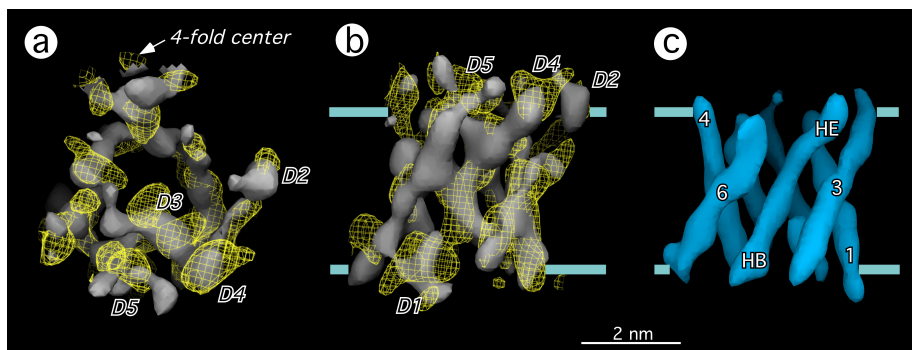
Figure 3.9: Comparison of independent 3D density maps of GlpF with AQP1. The two independent GlpF monomers are represented as shaded and wire frame surfaces; a, Top view from the periplasmic side; b, Side view from outside the tetramer. c, Equivalent side view of the AQP1 monomer rendered at 6.9 Å resolution. The membrane surfaces are indicated by light blue lines.

fitting orientations of an α-carbon model of the structure of AQP1 in the 3D map of GlpF [16] showed that the orientation with the more protruding surface being extracellular fits better (with a "rottrans" score of 0.62; see materials and methods) than orientations with the opposite sidedness (with a score of 0.51). (3) The deviation of helix 1 from the quasi two-fold symmetry of the monomer with respect to an axis in the membrane plane [11, 42], which is more pronounced in GlpF than in AQP1, allowed helix 1 and hence the sidedness to be identified. This assignment corroborated the results of criteria (1) and (2). The superposition of the GlpF monomer and the AQP1 atomic model shown as ribbons (figure 3.10) confirms the strong similarity of these molecules as already suggested by figure 3.9. While the match of the two structures is pronounced in their centers, distinct differences are seen at the cytoplasmic surface (D1) and the extracellular surface (D2-D5). Considering the GlpF sequence (figure 3.10e), additional residues at the N-terminus are tentatively assigned to domain D1, the additional residues in loops C (Y99-H119 and V126-A132) to the extension of helix 3 (D2) and a density closer to the interior of the monomer (D3), and additional residues in loop E (A218-D229) to the extensions of helix HE (D4) and helix 6 (D5). Since loop regions are always less well defined than the helices, higher resolution data are required to prove this hypothesis. However, the 6.9 Å map clearly shows that the additional residues in loops C and E do not restrict the channel but are found at the surface of the protein, located mainly at the periphery of the tetramer.

Homology modeling of GlpF channel

The pronounced structural similarity of GlpF and AQP1 shown in figure 3.10a-d and the strong conservation of critical residues [30] prompted us to build a model of the glycerol channel based on the AQP1 atomic model: In a first step all AQP1 residues were replaced by residues of GlpF, using the alignment based on multiple sequence analysis shown in figure 3.10e. This resulted in an overall reduction of the mass protruding into the channel by approx. 100 Da. With the exception of the site with the two aromatic residues W42 and Y138, a general
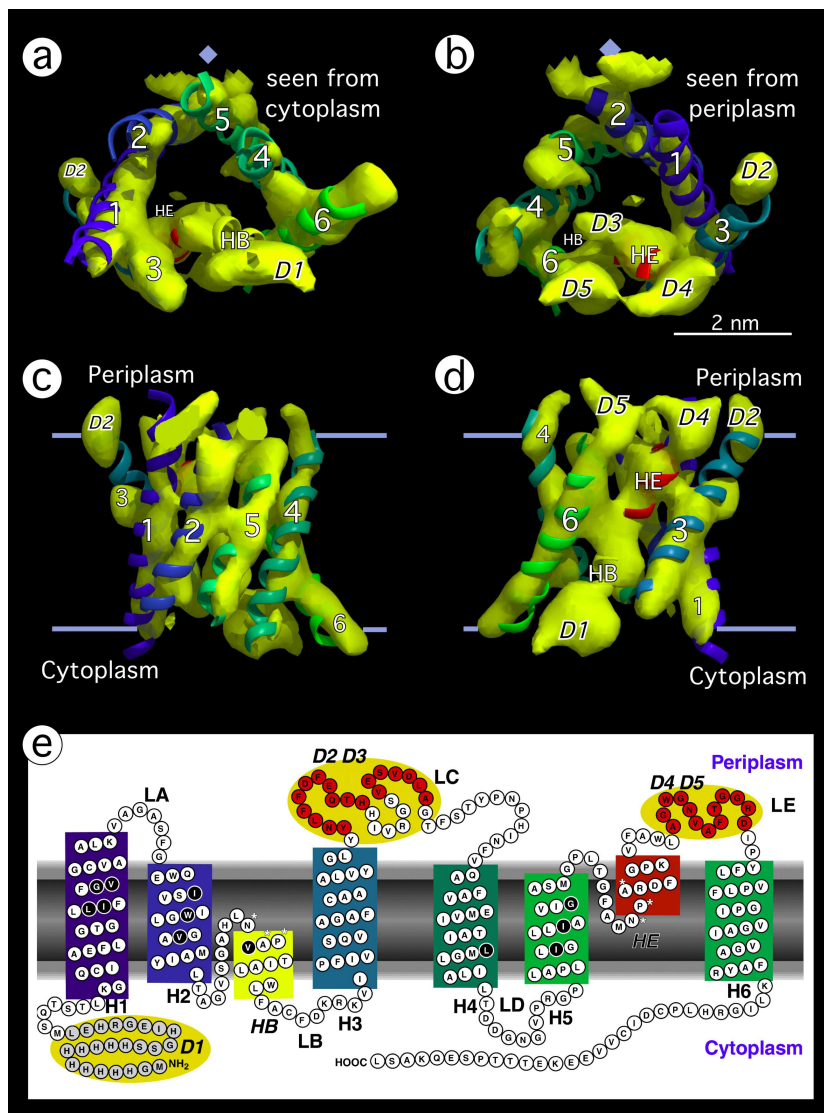
Figure 3.10: Superposition of the averaged GlpF monomer (yellow shapes) with the AQP1 atomic model (colored a-helices; [51]). Numbers indicate the helix segments of the primary sequence. The helix assignment was determined by cryo-electron microscopy [51], and also confirmed by sequence comparison [30] as well as directionality pattern analysis [16]. Helical segments in loops B and E are indicated by HB and HE. Additionally identified densities are labeled D1 through D5, see text. a,b, Top views from cytoplasmic and periplasmic side. c,d, Side views as seen from the four-fold symmetry axis of the tetramer (c) and from outside the tetramer (d). The helices of GlpF are highly tilted (H1: 28° against z-direction, H2: 23°, H3: 37°, H4: 22°, H5: 21°, H6: 38°). The maps are generated using the programs DINO and POVRAY (see Methods p. 64). (e) Topology model of GlpF, showing six transmembrane helices and two short helices in the functional loops B and E. The N-terminal 10-His tag and 11 spacer amino acids are shown in grey, while stars mark the NPA motifs. Black circular disks indicate the sites proposed to face the channel, based on the atomic model (Murata *et al.*, 2000 [51]) and alignment of 164 sequences (Heymann and Engel, 2000 [30]). GlpF has in comparison with AQP1 inserts of 18 residues in the periplasmic loop C and 13 residues in loop E, as displayed in red. The proposed interpretation of the peripheral densities D1 through D5 are marked by yellow areas.

.

widening of the channel was observed. A subsequent database search for possible orientations of Trp and Tyr in environments with similar backbone conformations revealed an alternative and equally probable orientation of these residues that eliminated the narrowing of the channel at this position [90]. Projection maps of both the atomic model of AQP1 and the putative GlpF model were then calculated to compare them with the experimental projection maps. While the excellent correlation between calculated and experimental map of AQP1 validates the approach to test an atomic model with a high-resolution projection map (Figure 3.11a), the wider pore region observed in the experimental projection map of GlpF is also observed in the calculated map (Figure 3.11b). This suggests that the structural model of the glycerol channel is correct within the experimental error.

To reveal the shape of the channel, the accessible channel surfaces were probed with the program HOLE [73]. While AQP1 exhibits a distinct eyelet with a minimal diameter of 2.8 Å that is close to a pronounced bend of the channel (Figure 3.11c), the GlpF channel appears to be slightly larger, rather uniform in size and free of bends, having a minimal pore diameter of 3.3 Å (Figure 3.11d). The bend in the AQP1 channel is related to F24, which is replaced by a Leu in GlpF. While 63% of the so far identified water channels have the residue pairs Phe/X (with X being mostly Leu) that form part of the eyelet [51], 15 out of 19 GLP subtypes exhibit the pair Leu/Leu, two Leu/Met and two Leu/Phe [30]. In some aquaporin subtypes, a Tyr is present instead of F24. Among these are AQP0 reported to possess pH dependent water capacity [53, 96], and AQP6, which becomes a chloride channel at pH 5.5 [95]. This indicates a possible role of Y24 in channel gating. Finally, the channel surrounding residues exhibit an amphiphilic nature: One side is hydrophobic, while the other is hydrophilic (Figure 3.11e). Thus, the glycerol channel has properties akin to maltoporin with its greasy slide that promotes passage of maltodextrins [72]. This property may partially explain the contradiction of glycerol diffusion but limited water capacity [44].

3.2.3   Conclusions

Electron crystallography combined with homology modeling is a powerful approach to elucidate the structure of a membrane protein. Strong sequence conservation within the aquaporin family, the structural homology between GlpF and AQP1 and the availability of an channel. The validity of this approach will be assessed by comparing the model with the structure determined by X-ray crystallography to 2.2 Å [23].

3.2.4   Methods

Cryo-electron microscopy   GlpF was over-expressed in *Escherichia coli*, purified on a Ni-column and 2D crystallized as described [8]. For cryo-electron microscopy [18], grids were prepared by trehalose embedding [32]. All microscopic work was done within ten days. Images were recorded at various tilt-angles up to 60° with a JEOL 3000SFF in spot scan mode, working at 300 kV, 4.2 K, and 70'000x nominal magnification with an electron dose of approx. 17 $e-/Å^2$. The loss of resolution normal to the tilt-axis in images of tilted samples was significantly reduced by employing the spot-scan procedure. Negatives were
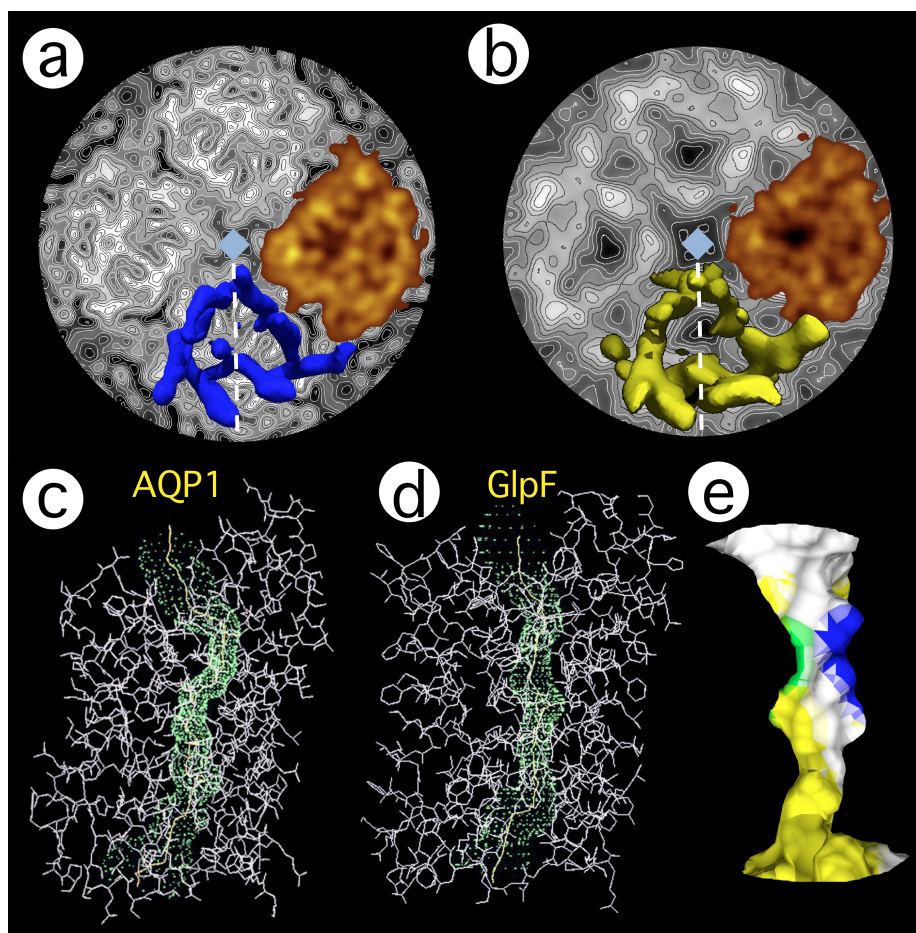
Figure 3.11: Atomic modeling of the GlpF based on the structure and sequence homology of GlpF and AQP1 and the atomic structure of AQP1 [51]. a, The 3.5Å AQP1 projection structure with the 3D map of the monomer at 6.9Å resolution (blue) and the projection of the atomic model (brown). b, The 3.7Å GlpF projection structure with the 3D map of the monomer at 6.9Å resolution (yellow) and the projection of the constructed model of GlpF. The dotted line indicates the pseudo two-fold symmetry axis of the monomer. c,d, Channels of AQP1 (c) and GlpF (d), calculated by HOLE [90]. e, The amphiphilic nature of the GlpF channel is revealed by color coding the accessible surfaces: green: aromatic residues; yellow: hydrophobic residues; white: polar residues ; blue: positively charged residues.

examined with a laser diffractometer and digitized with a ZEISS Phodis scanner (Carl Zeiss, Oberkochen, Germany) at 1Å/*pixel* on the specimen level or with a Leafscan-45 scanner (Leaf systems. Inc., Westborough, MA, USA) at 1.4 Å/*pixel*.

Image processing   Image processing was performed using the MRC crystallography program suite [27, 28]. Images were corrected for lattice distortions, taking the Fourier-filtered images themselves as references. Phases and amplitudes were measured and corrected for the tilted contrast transfer function. Images with two lattices of equal quality were processed for both crystal layers independently. Amplitudes and phases from processed images were merged imposing p4 symmetry. After phase origin refinement, lattice lines for the amplitudes and phases normal to the membrane plane were fitted and sampled at $(100 \ \mathring{A}) - 1$ to create a 3D data set of structure factors. The 3D dataset was used with the program MAKETRAN to create reference projections [37]. All images were then unbent with these synthetic references and merged again. A final 3D map was calculated using the CCP4 programs [1].

Homology modeling   A model of the structure of GlpF was built based on the atomic structure of AQP1 [51] and an alignment of the two sequences [30] using the WHATIF program [90]. Using the rotamer database of WHATIF, the side-chain conformations of W42 and Y138 were refined manually to select the most probable rotamer state for both residues that did not block the channel. Rottrans[2] was used to calculate the most favorable orientation of this model in the 3D electron-crystallographic map of GlpF, and for this orientation, a projection in the membrane plane was calculated.

---

[2]http://www.mpibpc.gwdg.de/abteilungen/071/bgroot/maptools.html

Chapter 4

Summary

Membrane proteins are responsible for a broad spectrum of biological functions such as signal transduction, structural functions, energy conversion or transport of matter across the membranes. Around 30% of the protein-sequences encode membrane-proteins [88, 80]: Most of them are not directly involved in cell-house-keeping functions but are indispensable for multicellular life. Therefore, many of these proteins are of high importance in various medical relevant areas, such as neurobiology, cell-cycle controlling or immune response, just to mention a few of them. Malfunctions of these proteins can result in severe diseases such as Cystic Fibrosis. Other membrane-proteins, such as the multidrug resistance-pump, are responsible for major medical problems *if* they are present: Examples are the resistance of microbes against antibiotics or ineffective treatments of cancer patients due to resistance of the cancer cell against the chemotherapeutic agents.

The medical relevance of these proteins was and is accompanied by a lack of structural information. However, significant progress was made in the last three years. Several leading structures were solved for some protein-families, mostly using large automated screening approaches. But others are still in the dark. Furthermore, the current structure exploration still fails in solving routinely the structure of specific membrane-proteins. More effort has to be put into the development of these methods for specifically crystallizing (in 2D or 3D) medically relevant proteins with the goal of bringing membrane protein structures to structural biology and medicine.

2D-crystallization is a promising approach for these difficult projects since the protein is reconstituted in its natural environment soon after purification. The protein can be kept under physiological conditions for the structural exploration. Some of the obtained 2D-crystals were reported to be still functional active such as the AQP1 crystals [92].

However, as with 3D-crystallization for X-ray crystallography, the 2D-crystallization is still the bottle-neck in electron crystallography. Chapter 2 describes the attempts to 2D-crystallize a highly flexible multidrug-resistance protein LmrA from *Lactococcus lactis*. This ABC-transporter was subjected to a broad crystallization pre-screen to find stabilizing conditions for subsequent crystallization experiments: First, various detergents were tested for their ability to preserve LmrA in a healthy state. Since no functionality test for solubilized LmrA was known, indirect methods to test the integrity of the protein had to be used, such as solubilization tests, electron microscopy of solubilized

LmrA or sucrose gradients. In the second part of the pre-screen the selected detergents were tested against various lipids for LmrA reconstitution. These reconstitution tests were done with the monolayer technique [41]. From these experiments we learned that the detergents $C_{12}E_8$, Triton X-100 and (with some restriction) DDM are most suitable for further crystallization tests. The lipid-screen revealed that synthetic lipids mimicking the membrane of *Lactococcus lactis* are better suitable for LmrA-reconstitution than other synthetic lipids (except DMPC). Especially the results for a POPG:cardiolipin mixture seemed to be promising. From the natural lipid-isolates, *Escherichia coli*-lipid, also containing cardiolipin has the ability to incorporate LmrA in lipid bilayers (see next paragraph).

In parallel, reconstitution and crystallization experiments were performed: A major problem was the proper reconstitution of LmrA. Tests of different detergent removal methods revealed, that LmrA reconstitutes nicely in *Escherichia coli*-lipid by a stepwise detergent-removal with bio-beads [65, 64]. In these experiments, fungi-like structures were visible as spikes sticking out for 6 *nm* of thick double-membranes. These structures were interpreted as the soluble part of LmrA. The measured dimensions are compatible with the findings of Chang *et al.*, 2001 [10] on MsbA, a LmrA homologue of *Escherichia coli*. Taken together, these results are a good starting point for further crystallization experiments, if the found conditions can be combined and the protein can be trapped in a specific confirmation using LmrA-inhibitors.

In chapter 3 the successful 2D-crystallization of GlpF, the glycerol facilitator protein of *Escherichia coli*, is described. To assess the GlpF structure, recombinant histidine tagged protein was overexpressed, solubilized in octylglucoside (OG) and purified to homogeneity. Negative stain electron microscopy of solubilized GlpF protein revealed a tetrameric structure of approximately 80 Å sidelength. Scanning transmission electron microscopy (STEM) yielded a mass of 170 *kDa* corroborating the tetrameric nature of GlpF. These results are contradictory to previous speculations that GlpF is a monomer [9, 39]. However, the tetrameric architecture has been confirmed by the atomic structure of GlpF [23].

Reconstitution of GlpF in the presence of lipids produced highly ordered two dimensional crystals, which diffracted electrons to 3.6 Å resolution. Cryo electron microscopy provided a 3.7 Å projection map exhibiting a unit cell comprised of two tetramers. In projection, GlpF is similar to AQP1, the erythrocyte water channel. However, the major density minimum within each monomer is distinctly larger in GlpF than in AQP1. This finding was confirmed with the comparison of the refined AQP1 model [14] and the x-ray structure of GlpF [23], see also figure 1.6 p. 12.

To obtain the three dimensional (3D) structure of GlpF, the two-dimensional crystals were tilted up to 62° in the electron microscope to get the side-views of the protein. The resulting 6.9 Å density map showed the GlpF helices to be similar to those of AQP1, the erythrocyte water channel. While the helix arrangement of GlpF does not reflect the larger pore diameter as seen in the projection map, additional peripheral densities observed in GlpF are compatible with the 31 additional residues in loops C and E, which accordingly do not interfere with the inner channel construction. Therefore, the atomic structure of AQP1 was used as a basis for homology modeling of the GlpF channel, which was predicted to be free of bends, wider, and more vertically oriented than the

AQP1 channel. Furthermore, the residues facing the GlpF channel exhibited an amphiphilic nature, being hydrophobic on one side and hydrophilic on the other side. This property was speculated to partially explain the contradiction of glycerol diffusion but limited water capacity. Both, the additional densities and the greasy slide similar to maltoporin [72] have also been observed in the atomic structure of GlpF [23]. The importance of the amphiphilic channel architecture is also corroborated by molecular dynamic calculations [35].

Publications

- T. Braun, R. J. McIlhinney, and G. Vergères. Myristoylation-dependent n-terminal cleavage of the myristoylated alanine-rich c kinase substrate (MARCKS) by cellular extracts. *Biochimie*, 82:1–11, 2000.

- T. Braun, A. Philippsen, M. Borgnia, P. Ager, W. Kühlbrandt, A. Engel, and H. Stahlberg. GlpF: A structural variant of the aquaporin tetramer. In S. Hohmann and S. Nielsen, editors, *Molecular biology and physiology of water and solute transport*. Academic Press, 2000, p. 13-22.

- T. Braun, A. Philippsen, S. Wirtz, M. J. Borgnia, P. Agre, W. Kühlbrandt, A. Engel, and H. Stahlberg. The 3.7Å projection map of the glycerol facilitator GlpF: A variant of the aquaporin tetramer. *EMBO Reports*, 2:183–189, 2000.

- H. Stahlberg[1], T. Braun[1], B. de Groot, A. Philippsen, M. J. Borgnia, P. Agre, W. Kühlbrandt, and A. Engel. The 6.9-Å structure of GlpF: A basis for homology modeling of the glycerol channel from *escherichia coli*. *Journal of Structural Biology*, 132:133–141, 2000.

- H. Stahlberg, D. Fotiatis, S. Scheuring, H. Rémigy, T. Braun, K. Mitsuoka, Y. Fujiyoshi, and A. Engel. Two dimensional crystals: A powerful approach to assess structure, function and dynamics of membrane proteins. *FEBS Letters*, 504:166–172, 2001.

- A. Ulrich, A. A. Schmitz, T. Braun, T. Yuan, H. J. Vogel, and G. Vergeres. Mapping the interface between calmodulin and MARCKS-related protein by fluorescence spectroscopy. *Proc. Natl. Acad. Sci. USA*, 97(10):5191–5196, 1999.

---

[1]These authors contributed equally to this work

Bibliography

[1] C. C. P. N. 4. The CCP4 suite: Programs for protein crystallography. *Acta Crystallog.*, 50:760–763, 1994.

[2] W. Baumeister, F. Karrenberg, R. Rachel, A. Engel, B. ten Heggeler, and W. O. Saxton. The major cell envelope protein of *Micrococcus radiodurans* (R1). Structural and chemical characterization. *Eur. J. Biochem.*, 125(3):535–544, 1982.

[3] P. R. Bevington. *Data Reduction and Error Analysis for the Physical Sciences*. McGrow-Hill Book Company, New York, 1969.

[4] R. Binet, S. Letoffe, J. M. Ghigo, P. Delepelaire, and C. Wandersman. Protein secretion by gram-negative bacterial ABC exporters–a review. *Gene*, 192(1):7–11, 1997.

[5] W. Boos, U. Ehmann, H. Forkl, W. Klein, M. Rimmele, and P. Postma. Trehalose transport and metabolism in *Escherichia coli*. *Journal Bacteriology*, 172(6):3450–3461, 1990.

[6] M. J. Borgnia and P. Agre. Reconstitution and functional comparison of purified GlpF and AqpZ, the glycerol and water channels from *Escherichia coli*. *PNAS*, 98(5):28882893, February 2001.

[7] M. J. Borgnia, D. Kozono, G. Calamita, P. C. Maloney, and P. Agre. Functional reconstitution and characterization of AqpZ, the *E. coli* water channel protein. *Journal Molecular Biology*, 291(5):1169–1179, 1999.

[8] T. Braun, A. Philippsen, S. Wirtz, M. J. Borgnia, P. Agre, W. Kuhlbrandt, A. Engel, and H. Stahlberg. The 3.7Å projection map of the glycerol facilitator GlpF: A variant of the aquaporin tetramer. *EMBO Reports*, 2:183–189, 2000.

[9] P. Bron, V. Lagree, A. Froger, R. Rolland, J. F. Hubert, C. Delamarche, S. Deschamps, I. Pellerin, D. Thomas, and W. Haase. Oligomerization state of MIP proteins expressed in *Xenopus* oocytes as revealed by freeze-fracture electron-microscopy analysis. *Journal Structural Biology*, 128(3):287–296, 1999.

[10] G. Chang and C. B. Roth. Structure of MsbA from e. coli: A homolog of the multidrug resistance atp binding cassette (abc) transporters. *Science*, 293(5536):1793–1800, 2001.

[11] A. Cheng, A. N. van Hoek, M. Yeager, A. S. Verkman, and A. K. Mitra. Three-dimensional organization of a human water channel. *Nature*, 387(6633):6227–6230, 1997.

[12] R. A. Crowther, R. Henderson, and J. M. Smith. MRC image processing programs. *J. Struct. Biol.*, 116(1):9–16, 1996.

[13] M. J. Daniels, M. J. Chrispeels, and M. Yeager. Projection structure of a plant vacuole membrane aquaporin by electron cryo-crystallography. *Journal of Molecular Biology*, 294(5):1337–1349, 1999.

[14] B. L. de Groot, A. Engel, and H. Grubmüller. A refined structure of human aquaporin-1. *FEBS Letters*, 504:206–211, 2001.

[15] B. L. de Groot and H. Grubmüller. Water permeation across biological membranes: Mechanism and dynamics of Aquaporin-1 and GlpF. *Science*, 214, December 2001.

[16] B. L. de Groot, J. B. Heymann, A. Engel, K. Mitsuoka, Y. Fujiyoshi, and H. Grubmüller. The fold of human aquaporin 1. *Journal of Molecular Biology*, 300(4):987–994, 2000.

[17] A. J. M. Driessen, T. Zheng, G. in t' Feld, J. A. F. Op den Kamp, and W. N. Konings. The lipid requireement of the branched-chain amino acid transport system of *Lactococcus Lactis* subsp. *Cremoris*. *Biochemistry*, 27:865–872, 1988.

[18] J. Dubochet, M. Adrian, J.-J. Chang, J.-C. Homo, J. Lepault, A. McDowall, and P. Schultz. Cryo-electron microscopy of vitrified specimens. *Quart. Rev. Biophys.*, 21:129–228, 1988.

[19] A. Engel, Y. Fujiyoshi, and P. Agre. The importance of aquaporin water channel protein structures. *EMBO Journal*, 19(5):800–806, 2000.

[20] D. Fotiadis, L. Hasler, D. J. Müller, H. Stahlberg, J. Kistler, and A. Engel. Surface tongue-and-groove contours on lens MIP facilitate cell-to-cell adherence. *Journal of Molecular Biology*, 300(4):779–789, 2000.

[21] J. Frank, M. Radermacher, P. Penczek, J. Zhu, Y. Li, M. Ladjadj, and A. Leith. SPIDER and WEB: Processing and visualization of images in 3D electron microscopy and related fields. *J. Struct. Biol.*, 116(1):190–199, 1996.

[22] A. Froger, B. Tallur, D. Thomas, and C. Delamarche. Prediction of functional residues in water channels and related proteins. *Protein Sci.*, 7(6):1458–1468, 1998.

[23] D. Fu, A. Libson, L. J. Miercke, C. Weitzman, P. Nollert, J. Krucinski, and R. M. Stroud. Structure of a glycerol-conducting channel and the basis for its selectivity. *Science*, 290(5491):481–486, 2000.

[24] Y. Fuiyoshi. The structural study of membrane proteins by electron crystallography. *Advanced Biophysics*, 35:25–80, 1998.

[25] M. B. Gorin, S. B. Yancey, J. Cline, J.-P. Revel, and J. Horwitz. The major intrinsic protein (MIP) of the bovine lens fiber membrane: Characterization and structure based on cDNA cloning. *Cell*, 39:49–59, 1984.

[26] L. Hasler, T. Walz, P. Tittmann, H. Gross, J. Kistler, and A. Engel. Purified lens major intrinsic protein (MIP) forms highly ordered tetragonal two-dimensional arrays by reconstitution. *Journal Molecular Biology*, 279(4):855–864, 1998.

[27] R. Henderson, J. M. Baldwin, T. Ceska, F. Zemlin, E. Beckmann, and K. H. Downing. Model for the structure of bacteriorhodopsin based on high-resolution electron cryo-microscopy. *J. Mol. Biol.*, 213:899– 929, 1990.

[28] R. Henderson, J. M. Baldwin, K. H. Downing, J. Lepault, and F. Zemlin. Structure of purple membrane from *Halobacterium halobium*: Recording, measurement and evaluation of electron micrographs at 3.5 Å resolution. *Ultramicroscopy*, 19:147–178, 1986.

[29] R. Henderson and P. N. Unwin. Three-dimensional model of purple membrane obtained by electron microscopy. *Nature*, 257(5521):228–232, 1975.

[30] B. Heymann and A. Engel. Structural clues in the sequences of the aquaporins. *Journal Molecular Biology*, 295(4):1039–1053, 2000.

[31] J. B. Heymann and A. Engel. Aquaporins: Phylogeny, structure, and physiology of water channels. *News Physiol. Sci.*, 14:187–193, 1999.

[32] T. Hirai, K. Murata, Y. Kimura, and Y. Fujiyoshi. Trehalose embedding technique for high-resolution electron crystallography: Application to structural study on bacteriorhodopsin. *J. Elec. Microsc.*, 48(5):653–685, 1999.

[33] D. L. Jack, N. M. Yang, and J. Milten H. Saier. The drug/metabolite transporter superfamily. *European Journal of Biochemistry*, 268:3620–3639, 2001.

[34] B. K. Jap, M. Zulauf, T. Scheybani, A. Hefti, W. Baumeister, U. Aebi, and A. Engel. 2D crystallization: From art to science. *Ultramicroscopy*, 46(1-4):45–84, 1992.

[35] M. O. Jensen, E. Tajkhorshid, and K. Schulten. The mechanism of glycerol conduction in aquaglyceroporins. *Structure*, 9:1083–1093, November 2001.

[36] J. S. Jung, G. M. Preston, B. L. Smith, W. B. Guggino, and P. Agre. Molecular structure of the water channel through aquaporin CHIP. The hourglass model. *Journal of Biological Chemistry*, 269(20):14648–14654, 1994.

[37] E. R. Kunji, S. von Gronau, D. Oesterhelt, and R. Henderson. The three-dimensional structure of halorhodopsin to 5Å by electron crystallography: A new unbending procedure for two-dimensional crystals by using a global reference structure. *Proc. Natl. Acad. Sci. USA*, 97(9):4637–4642, 2000.

[38] V. Lagree, A. Froger, S. Deschamps, J. F. Hubert, C. Delamarche, G. Bonnec, D. Thomas, J. Gouranton, and I. Pellerin. Switch from an aquaporin to a glycerol channel by two amino acids substitution. *Journal of Biological Chemistry*, 274(11):6817–6819, 1999.

[39] V. Lagree, A. Froger, S. Deschamps, I. Pellerin, C. Delamarche, G. Bonnec, J. Gouranton, D. Thomas, and J. F. Hubert. Oligomerization state of water channels and glycerol facilitators. involvement of loop E. *Journal of Biological Chemistry*, 273(51):33949–33953, 1998.

[40] V. Lagree, I. Pellerin, J. F. Hubert, F. Tacnet, F. Le Caherec, N. Roudier, D. Thomas, J. Gouranton, and S. Deschamps. A yeast recombinant aquaporin mutant that is not expressed or mistargeted in *Xenopus* oocyte can be functionally analyzed in reconstituted proteoliposomes. *Journal of Biological Chemistry*, 273(20):12422–12426, 1998.

[41] D. Lévy, G. Mosser, O. Lambert, G. S. Moeck, D. Bald, and J.-L. Rigaud. Two-dimensional crystallization on lipid layer: A successful approach for membrane proteins. *Journal of Structural Biology*, 127:44.52, 1999.

[42] H. Li, S. Lee, and B. Jap. Molecular design of Aquaporin-1 water channel as revealed by electron crystallography. *Nature Structural Biology*, 4(4):263–265, 1997.

[43] A. Margolles, M. Putman, H. W. van Veen, and W. N. Konings. The purified and functionally reconstituted multidrug transporter LmrA of *Lactococcus lactis* mediates the transbilayer movement of specific fluorescent phospholipids. *Biochemistry*, 38(49):16298–16306, 1999.

[44] C. Maurel, J. Reizer, J. I. Schroeder, M. J. Chrispeels, and J. Saier, M. H. Functional characterization of the *Escherichia coli* glycerol facilitator, GlpF, in *Xenopus* oocytes. *Journal of Biological Chemistry*, 269(16):11869–11872, 1994.

[45] M. J. Memieux, R. A. F. Reithmeier, and D.-N. Wang. Importance of detergent and phospholipid in the crystallization of human erythrocyte anion exchanger membrane domain. *Journal Structural Biology*, 2002. In press.

[46] H. Michel. Membrane proteins of known structure, 2002. URL: http://www.biophys.mpg.de/michel/public/memprotstruct.html.

[47] J. Milton H. Saier and I. T. Paulsen. Phylogeny of multidrug transporters. *Seminars in Cell Developmental Biology*, 12:3620–3639, 2001.

[48] K. Mitsuoka, K. Murata, T. Walz, T. Hirai, P. Agre, J. B. Heymann, A. Engel, and Y. Fujiyoshi. The structure of Aquaporin-1 at 4.5-Å resolution reveals short alpha-helices in the center of the monomer. *Journal of Structural Biology*, 128(1):34–43, 1999.

[49] S. Müller and A. Engel. Mass measurement in the scanning transmission electron microscope: A powerful tool for studying membrane proteins. *J. Struct. Biol.*, 121(2):219–230, 1998.

[50] S. Müller, K. Goldie, R. Bürki, R. Häring, and A. Engel. Factors influencing the precision of quantitative scanning transmission electron microscopy. *Ultramicroscopy*, 46:317–334, 1992.

[51] K. Murata, K. Mitsuoka, T. Hirai, T. Walz, P. Agre, J. Heymann, A. Engel, and Y. Fujiyoshi. Structural determinants of water permeation through Aquaporin-1. *Nature*, 407(October):599–605, 2000.

[52] A. G. Murzin, S. E. Brenner, T. Hubbard, and C. Chothia. SCOP: A structural classification of proteins database for the investigation of sequences and structures. *Journal Molecular Biology*, 247:536540, 1995.

[53] K. L. Nemeth-Cahalan and J. E. Hall. pH and calcium regulate the water permeability of Aquaporin 0. *Journal Biological Chemistry*, 275(10):6777–6782, 2000.

[54] J. H. Park and J. Saier, M. H. Phylogenetic characterization of the MIP family of transmembrane channel proteins. *Journal of Membrane Biology*, 153(3):171–180, 1996.

[55] P. Penczek, M. Radermacher, and J. Frank. Three-dimensional reconstruction of single particles embedded in ice. *Ultramicroscopy*, 40(1):33–53, 1992.

[56] G. E. Pfyffer. Drug-resistant tuberculosis: resistance mechanisms and rapid susceptibility testing. *Schweizerische Medizinische Wochenschrift*, 130:1909–1913, 2000.

[57] G. M. Preston and P. Agre. Isolation of the cDNA for erythrocyte integral membrane protein of 28 kilodaltons: Member of an ancient channel family. *Proc. Nat. Acad. Sci. USA*, 88:11110–11114, 1991.

[58] G. M. Preston, T. P. Carroll, W. B. Guggino, and P. Agre. Appearance of water channels in *Xenopus* oocytes expressing red cell CHIP28 protein. *Science*, 256:385–387, 1992.

[59] Q. Qu and F. J. Sharon. FRET analysis indicates that the twi ATPase active site of the P-glycoprotein multidrug transporter are closely associated. *Biochemistry*, 40:1413–22, 2001.

[60] Y. Raviv, H. B. Pollard, I. Bruggemann, E. P. Pastan, and M. M. Gottesmann. Photosensitized labeling of a functional multidrug transporter in living drug-resistant tumor cells. *Journal of Biological Chemistry*, 265(7):3975–3980, March 1990.

[61] H. Remigy. *Crystallization of something and building a huge machine*. PhD thesis, Universität Basel, 2001.

[62] J.-L. Riagaud, M. Chami, O. Lambert, D. Levy, and J.-L. Ranck. Use of detergent in two-dimensional crystallisation of membrane proteins. *Biochim. Biophys. Acta.*, 2000.

[63] J.-L. Rigaud, D. Levy, G. Mosser, and O. Lambert. Detergent removal by non-polar polystyrene beads. *Eur Biophys Journal*, 25:305319, 1998.

[64] J.-L. Rigaud, G. Mosser, J.-J. Lacapere, A. olofsson, D. Levy, and J.-L. Ranck. Bio-beads: An efficient strategy for two-dimensional crystallisation of membrane proteins. *Journal of Structural Biology*, 118:226–35, 1997.

[65] J.-L. Rigaud, B. Pitard, and D. Levy. Reconstitution of membrane proteins into liposomes: Application to energy-transducing membrane proteins. *BBA*, 1231:223–46, 1995.

[66] P. Ringler, M. J. Borgnia, H. Stahlberg, P. C. Maloney, P. Agre, and A. Engel. Structure of the water channel AqpZ from *Escherichia coli* revealed by electron crystallography. *Journal Molecular Biology*, 291(5):1181–1190, 1999.

[67] P. Ringler, B. Heymann, and A. Engel. Two-dimensional crystallisation of membrane proteins. Technical report, MIH Biozentrum Uni Basel, 1999.

[68] M. F. Rosenberg, Q. Mao, A. Holzenburg, R. C. Ford, R. G. Deeley, and S. P. C. Cole. The structure of the multidrug resistance protein 1 (mrp1/abcc1). *Journal of Biological Chemistry*, 276(19):16076–16082, May 2001.

[69] J. I. Ruiz and B. Ochoa. Quantification in the subnanomolar range of phosphilipids and neutral lipids by monodimensional thin-layer chromatography and image analysis. *Journal of Lipid Research*, 38:1482–1489, July 1997.

[70] S. Scheuring, P. Ringler, M. Borgnia, H. Stahlberg, D. J. Muller, P. Agre, and A. Engel. High resolution AFM topographs of the *Escherichia coli* water channel aquaporin Z. *EMBO Journal*, 18(18):4981–4987, 1999.

[71] S. Scheuring, P. Tittmann, H. Stahlberg, P. Ringler, M. Borgnia, P. Agre, H. Gross, and A. Engel. The aquaporin sidedness revisited. *Journal of Molecular Biology*, 299(5):1271–1278, 2000.

[72] T. Schirmer, T. A. Keller, Y. F. Wang, and J. P. Rosenbusch. Structural basis for sugar translocation through maltoporin channels at 3.1Å resolution. *Science*, 267(5197):473–474, January 1995.

[73] O. Smart, J. Neduvelil, X. Wang, B. Wallace, and M. Sansom. HOLE: A program for the analysis of the pore dimensions of ion channel structural models. *J. Mol. Graphics*, 14:354–360, 1996.

[74] B. L. Smith and P. Agre. Erythrocyte Mr 28,000 transmembrane protein exists as a multisubunit oligomer similar to channel proteins. *Journal Biological Chemistry*, 266(10):6407–6415, 1991.

[75] H. Stahlberg, T. Braun, B. de Groot, A. Philippsen, M. J. Borgnia, P. Agre, W. Kühlbrandt, and A. Engel. The 6.9-å structure of GlpF: A basis for homology modeling of the glycerol channel from *escherichia coli*. *Journal of Structural Biology*, 132:133141, 2000.

[76] D. Stock, A. G. W. Leslie, and J. E. Walker. Molecular architecture of the rotary motor in ATP synthase. *Science*, 286:1700–1705, November 1999.

[77] H. Sui, B.-G. Han, J. K. Lee, P. Walian, and B. K. Jap. Structural basis of water-specific transport through the AQP1 water channel. *Nature*, 414:872–878, December 2001.

[78] C. G. Tate, E. R. S. Kunji, M. Lebendiker, and S. Schuldiner. The projection structure of EmrE, a proton linked multidrug transporter from *Escherichia coli*, at 7Å resolution. *EMBO Journal*, 20:77–81, January 2001.

[79] C. Toyoshima, M. Nakasako, H. Nomura, and H. Ogawa. Crystal structure of the calcium pump of sarcoplasmic reticulum at 2.6Å resolution. *Nature*, 405, June 2000.

[80] I. Ubarretxena-Belandia and D. M. Engelman. Helical membrane proteins: Diversity of functions in the context of simple architecture. *Annual Reviews Biochemistry*, 11:370376, 2001.

[81] P. N. Unwin and R. Henderson. Molecular structure determination by electron microscopy of unstained crystalline specimens. *J. Mol. Biol.*, 94(3):425–440, 1975.

[82] M. van Heel. Similarity measures between images. *Ultramicroscopy*, 21(1):95–100, 1987.

[83] H. W. van Veen, R. Callaghan, L. Soceneantu, A. Sardini, W. N. Konings, and C. F. Higgins. A bacterial antibiotic-resistance gene that complements the human multidrug-resistance P-glycoprotein gene. *Nature*, 391(6664):291–295, 1998.

[84] H. W. van Veen, A. Margolles, M. Muller, C. F. Higgins, and W. N. Konings. The homodimeric ATP-binding cassette transporter LmrA mediates multidrug transport by an alternating two-site (two-cylinder engine) mechanism. *EMBO Journal*, 19(11):2503–2514, 2000.

[85] H. W. van Veen, A. Margolles, M. Putman, K. Sakamoto, and W. N. Konings. Multidrug resistance in *Lactic acid* bacteria: Molecular mechanisms and clinical relevance. *Antonie Van Leeuwenhoek*, 76(1-4):347–352, 1999.

[86] H. W. van Veen, M. Putman, A. Margolles, K. Sakamoto, and W. N. Konings. Structure-function analysis of multidrug transporters in *Lactococcus lactis*. *Biochimica Biophysica Acta*, 1461(2):201–206, 1999.

[87] H. W. van Veen, K. Venema, H. Bolhuis, I. Oussenko, J. Kok, B. Poolman, A. J. Driessen, and W. N. Konings. Multidrug resistance mediated by a bacterial homolog of the human multidrug transporter MDR1. *Proc. Natl. Acad. Sci. U S A*, 93(20):10668–10672, 1996.

[88] J. Venter, M. D. Adams, E. Myers, P. Li, R. Mural, G. Sutton, H. Smith, M. Yandell, C. Evans, R. Holt, J. Gocayne, P. Amanatides, R. Ballew, D. Huson, J. Wortman, Q. Zhang, C. Kodira, X. Zheng, L. Chen, M. Skupski, G. Subramanian, P. Thomas, J. Zhang, G. L. Gabor Miklos, C. Nelson, S. Broder, A. Clark, J. Nadeau, V. McKusick, N. Zinder, A. Levine, R. Roberts, M. Simon, C. Slayman, M. Hunkapiller, R. Bolanos, A. Delcher, I. Dew, D. Fasulo, M. Flanigan, L. Florea, A. Halpern,

S. Hannenhalli, S. Kravitz, S. Levy, C. Mobarry, K. Reinert, K. Remington, J. Abu-Threideh, E. Beasley, K. Biddick, V. Bonazzi, R. Brandon, M. Cargill, I. Chandramouliswaran, R. Charlab, K. Chaturvedi, Z. Deng, V. Di Francesco, P. Dunn, K. Eilbeck, C. Evangelista, A. Gabrielian, W. Gan, W. Ge, F. Gong, Z. Gu, P. Guan, T. Heiman, M. E. Higgins, R. R. Ji, Z. Ke, K. A. Ketchum, Z. Lai, Y. Lei, Z. Li, J. Li, Y. Liang, X. Lin, F. Lu, G. V. Merkulov, N. Milshina, H. M. Moore, A. K. Naik, V. A. Narayan, B. Neelam, D. Nusskern, D. B. Rusch, S. Salzberg, W. Shao, B. Shue, J. Sun, Z. Wang, A. Wang, X. Wang, J. Wang, M. Wei, R. Wides, C. Xiao, C. Yan, A. Yao, J. Ye, M. Zhan, W. Zhang, H. Zhang, Q. Zhao, L. Zheng, F. Zhong, W. Zhong, S. Zhu, S. Zhao, D. Gilbert, S. Baumhueter, G. Spier, C. Carter, A. Cravchik, T. Woodage, F. Ali, H. An, A. Awe, D. Baldwin, H. Baden, M. Barnstead, I. Barrow, K. Beeson, D. Busam, A. Carver, A. Center, M. L. Cheng, L. Curry, S. Danaher, L. Davenport, R. Desilets, S. Dietz, K. Dodson, L. Doup, S. Ferriera, N. Garg, A. Gluecksmann, B. Hart, J. Haynes, C. Haynes, C. Heiner, S. Hladun, D. Hostin, H. J, H. T, I. C, J. J, K. F, K. L, K. S, L. A, M. F, M. D, M. S, M. T, M. I, M. M, M. L, M. B, N. K, P. C, P. E, P. V, Q. H, R. M, R. R, R. YH, R. D, R. B, S. R, S. C, S. M, S. E, S. R, S. E, T. R, T. NN, T. S, V. C, W. G, W. J, W. S, W. M, W. S, W.-D. E, W. K, Z. J, Z. K, A. JF, G. R, C. MJ, S. KV, K. B, K. A, M. H, L. B, H. T, N. A, D. K, M. A, G. N, S. S, B. V, I. S, L. R, S. R, W. B, Y. S, A. D, B. A, B. J, B. L, C. M, C.-S. J, C. P, C. YH, C. M, D. C, M. A, D. M, D. M, E. D, E. S, F. C, G. H, G. S, G. K, G. A, G. M, G. K, G. B, H. M, H. J, H. S, H. J, J. D, J. C, J. J, K. J, K. L, K. C, L. A, L. M, L. X, L. J, M. D, M. W, M. J, M. S, N. M, N. T, N. N, N. M, P. S, P. J, P. M, R. W, S. R, S. J, S. M, S. T, S. A, S. T, T. R, V. E, W. M, W. M, W. D, W. M, X. A, Z. A, and X. Zhu. The sequence of the human genome. *Science*, 291, February 2001.

[89] R. T. Voegele, G. D. Sweet, and W. Boos. Glycerol kinase of *Escherichia coli* is activated by interaction with the glycerol facilitator. *Journal Bacteriol.*, 175(4):1087–1094, 1993.

[90] G. Vriend. WHAT IF: A molecular modeling and drug design program. *J. Mol. Graph.*, 8(1):52–56, 1990.

[91] T. Walz, T. Hirai, K. Murata, J. Heymann, K. Mitsuoka, Y. Fujiyoshi, B. Smith, P. Agre, and A. Engel. The three-dimensional structure of Aquaporin-1. *Nature*, 387(6633):624–627, 1997.

[92] T. Walz, B. L. Smith, P. Agre, and A. Engel. The three-dimensional structure of human erythrocyte aquaporin CHIP. *EMBO Journal*, 13(13):2985–2993, 1994.

[93] T. Walz, D. Typke, B. Smith, P. Agre, and A. Engel. Projection map of aquaporin-1 determined by electron crystallography. *Nature Structural Biology*, 2(9):730–732, 1995.

[94] P. J. Werten, L. Hasler, J. B. Koenderink, C. H. Klaassen, W. J. de Grip, A. Engel, and P. M. Deen. Large-scale puriccation of functional recombinant human aquaporin-2. *FEBS letters*, 504:200–205, 2001.

[95] M. Yasui, A. Hazama, T. H. Kwon, S. Nielsen, W. B. Guggino, and P. Agre. Rapid gating and anion permeability of an intracellular aquaporin. *Nature*, 402(6758):184–187, 1999.

[96] T. Zeuthen and D. A. Klaerke. Transport of water and glycerol in aquaporin 3 is gated by H^+. *Journal of Biological Chemistry*, 274(31):21631–21636, 1999.

Curriculum vitae

Personal

Born: February 8th 1973

Citizenship: Swiss (Basel)

marital status : Unmarried

Education

1980 - 1985: Primary school (Allschwil)

1985 - 1989: Grammar school (Allschwil)

1989: Entry in high school (Mathematisches Naturwissenschaftliches Gymnasium), Basel

1993: Matura (Mathematisches Naturwissenschaftliches Gymnasium); Beginning of studies of Biologie II at the Biocentre of the Universiy of Basel

1998: Diploma degree in Biology II, University of Basel

1999: Start of PhD thesis

Working experiences

- October 1996 – February 1998: Diploma thesis by PD Dr. G. Vergères (Biozentrum Universität Basel, Departement Biophysical Chemistry, group of Prof. Schwarz)

- Practical as technical assistant in the same laboratory for further 6 months.

- January 1999: Start PhD thesis in the group of Andreas Engel (Maurice E. Müller Institute, Biozentrum Basel)

Fields of training and research expiereince

- Protein chemistry and 2D-crystallization

- High resolution electron-microscopy

- Image processing (MRC program suite, Spider, Semper)

Current research work

- 2D-crystallization of LmrA, a multidrug transporter from *Lactococcus lactis*, which belongs to the ABC-Transporter.

- 2D-crystallization of PM28, a regulated plant aquaporin.

- Single particle analysis of the McrBC complex, a DNAse which belongs to the AAA-protein-family.

Other experiences

- Experiences in science communication (organisation of public discussions, writing of newspaper articles)